

For Reference

NOT TO BE TAKEN FROM THIS ROOM

For Reference

NOT TO BE TAKEN FROM THIS ROOM

Ex LIBRIS
UNIVERSITATIS
ALBERTAENSIS



1970
297
UNIVERSITY OF ALBERTA
THE UNIVERSITY OF ALBERTA

THE KINETICS OF THE OXIDATION OF FERROCYANIDE
BY HORSERADISH PEROXIDASE COMPOUNDS I AND II

by



BRIAN B. HASINOFF

A THESIS

SUBMITTED TO THE FACULTY OF GRADUATE STUDIES
IN PARTIAL FULFILMENT OF THE REQUIREMENTS FOR THE DEGREE
OF DOCTOR OF PHILOSOPHY

DEPARTMENT OF CHEMISTRY

EDMONTON, ALBERTA

Spring, 1970

Thesis
1970
23D

UNIVERSITY OF ALBERTA

FACULTY OF GRADUATE STUDIES

The undersigned certify that they have read, and recommend to the Faculty of Graduate Studies for acceptance, a thesis entitled

"THE KINETICS OF THE OXIDATION OF FERROCYANIDE BY

HORSE RADISH PEROXIDASE COMPOUNDS I AND II"

submitted by Brian B. Hasinoff in partial fulfilment of the requirements for the degree of Doctor of Philosophy.

ABSTRACT

The kinetics of the oxidation of ferrocyanide by both horseradish peroxidase compounds I and II (HRP-I, HRP-II) have been studied as a function of pH at 25°. The apparent second order rate constant, k_{2app} , for the reaction of HRP-I with ferrocyanide varied from $4.1 \times 10^7 \text{ M}^{-1} \text{ sec}^{-1}$ to $5.5 \times 10^5 \text{ M}^{-1} \text{ sec}^{-1}$ over the pH range 3.7 to 11.3. The value of k_{3app} for the reaction of HRP-II with ferrocyanide varied from $1.3 \times 10^7 \text{ M}^{-1} \text{ sec}^{-1}$ to $2.4 \times 10^2 \text{ M}^{-1} \text{ sec}^{-1}$ over the pH range 2.8 to 10.3. The pH dependence of the HRP-I-ferrocyanide reaction has been interpreted in terms of a single ionization of pK 5.3 at the active site of HRP-I. The pH dependence of the HRP-II-ferrocyanide reaction has been interpreted in terms of three ionizations with pK's of 3.4, 5.2 and 8.6 at the active site of HRP-II.

The steady state kinetics of the HRP catalyzed oxidation of ferrocyanide by H_2O_2 were studied by the measurement of initial reaction velocities. Rate constants obtained by the steady state method were in agreement with those obtained from studies of isolated reactions on the stopped flow apparatus. The kinetic results can be correlated with conclusions drawn from previous kinetic studies on native HRP and with current ideas on the structures of HRP-I and HRP-II.

The kinetics of the binding of imidazole to ferri-protoporphyrin IX (hemin) in aqueous ethanol (44.5 weight %)

were studied at 25° using the temperature jump relaxation technique. The reaction was studied both as a function of imidazole concentration and hydrogen ion concentration. The acid dissociation constant for imidazolium ion was determined by acid-base titration and that of the protonated hemin species by spectrophotometric titration. The kinetic results may be explained quantitatively by a reaction in which imidazolium and imidazole bind at different rates to the basic hemin species. A comparison of the rates of ethanol exchange and imidazole binding to hemin favoured imidazolium ion substitution on the hydroxy hemin species by a S_N1 ion pair mechanism.

Acknowledgements

I would like to thank my research director, Dr. H. B. Dunford, for the encouragement and advice he has given me throughout the course of my research. I would also like to thank my fellow graduate students and the post doctorate fellows for many helpful discussions.

I would also like to make an acknowledgement to Dr. R. B. Jordan and Dr. N. S. Angerman without whose collaboration part of this research would not have been possible.

CONTENTS	PAGE
Abstract.....	i
Acknowledgements.....	iii
List of Tables.....	vi
List of Figures.....	viii

Chapter 1

Introduction

1.01	Horseradish Peroxidase.....	1
1.02	Hemin.....	9
1.03	Study of Fast Reactions.....	17

Chapter 2

Design Improvements to the Stopped-Flow Apparatus

2.01	Design Considerations.....	24
2.02	Measurement and Calculation of the Instru- mental Parameters Describing the Performance of the Stopped-Flow Apparatus.....	30
2.03	Construction.....	35

Chapter 3

The Kinetics of the Oxidation of Ferrocyanide by Horseradish Peroxidase Compounds I and II

3.01	Introduction.....	37
3.02	Experimental.....	39
3.03	Results.....	42
3.04	Discussion.....	70

Chapter 4

The Temperature Jump Kinetics of the Binding of
Imidazole to Ferriprotoporphyrin IX

4.01	Introduction.....	78
4.02	Experimental.....	80
4.03	Results.....	84
4.04	Discussion.....	100
	Bibliography.....	109

Appendix 1

The Analysis of Second Order Kinetic Data Obtained on a Stopped-Flow Apparatus.....	118
--	-----

Appendix 2

Derivation of the Initial Velocity Expression for the Steady State HRP Catalyzed Oxidation of Ferro- cyanide by Hydrogen Peroxide with a Calculation of the Attainment of Steady State Conditions.....	126
---	-----

Appendix 3

Purification of HRP by Sephadex Column Chromatography	135
---	-----

Appendix 4

Derivation of the Steady State Relaxation Time for the Binding of Imidazole to Hemin.....	139
--	-----

List of Tables

Table		Page
1.01	Amino Acid Composition of the HRP Isozymes.	3
1.02	Spectroscopic Features of HRP and its Hydrogen Peroxide Derivatives.....	7
1.03	The pK Values of Ionizations Found on Various Species of HRP.....	10
1.04	Comparison of Various Kinetic Methods Giving Minimum Reaction Half Times of $t_{1/2}$	19
3.01	Apparent Rate Constants for the HRP-II - Ferrocyanide Reaction at 25.0° and $\mu = 0.11$.	49
3.02	Rate and Ionization Constants Obtained by Non-linear Least Squares Analysis for the Reaction of HRP-II with Ferrocyanide.....	54
3.03	Apparent Rate Constants for the HRP-I - Ferrocyanide Reaction at 25.0° and $\mu = 0.11$.	58
3.04	Rate and Ionization Constants Obtained by Non-linear Least Squares Analysis for the Reaction of HRP-I with Ferrocyanide.....	61
3.05	Initial Velocity Data for the HRP Catalyzed Oxidation of Ferrocyanide at 25.0°, $\mu = 0.11$ and pH = 4.79.....	64
3.06	Initial Velocity Data for the HRP Catalyzed Oxidation of Ferrocyanide at 25.0° and $\mu = 0.11$	67

List of Tables

Table		Page
3.07	Rate Constants for the HRP Catalyzed Oxidation of Ferrocyanide by H_2O_2 at 25.0° and $\mu = 0.11$	68
3.08	The pK Values for Ionizations at the Active site of HRP Deduced from Kinetic Studies at 25.0° and $\mu = 0.11$	71
3.09	Comparison of Apparent Rate Constants for the Reaction of HRP-I and HRP-II with Various Substrates at Select pH Values.....	76
4.01	Apparent Rate and Equilibrium Constants for the Binding of Imidazole to Hemin at 25° and Ionic Strength 0.11	94
4.02	Rate and Equilibrium Constants Determined from Non-linear Least Squares Analysis of pH* Dependence of the k_{lapp} Data.....	103
A2.01	Normalized Concentration Derivatives Under Pseudo First Order Conditions at pH $4.79..$	132

List of Figures

	PAGE
1.01 The Relationship of the Different forms of HRP to One Another.....	6
1.02 Ferriprotoporphyryn IX or Hemin.....	11
1.03 Placement of the Nitrogen Atoms About the Central Metal Ion.....	12
1.04 Schematic of a Temperature Jump Apparatus..	22
2.01 Design Details of the Stopped-Flow Apparatus.....	27
2.02 Design Details of the Stopped-Flow Apparatus.....	29
2.03 Semilogarithmic Plot of Voltage <u>vs.</u> Time for the Reaction of Ferricyanide and Ascorbic Acid.....	34
3.01 Plot of Absorbance <u>vs.</u> Wavelength at the Times Indicated Showing the Conversion of HRP-II to HRP.....	44
3.02 Plot of $k_{3\text{obs}}$ <u>vs.</u> $[\text{Fe}(\text{CN})_6^{4-}]$ at pH 5.90 for the HRP-II - Ferrocyanide Reaction.....	46
3.03 Semilogarithmic Plot of $k_{2\text{app}}$ and $k_{3\text{app}}$ <u>vs.</u> pH for the Reaction of HRP-I and HRP-II with Ferrocyanide.....	48
3.04 Plot of $k_{2\text{obs}}$ <u>vs.</u> $[\text{Fe}(\text{CN})_6^{4-}]$ at pH 7.86 for the HRP-I - Ferrocyanide Reaction.....	57

3.05	Plot of Initial Steady State Velocity, v , <u>vs.</u> [HRP] ₀ at pH 4.79 and Constant Initial Con- centrations of Ferrocyanide and H ₂ O ₂	63
3.06	Plot of [HRP] ₀ / v <u>vs.</u> $1/[\text{Fe}(\text{CN})_6^{4-}]_0$ at the pH Values Shown.....	66
3.07	Plot of [HRP] ₀ / v <u>vs.</u> $1/[\text{H}_2\text{O}_2]_0$ at a pH of 4.82 and Constant Initial Concentrations of Ferrocyanide and HRP.....	69
4.01	Oscilloscope trace of Voltage <u>vs.</u> Time.....	82
4.02	Plot of α , the Fraction of the Protonated Hemin Species Present <u>vs.</u> pH*.....	87
4.03	Plot of Absorbance <u>vs.</u> Wavelength.....	89
4.04	Plot of $\log [(A_r - A_s)/(A_s - A_\infty)]$ <u>vs.</u> $\log [\overline{\text{Im}}]$.	91
4.05	Plot of $\Delta A/[\overline{\text{Im}}]^2$ <u>vs.</u> ΔA	93
4.06	Plot of K_{app} <u>vs.</u> pH*.....	95
4.07	Plot of $1/\tau$ <u>vs.</u> $[\overline{\text{Im}}]$ for Imidazole Binding to Hemin at pH* 8.82.....	97
4.08	Plot of k_{lapp} <u>vs.</u> pH*.....	98
A1.01	A Hypothetical Stopped-Flow Oscilloscope Trace of Voltage <u>vs.</u> Time.....	120
A2.01	Computer Calculated Relative Concentrations of Various HRP Species <u>vs.</u> Time at pH 4.79.	130
A3.01	Absorbances at 403 and 280 m μ and <u>R.Z.</u> Plotted <u>vs.</u> Effluent Volume.....	137

CHAPTER 1

Introduction

1.01 Horseradish Peroxidase

Horseradish peroxidase (EC 1.11.1.7; donor: H_2O_2 oxidoreductase) is an enzyme that catalyzes the oxidation of certain substrates by methyl hydrogen peroxide, ethyl hydrogen peroxide and hydrogen peroxide.

As early as 1810 the catalytic properties of fresh horseradish root were recognized (Planche, 1810). However, a proportional relationship between peroxidase activity and absorption in the Soret region was not shown until 1931 (Kuhn et al., 1931). Reasonably pure preparations of horseradish peroxidase, HRP, were first obtained by Keilin and Mann (1937). Peroxidases are found in plants, animals and microorganisms. Horseradish roots, Japanese radish, turnips, and fig sap all contain relatively high concentrations of peroxidase and serve as sources. Peroxidases are also present in milk, the thyroid gland, human saliva and blood plasma (Saunders et al., 1964).

Purification and Separation

A number of isozymes of HRP from horseradish roots have been observed by several workers (Theorell, 1942; Paul, 1958; Kasinky and Hackett, 1968; Shannon et al., 1966). The amino acid composition of the most abundant isozymes of HRP as determined by Shannon et al. (1966) are listed in Table

(1.01). All isozymes found for HRP contained ferriprotoporphyrin IX as their prosthetic group as do most of the other plant peroxidases. The molecular weight of HRP is approximately 40,000 (Keilin and Hartree, 1951). HRP is unusual as an enzyme because it is a glycoprotein. Carbohydrate analysis has shown that neutral and amino sugars account for 18% of the enzyme (Shannon et al., 1966). The neutral sugars in the different isozymes include galactose, arabinose, xylose, fucose and mannose. The amino sugars include mannosamine and galactosamine. The function or the mode of attachment of these sugars to the protein is as yet unknown. Separation of the carbohydrate and protein portions of the molecule was not achieved throughout normal separation procedures (Paul, 1963). Keilin and Hartree (1951) described properties of HRP in its alkaline and reduced forms as well as the compounds it forms with carbon monoxide, cyanide, azide, fluoride and hydrogen peroxide. They also concluded that a water molecule normally occupies the sixth co-ordination position of the Fe(III) ion of HRP.

The purification procedure of commercial samples of HRP is described in Appendix 3.

Reaction of HRP with Oxidizing Agents

HRP was first observed to form spectroscopically distinct compounds with hydrogen peroxide over 30 years ago (Keilin and Mann, 1937). When H_2O_2 is added to a dilute (10^{-5}M) solution of a highly purified HRP preparation the brown colour initially present gives way to a green colour.

Table 1.01

Amino Acid Composition of the HRP Isozymes^a

<u>Amino acid</u>	<u>Isozyme C</u> (gm residue/100 gm protein)	<u>Isozyme B</u>
lysine	1.8	1.8
histidine	1.0	1.1
arginine	8.2	8.5
aspartic acid	14.5	15.5
threonine	5.8	6.6
serine	4.7	5.0
glutamic acid	6.2	6.6
proline	4.0	4.2
glycine	2.2	2.5
alanine	4.0	4.4
half-cystine	0.9	1.0
isoleucine	3.6	3.7
leucine	10.1	10.9
tyrosine	2.0	1.8
phenylalanine	8.3	8.8

^a from Shannon et al. (1966)

Upon standing for several minutes or on adding a small amount of reducing agent such as p-cresol the green colour gives way to a red one. With an enzyme preparation that is less pure, the reducing agent present in the preparation (endogenous donor) causes the green compound to change immediately to the red one. When an excess of the reducing agent is added, the original brown colour of the solution is returned. The green compound that precedes the red one is known as horseradish peroxidase compound I and is abbreviated to HRP-I. HRP-I was first observed by Theorell (1941) who used HRP of reasonably high purity obtained by repeated fractional crystallization. The red compound following HRP-I formation is known as compound II or HRP-II. At higher hydrogen peroxide concentrations a bright red compound, HRP-III, is formed. Changes from HRP-I, HRP-II, and HRP-III to HRP are reversible as HRP can be reformed in the presence of an oxidizable substrate. Under conditions where HRP-III is present for a number of minutes the enzyme activity is reduced (Chance, 1952). At excessively high concentrations of hydrogen peroxide an irreversible change takes place with the formation of the emerald green compound IV, HRP-IV, (Chance, 1949a). Chance (1949b) showed that HRP-I precedes HRP-II and that HRP-II is formed only from HRP-I. George (1952, 1953a) titrated HRP-II with ferrocyanide and showed that HRP-II was converted to HRP by a one-electron reduction. Similarly Chance (1952b) showed that the conversion from HRP-I to HRP-II also involved

a one-electron reduction. Thus HRP-I retains the two oxidizing equivalents of hydrogen peroxide and HRP-II only one. Only HRP-I and HRP-II are thought to be enzymatically important intermediates in the peroxidatic oxidation of substrates. The relationship between each of these forms of the enzyme, illustrated with ferrocyanide as the substrate, are shown in Figure (1.01). The features of the absorption spectra of HRP, HRP-I, HRP-II, and HRP-III are listed in Table (1.02).

HRP-I may be formed from hydrogen peroxide, methyl hydrogen peroxide, and ethyl hydrogen peroxide (Chance, 1949b). The reaction of HRP and peroxide is first order in each of the reactants. For reaction (1.01) (Chance, 1963):



where R = HOOH, MeOOH, EtOOH

the second order rate constants for each of hydrogen peroxide, methyl hydrogen peroxide and ethyl hydrogen peroxide are: 9×10^6 , 1.5×10^6 , $3.6 \times 10^6 \text{ M}^{-1}\text{sec}^{-1}$. In addition to the three peroxides known to give rise to HRP-I and HRP-II, a number of strong oxidizing agents (HOCl , HOBr , NaClO_2 , ClO_2 , KBrO_3 , KIO_4 and O_3) cause similar reactions (George, 1953b).

Reaction with Reducing Agents

The HRP - hydrogen peroxide system is known to oxidize inorganic ions such as ferrous ion, ferrocyanide, chloroiridate, nitrite, and iodide (Paul, 1963) as well as numerous organic substrates including aniline, mesidine,

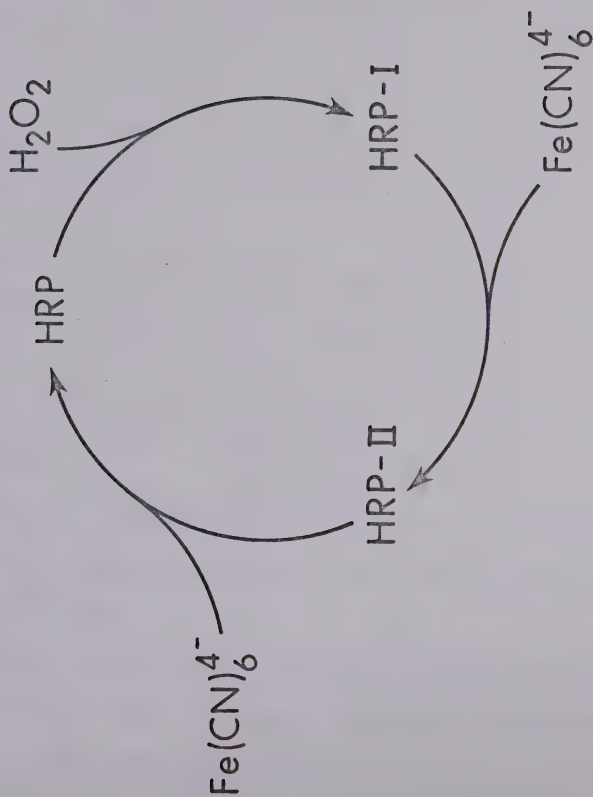


Figure 1.01: The relationship between HRP-I, HRP-II and HRP with ferrocyanide and hydrogen peroxide as substrates.

Table 1.02

Spectroscopic Features of HRP and its Hydrogen Peroxide
Compounds^{a,b,c}

HRP

λ_{\max}	403	497	530	580	641
ϵ_{mM}	91	10.0	7.5	2.5	2.8

HRP-I

λ_{\max}	410
ϵ_{mM}	48

HRP-II

λ_{\max}	418	527	558
ϵ_{mM}	95	8.5	8.5

HRP-III

λ_{\max}	416	546	583
ϵ_{mM}	106	10	8.5

^a With λ_{\max} the band position in $\text{m}\mu$ and ϵ_{mM} the millimolar absorptivities

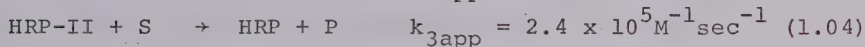
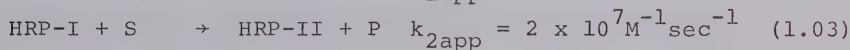
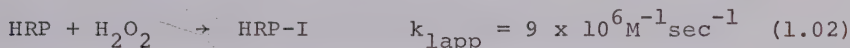
^b From Paul (1963) and Brill and Williams (1961).

^c In addition, the following isosbestic points exist between each of the compounds (Chance, 1963a):

<u>Compounds</u>	<u>Wavelength</u>
HRP-I - HRP-II	395 $\text{m}\mu$
HRP - HRP-II	410 $\text{m}\mu$
HRP - HRP-I	427 $\text{m}\mu$

p-cresol, and tyrosine (Saunders et al., 1964).

Chance (1963a) studied the kinetics of the reaction of HRP-I and HRP-II with a number of oxidizable substrates including p-aminobenzoic acid, nitrite, and ascorbic acid. In general the rate constant for the reaction of HRP-I with substrate is generally 40 to 100 times faster than for HRP-II. Thus the reaction of HRP-II with substrate is usually the overall rate determining step in the enzyme reaction. In the case of p-aminobenzoic acid acting as substrate, S, and giving product, P, the rate constants for the individual reactions determined by Chance (1963a) are:



The second order rate constants are subscripted as apparent rate constants as they may show considerable pH dependence.

A recent stopped-flow study of the hydrogen peroxide oxidation of luminol by HRP has indicated the second order apparent rate constants, $k_{2\text{app}}$ and $k_{3\text{app}}$, to be $2.3 \times 10^6 \text{M}^{-1}\text{sec}^{-1}$ and $7.2 \times 10^4 \text{M}^{-1}\text{sec}^{-1}$ (Cormier and Prichard, 1968) at pH 8.0.

Reaction of HRP with Ligands

HRP reacts with a variety of ligands including cyanide, fluoride, azide, hydrogen sulfide, nitric oxide, and hydroxide (Keilin and Hartree, 1951). The kinetics of ligand binding to HRP has been used as a probe to gain

information about proton ionizations at the active site of the enzyme (Dunford and Alberty, 1967; Ellis and Dunford, 1968).

Ionizable Groups at the Active Site of HRP

A number of studies have measured proton ionizations associated with the active site of HRP. Values of the acid dissociation constants are listed as pK 's in Table (1.03). The physical techniques used to measure these ionization constants include spectrophotometric, magnetometric, and potentiometric titration as well as kinetic methods. It is generally agreed that the pK values on HRP in the range 10.8 to 11.3 are associated with the formation of an hydroxide complex on the single iron atom of HRP (Ellis and Dunford, 1969). No general agreement exists as to the nature or even the presence of the other ionizations.

1.02 Hemin

The porphyrin ring system has unique chelating properties towards certain metal cations. The metalloporphyrins constitute the functional group of a wide range of biologically important compounds. Ferriprotoporphyrim IX or hemin, an iron(III) porphyrin, which is the prosthetic group of HRP, is shown in Figure (1.02).

Table 1.03

The pK Values Found on Various Species of HRP

Species	pK	T (°)	μ	Method
HRP ^a	4, 5.0	-	-	Spec
HRP ^b	10.91	20	not constant	Spec
HRP ^b	11.27	20	~0.06	Mag
HRP ^c	10.56	30	0.07-0.19	Pot
HRP ^d	11.0	25.0	0.11	Spec
HRP ^e	4.1, 6.4, 10.8	25.0	0.11	Kin-CN ⁻
HRP ^{e,f}	4.3, 6.1	25.0	0.11	Kin-F ⁻
HRP-CN ^e	6.7, 10.7	25.0	0.11	Kin-CN ⁻
HRP-F ^e	5.2	25.0	0.11	Kin-F ⁻
HRP-II ^g	3.4, 5.2, 8.6	25.0	0.11	Kin-Fe(CN) ₆ ⁴⁻
HRP-I ^g	5.3	25.0	0.11	Kin-Fe(CN) ₆ ⁴⁻

Spec: spectrophotometric equilibrium titration

Mag: magnetometric equilibrium titration

Pot: potentiometric equilibrium titration

Kin-CN⁻: kinetically, cyanide binding.

Kin-F⁻: kinetically, fluoride binding

Kin-Fe(CN)₆⁴⁻: kinetically, Fe(CN)₆⁴⁻ substrate

^a (Theorell and Paul, 1944); ^b (Theorell, 1942); ^c (Harbury, 1957);

^d (Ellis and Dunford, 1969); ^e (Ellis and Dunford, 1968);

^f (Dunford and Alberty, 1967); ^g see Chapter 3.



Figure 1.02: Ferriproteoporphyrin IX or Hemin.

Structure

The chelation of a metal ion by a porphyrin involves the displacement of two protons from the nitrogen atoms to form a structure that is almost square planar.

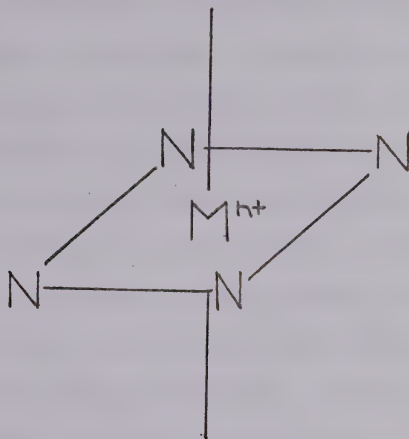


Figure 1.03: Placement of the Nitrogen Atoms About the Central Metal Ion.

The fifth and sixth co-ordination positions above and below the plane of the nitrogen atoms are available for further co-ordination to form octahedral or square pyramidal structures. The x-ray structural determination of chloro-hemin, the mono chloro derivative of ferriprotoporphyrin IX, has indicated that the compound is nearly square pyramidal with a 0.48 \AA out-of-plane displacement of the iron atom (Koenig, 1965). The Fe-Cl distance was found to be 2.22 \AA .

and the Fe-N distance 2.00 \AA . The x-ray structure of the bis(imidazole)- $\alpha, \beta, \gamma, \delta$ -tetraphenyl-porphinato iron(III) chloride has been determined (Countryman et al., 1969) and the environment of the iron atom is more nearly octahedral than the chlorohemin compound with only a slight (0.009 \AA) out-of-plane displacement. Magnetic susceptibility measurements of chlorohemin (Pauling and Coryell, 1936) and aquohydroxyferriproto-porphyrin IX (Coryell et al., 1937) have indicated that these compounds are mainly present in their high spin state. A number of other solid hemins with ligands such as bromide, formate, acetate, azide and propionate are also high spin (Rawlinson and Scutt, 1952). The solid bis(cyanide) and the bis(imidazole) hemins are low spin complexes (Countryman et al., 1969).

Hemin as the Prosthetic Group of Heme Proteins

The ferric and ferro protoporphyrin IX's are found in a number of heme proteins (Falk, 1964) and among these are the hemoglobins, myoglobins, peroxidases, catalases, and cytochrome b's. Hemoglobin and myoglobin reversibly complex molecular oxygen. Peroxidase and catalase oxidize a variety of substrates with hydrogen peroxide. The function of the cytochromes involves oxidation and reduction in the electron transport chain. When the metalloporphyrin is a functional group in a protein it undergoes

co-ordination with some amino acid residue of the protein and the solvent. In ferrimyoglobin (metmyoglobin) the fifth and sixth co-ordination positions are occupied by an imidazole nitrogen of a histidine residue and a water molecule (Nobbs et al., 1966). In ferrous myoglobin the water molecule is absent.

Properties of Hemin in Solution

Hemin, when dissolved in an alkaline solution, is known to form dimers and polymers (Clark and Perkins, 1940; Cowgill and Clark, 1952; Davies, 1952; Inada and Shibata, 1962; Maehly and Akeson, 1958; Jordan and Bednarski, 1964). When the pH is lowered in aqueous solution the first change is protonation of an hydroxide ligand which is 50% complete at pH 6.7 (Shack and Clark, 1947). It is postulated that this conversion is from the dimeric diaquo species to the dimeric hydroxyaquo species. The formation of the dimer is known to be inhibited by large concentrations of ethanol (Davies, 1940; Maehly and Akeson, 1958; Vestling, 1940), ethylene glycol (Smith, 1957), pyridine (Phillips, 1960) and dimethyl formamide (Scheler, 1960). Aqueous detergent solutions are also known to favour formation of the monomers (Dempsey et al., 1961).

Equilibria of Ligand Substitution on Hemin

A great deal of data on the binding of ligands to hemin in a variety of solvents and solvent mixtures has been published. Studies of the systems most relevant to the imidazole binding study are reviewed here briefly.

Shack and Clark (1947) have studied the reaction of cyanide, pyridine and the acid ionization of the dimeric hemin in aqueous solution. Both cyanide and pyridine cause the dimer to break up to form the monomeric disubstituted complexes. The equilibrium is of the type:



where M_2 is the dimer, M the monomer, and L the cyanide or pyridine ligands. Cowgill and Clark (1952) studied a series of substituted imidazoles in co-ordination with iron (III) mesoporphyrin and found a rough relationship between the acid dissociation constants of the imidazoles and their equilibrium binding constants. Scheler (1960) studied the binding of imidazole, cyanate, azide, fluoride, and formate to hemin in dimethyl formamide-water solution and found that for formate, fluoride, cyanate, and azide the equilibrium was of the type:



and for imidazole and cyanide of the type:



Gallagher and Elliott (1965) studied the titration of hemin with pyridine over a wide range of pyridine concentrations and obtained evidence for the break up of the dimer to form the monomeric pyridine substituted compound. A similar effect was noted with caffeine and imidazole (Gallagher and Elliott, 1967; 1968) in which they proposed that the dimer was formed by hydrophobic interaction between the two planar aromatic rings of the porphyrins leaving all four co-ordination positions of the dimer open to the solvent. A spectral study of a histidine and a histidine-glutamic acid copolymer complex with hemin indicated that at pH 6.2 one co-ordination position of the hemin was occupied by the imidazole of a histidine residue and the other by a water molecule or a glutamic acid residue. On raising the pH to 7.2 a dihistidine type spectrum was observed. The binding of a lysine polymer with hemin gave a compound that was spectrally analogous with ferricytochrome c (Blauer and Ehrenberg, 1963). Imidazole, pyridine, and glycine binding to the ferriheme, peptide of cytochrome c indicated the ionization of an iron co-ordinated imidazole with a pK of 11.1 (Harbury and Loach, 1960).

Kinetic Studies of Ligand Binding to Hemin

The binding of imidazole to hemin in an ethanol-water solvent is described in detail in Chapter 4.

(Hasinoff et al., 1969; Angerman et al., 1969). Gallagher and Elliott (1968) followed the break up of the hemin dimer to form bisimidazole hemin monomer by means of a stopped flow apparatus. Fleisher et al., (1968) studied cyanide binding to iron(III) hematoporphyrin in alkaline aqueous media. A discussion of these results is included in Section 4.04.

1.03 Study of Fast Reactions

Introduction

The flow technique for the rapid mixing of two reactant solutions was first developed by Hartridge and Roughton (1923). In the stopped flow method two reactant solutions are mixed rapidly (~ 1 msec.) and which then flow down to an observation chamber for spectrophotometric study. The flow is then stopped suddenly and the reaction may be followed spectrophotometrically for several milliseconds after mixing. Both Chance (1963b) and Gibson (1954) were instrumental in bringing about technological improvements that reduced the mixing time to about 1 msec and greatly increased the ease of operation and the economy of mixing the reactants. A description of a stopped-flow apparatus built in this laboratory is described in Chapter 2. The relaxation techniques described below, also have greatly extended the time range for measuring chemical reactions in

solution and these include: temperature-jump, electric field jump, pressure-jump, and ultrasonic absorption.

These techniques were developed and refined by Eigen and are reviewed thoroughly by Eigen and de Maeyer (1953). The minimum measurable reaction half-times, $t_{1/2}$, for the various flow and relaxation, as well as magnetic spin resonance techniques are compared in Table (1.04).

Relaxation Methods

When a reaction mixture is at equilibrium and some external parameter that determines the equilibrium conditions is changed, the reactants "relax" to the new equilibrium with a characteristic relaxation time. The external parameter may be temperature, pressure, or electric field. The relaxation time, τ , that characterizes the relaxation to equilibrium is a function of the rate constants in the reaction under study. The method can be best illustrated by deriving a relaxation time for a simple chemical reaction:



for which the differential rate law is:

$$-\frac{d[C]}{dt} = k_{-1}[C] - k_1[A][B] \quad (1.09)$$

Consider that upon a stepwise perturbation of some external parameter the concentrations change by the small amount

Table 1.04

Comparison of Various Kinetic Methods Giving

Minimum Reaction Half-times of $t_{\frac{1}{2}}^a$

<u>Method</u>	<u>$t_{\frac{1}{2}}$</u> (sec)
Flow	
Continuous flow	10^{-3}
Stopped-flow	10^{-3}
Accelerated flow	10^{-3}
Relaxation	
Temperature-jump	10^{-6}
Pressure-jump	10^{-4}
Electric field jump	10^{-7}
Ultrasonic absorption	10^{-9}
Magnetic spin resonance	
N.M.R.	10^{-4}
E.S.R.	10^{-10}

^a from Caldin (1964a)

$\Delta[A]$, $\Delta[B]$, and $\Delta[C]$ and

$$[A] = [\bar{A}] + \Delta[A] \quad (1.10)$$

$$[B] = [\bar{B}] + \Delta[B] \quad (1.11)$$

$$[C] = [\bar{C}] + \Delta[C] \quad (1.12)$$

where the bars represent equilibrium concentrations. From the stoichiometry of the reaction it is also known that:

$$\Delta[C] = -\Delta[A] = -\Delta[B] \quad (1.13)$$

Substituting equation (1.10-1.12) in equation (1.09)

$$\begin{aligned} -\frac{d\Delta[C]}{dt} &= \{k_1([\bar{A}] + [\bar{B}]) + k_{-1}\} \Delta[C] \\ &\quad - k_1[\bar{A}][\bar{B}] + k_{-1}[\bar{C}] - k_1(\Delta[C])^2 \end{aligned} \quad (1.14)$$

At equilibrium:

$$\frac{d[C]}{dt} = 0 \quad (1.15)$$

and from equation (1.09)

$$k_{-1}[\bar{C}] - k_1[\bar{A}][\bar{B}] = 0 \quad (1.16)$$

Also as the term $-k_1(\Delta[C])^2$ is small it can be dropped from equation (1.14) and along with equation (1.16) the result is:

$$-\frac{d\Delta[C]}{dt} = (k_1([\bar{A}] + [\bar{B}]) + k_{-1}) \Delta[C] \quad (1.17)$$

Integration of equation (1.17) gives:

$$\Delta[C] = \Delta[C]_0 e^{-t/\tau} \quad (1.18)$$

where $\Delta[C]_0$ is the concentration change at time zero. The reciprocal relaxation time is given by:

$$(\tau)^{-1} = k_1([\bar{A}] + [\bar{B}]) + k_{-1} \quad (1.19)$$

Thus it can be seen that the reversible second order-first order reaction (1.08) is described by a simple first order process. Measurement of τ at different concentrations of $([\bar{A}] + [\bar{B}])$ allows the determination of the two rate constants k_1 and k_{-1} .

Temperature-jump Method

In the temperature-jump method, the temperature of a reaction system at equilibrium is increased rapidly, and the rate of relaxation to the new equilibrium is followed. The change in equilibrium depends upon the thermodynamic equation:

$$\frac{d \ln K}{dT} = \frac{\Delta H}{RT^2} \quad (1.20)$$

If ΔH for the reaction under study is zero, its equilibrium will not be changed by an increase in temperature. In the temperature-jump apparatus, built in this laboratory, and described by Hasinoff et al., (1969) and Ellis (1968) as well as in Chapter 4, a voltage discharge of 20 kV was sufficient to raise the temperature of 1 ml of solution approximately 6°. The apparatus is described schematically in Figure (1.04). The energy used in heating is equal to $\frac{1}{2}CV^2$, where C is the capacitance of the high voltage

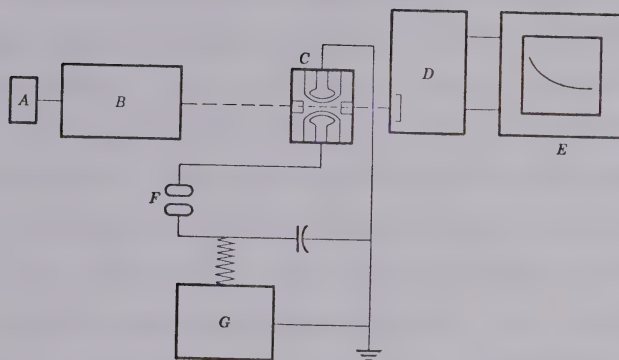


Figure 1.04: Schematic of Temperature-jump Apparatus

- A: Light source
- B: Monochromator
- C: Temperature-jump cell
- D: Photo multiplier
- E: Oscilloscope
- F: Spark gap
- G: High Voltage power supply

capacitor and V is the voltage to which the capacitor is charged, if losses in energy due to the inductance of the apparatus are negligible. It can also be shown that the temperature rise in the solution is determined by the total resistance and capacitance in the discharge circuit and that the relaxation time of the heating time constant for the heating of the solution in the cell is given by $RC/2$ (Amdur and Hammes, 1966). The heating time constant for the apparatus in this laboratory has been calculated to be about 5 μsec (Ellis, 1968). Thus reactions occurring in times much larger than 5 μsec are considered to undergo an instantaneous temperature perturbation. The resistance, R , and hence the heating time constant is kept low by the addition of an inert electrolyte such as KNO_3 to the reaction mixture.

Study of Fast Reactions in Biological Systems

Both flow and relaxation techniques have been applied successfully to the study of biological systems. These techniques are well suited to the study of enzyme reactions as these reactions are often extremely rapid. The application of flow techniques to biological systems has been thoroughly reviewed by Chance (1963a) and Roughton (1963). Hammes (1968a) has recently reviewed the application of relaxation techniques to biological systems and Eigen and Hammes (1963) have reviewed the study of elementary steps in enzyme mechanisms.

CHAPTER 2

Design Improvements to the Stopped-Flow Apparatus

A stopped-flow apparatus was constructed that offered a number of improvements over a stopped-flow apparatus in previous use in this laboratory (Ellis, 1968).

2.01 Design Considerations

The optical efficiency of the stopped-flow apparatus was greatly increased by a more efficient light collecting lens system. A conical quartz lens (Esco products, optical Al quartz lens, 1/2" OD x 3/4" long with a focal length of 1") was placed at the entrance port of the observation chamber and likewise an identical lens was placed at the exit port. Light incident on the entrance lens from the monochromator projected an image of the monochromator slit on the active surface of the photomultiplier. With this arrangement very little of the light emanating from the monochromator was lost.

Cavitation occurs in a rapidly flowing fluid when there is a local pressure drop across an orifice or sharp edge causing the liquid to vaporize (Chance, 1964). Dissolved air in the solution may diffuse into the cavity in the fluid, forming small bubbles that persist and interfere with the spectrophotometric observation of the solution. Cavitation may be eliminated or minimized by:

- (i) designing a mixing and observation chamber that avoids

sharp edges, turns, and has orifices decreasing in cross sectional area as the fluid flows downstream.

(ii) applying a back pressure to the fluid so that the drop in pressure never falls below the pressure required for cavitation (Chance, 1964).

(iii) degassing the solution so that bubbles do not form as a result of cavitation.

The mixing and observation chambers in this apparatus were designed to eliminate cavitation by (i). The performance of the apparatus was such that neither conditions (ii) nor (iii) were necessary for successful operation of the stopped-flow apparatus. The channels in the mixing block were designed such that when going downstream at any turn or orifice a decrease in cross sectional area occurs which increases the pressure at these points and prevents cavitation. Also, where possible, the angles at which turns occurred were made obtuse. This has the effect of decreasing the cross sectional area at the turn to a minimum. The previous stopped-flow apparatus did not incorporate these features and was subject to cavitation.

If efficient mixing is to occur in a stopped-flow apparatus the velocity of the fluids mixing must be above a certain critical value such that the flow is turbulent and eddying occurs. This critical velocity, u_c , in cm/sec, has been found empirically to relate to the diameter of the tube through which the liquid is flowing, d in cm, and the density, ρ in gm/cm^3 and the viscosity, η in poise, of the

liquid by the equation:

$$u_c = \frac{N_R \eta}{\rho d} \quad (2.01)$$

where N_R is the Reynolds' number, a unitless number equal to about 2000 (Caldin, 1964b). In the observation chamber, which is a tube 0.2 cm in diameter, it can be calculated that u_c has a value of 100 cm/sec. The experimentally measured value of the flow velocity in the observation chamber was 310 cm/sec as discussed in Section 2.02. This value is much larger than that calculated for u_c from equation (2.01) so it can be assumed that the mixing in this apparatus is aided by the attainment of turbulent flow conditions.

The mixing chamber of the stopped-flow apparatus is similar in principle to that constructed by Ellis (1968). In effect, mixing is accomplished by a 12 jet mixer. The mixing process can best be described by referring to the diagram of the mixing chamber in Figure (2.01). Each of the channels leading from the driving syringes split the stream of liquid into four separate streams by the "splitter". Each of the four newly created streams from the splitter are recombined at the extremities of the mixer creating 8 of the 12 jets bringing the number of streams down to 4. These four streams are again joined in the central portion of the mixer giving an effective total of 12 jets for the whole mixer assembly. From the central portion of the mixer the single recombined stream leads to the observation chamber.

Flow apparatuses constructed by other workers have anywhere from 2 (Strittmatter, 1964) to 18 jets (Chance, 1964b). The previous model of the stopped-flow apparatus was driven by pushing the thumb on a plunger against the driving syringes. It was found that upon pushing the plunger the whole apparatus would move slightly out of the light path causing an erroneous voltage reading on the oscilloscope. Also it was not possible to obtain reproducible driving times, and dead times when operating the stopped-flow manually. When studying very fast reactions it is important to have reproducible driving times.

To drive the syringes containing the reactant solutions, a pneumatically operated piston device was constructed and this is shown in Figure (2.02). The laboratory compressed air line in series with a reducing valve and gauge, set at 15 p.s.i., provided adequate force on the driving syringes. The mixing block and driving platform are joined only by flexible Teflon tubing and hence vibrations or movements in the driving platform are not transferred to the optical path of the mixing block.

The temperature of the apparatus was thermostatically controlled by a number of water jackets and baffles. Thermostatic control of the mixing block is provided for by the copper water jackets I and J in Figure (2.01) which are bolted onto the mixing block. The driving syringes are kept at a constant temperature by their individual water jackets completely surrounding the syringes and labelled

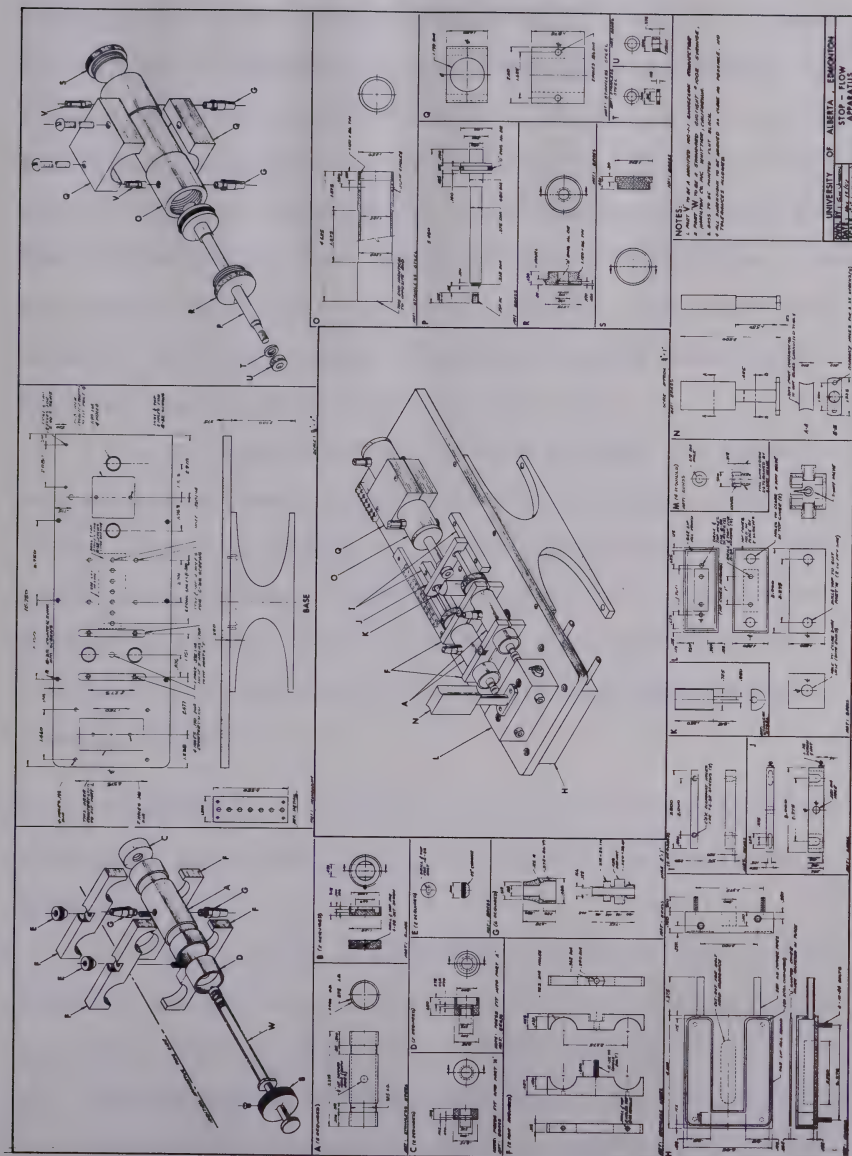


Figure 2.02: Design Details of the Stopped-Flow Apparatus.

parts B to D in Figure (2.02). The area directly under the 3-way valve (3LL3 Hamilton Syringe Co.), part L in Figure (2.02) has its temperature thermostatically controlled by a large copper water jacket, part H, bolted to the driving platform. In addition, a large copper helical coil containing rapidly flowing water thermostatically controls the temperature of the space where the Teflon tubing runs from the driving platform to the mixing block. Glass wool and aluminum foil were placed around the coil to ensure that this gap was filled by dead air space only.

The apparatus was designed so that the cooling jackets holding the Hamilton gas tight syringes (2.5 ml, 1002LL, Hamilton Syringe Co.) were interchangeable. Thus syringes of different sizes may be inserted in different syringe jackets so that the stopped flow apparatus can function for relaxation concentration-jump experiments. (Hammes, 1968).

2.02 Measurement and Calculation of the Instrumental Parameters Describing the Performance of the Stopped-Flow Apparatus

A number of instrumental parameters are used to describe the performance characteristics of a stopped-flow apparatus (Czerlinski, 1966b). Among them are:

(i) Mixing time -- the time required to mix two solutions in a stopped-flow apparatus, which is approximately 1 msec if the critical velocity for turbulent flow has been

exceeded (Caldin, 1964c).

- (ii) Driving time -- the time elapsed to drive the syringe plungers from stop to stop. This was measured from a triggered oscilloscope trace to be 55 msec.
- (iii) Volume flow rate -- the rate of volume flow in ml/sec past any given point. It is calculated by dividing the volume of solution used in each experiment by the drive time.

$$\begin{aligned} \text{volume flow rate} &= \text{ml ejected} / \text{drive time} \\ &= 0.53 \text{ ml} / 5.5 \times 10^{-2} \text{ sec} = 9.6 \text{ ml/sec} \quad (2.02) \end{aligned}$$

- (iv) Flow velocity -- the linear velocity in the direction of flow of the fluid at any given point and is in units of cm/sec. It is calculated by dividing the volume flow rate by the cross sectional area of the channel. In the observation chamber the flow velocity is:

$$\begin{aligned} \text{flow velocity} &= \text{volume flow rate} / \text{cross section area} \\ &= (9.6 \text{ cm}^3/\text{sec}) / 0.0314 \text{ cm}^2 = 3.1 \times 10^2 \text{ cm/sec} \quad (2.03) \end{aligned}$$

- (v) Completeness of expelling old solution -- the number of times that the observation chamber is swept out by fresh solution for each experiment. It is calculated by dividing the number of ml used per experiment by the volume of the observation chamber

$$\begin{aligned} \text{completeness of expelling old solution} &= \\ 0.53 \text{ ml} / 0.0314 \text{ ml} &= 17 \text{ times} \quad (2.04) \end{aligned}$$

- (vi) Dead time -- the time elapsed for solution to flow from the mixing chamber to the observation chamber. Because

of the dead time of the stopped flow apparatus the observed zero time of the reaction differs from the real zero time by an amount equal to the dead time. As it is not known exactly where the reactants mix completely as they flow through the mixing chamber, or as there is no one single point at which this happens, the dead time cannot be defined with a large degree of certainty. However, it can be calculated approximately, by dividing the distance the solution travels from the point where the reactants first come in contact in the mixing chamber to a point one half the distance along the observation chamber by the flow velocity in the observation chamber:

$$\begin{aligned} \text{dead time} &= \text{distance} / \text{flow velocity} = \\ 1.6 \text{ cm} / (3.1 \times 10^2 \text{ cm/sec}) &= 5.2 \times 10^{-3} \text{ sec} \quad (2.05) \end{aligned}$$

There is, additionally, an experimental method for measuring the dead time of the stopped-flow apparatus and this is described next. Ferricyanide is reduced by ascorbic acid and the reaction is well defined. It is first order in each of ferricyanide and ascorbic acid. In addition the molar absorptivity of ferricyanide is much larger than that of ferrocyanide (Birk, 1969) and both ascorbic acid and its oxidation products are colorless compared to the absorbance due to ferricyanide. The experimental procedure for measuring the dead time involves studying the reaction at a constant concentration of ferricyanide but at different concentrations of ascorbic acid so that the pseudo first

order rate constant for the reaction is changed. Suitable reactant solutions were prepared by dissolving 7.4 mg of $K_4Fe(CN)_6$ in 250 ml of water and 1 gm of ascorbic acid titrated to approximately pH 9.2 in 100 ml of water. Each of the reactant solutions were placed in the reservoir syringes and the reaction was studied at these initial concentrations. The pseudo first order rate constant is changed by successively diluting the ascorbic acid solution in the reservoir syringe by about one half each time for three or four experiments.

As explained previously the point at which the flow has stopped does not mark the zero time for the reaction but differs from the true elapsed time for the reaction by the amount of the dead time. But each of these reactions studied at different concentrations of ascorbic acid must have had the same initial concentration and hence the same absorbance. Thus when a semilogarithmic plot of photo-multiplier voltage change, (which is proportional to absorbance and hence concentration at absorbances less than 0.02 absorbance units) vs. time is made the common intersection of all the straight lines must be at a point equal to the true start of the reaction or the dead time behind the apparent zero time of the reaction. The plots are shown in Figure (2.03) and the dead time was determined to be 5 msec from their intersection. The dead time calculated from the flow velocity was 5.2 msec., equation (2.05), and is thus in good agreement with that found experimentally.

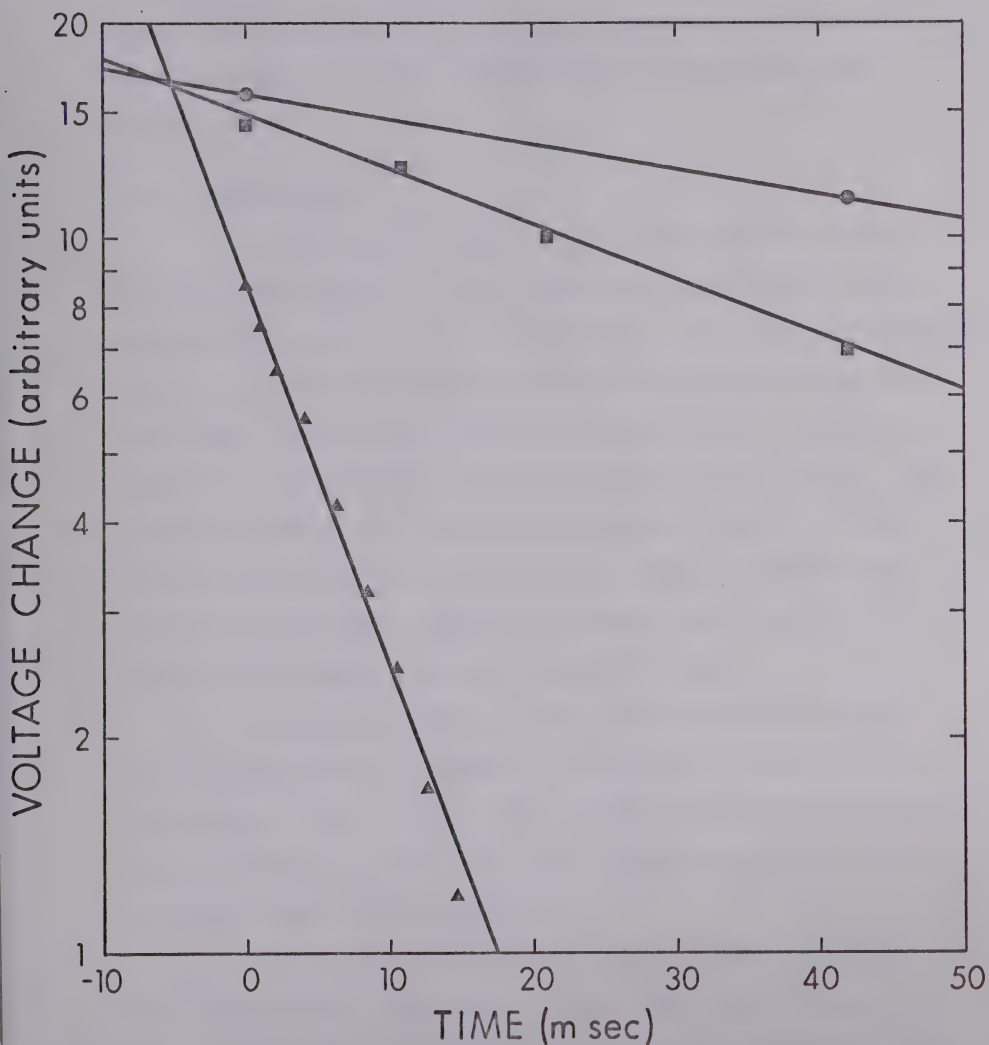


Figure 2.03: Semilogarithmic plot of voltage vs. time for the reaction of ferricyanide and ascorbic acid. The dead time, determined from the common intersection of the straight lines, is 5 msec.

The addition of the pneumatic drive to the stopped-flow apparatus resulted in a two-fold improvement in dead time over the previous model constructed in this laboratory (Ellis, 1968).

2.03 Construction

Plexiglas was used for the construction of the mixing block because it is transparent, reasonably inert, and is fairly easy to work and machine. The only materials that the reactant solutions come in contact with are glass (syringes), Teflon (syringes, tubing, valves), stainless steel (tubing adapters) and Plexiglas (mixing block). The sectional method of construction (parts A to F in Figure (2.01)) was chosen since it offered ease of construction as well as a convenient method of cleaning the mixing and observation chambers after a period of use.

To prevent stray light from travelling through the mixing block, one surface of part D of Figure (2.01) was painted black. Tests with solutions of very high optical absorbance in the light path indicated that the amount of stray light was negligible.

Previous models of temperature-jump cells and of a stopped flow apparatus (Ellis, 1968) with quartz lenses were found to leak solution at the interface of the lens and the Plexiglas whether they were glued with epoxy cement or a mixture of Plexiglas and solvent. The problem was particularly severe after the apparatus had been in use

for several months. The problem was remedied satisfactorily on the design of the stopped flow apparatus described here by employing a press fit of the quartz conical lenses. Parts A and F in Figure (2.01) contain a rubber gasket that evenly distributes pressure on the lens ensuring a tight fit onto the ends of the observation tube.

CHAPTER 3

The Kinetics of the Oxidation of Ferrocyanide by
Horseradish Peroxidase Compounds I and II

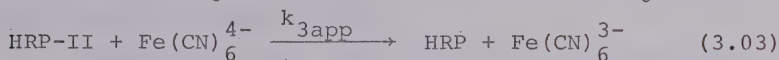
3.01 Introduction

Horseradish peroxidase (EC 1.11.1.7; donor: H_2O_2 oxidoreductase) was first observed to form a spectroscopically distinct compound, HRP-II¹, with H_2O_2 over 30

¹ Abbreviations used: HRP: horseradish peroxidase; HRP-I, HRP-II, HRP-III, HRP-CN, HRP-F: compounds I, II and III, cyanide and fluoride complexes of HRP; R.Z.: purity number; P-II, HP-II, $\text{H}_2\text{P-II}$, $\text{H}_3\text{P-II}$: states of ionization of HRP-II; P-I, HP-I: states of ionization of HRP-I; ferrocyanide: hexacyanoferrate(II) without regard to state of protonation; ferricyanide: hexacyanoferrate (III); K_A , K_B : the acid dissociation constants of $\text{HFe}(\text{CN})_6^{3-}$ and $\text{H}_2\text{Fe}(\text{CN})_6^{2-}$; K_1 , K_2 , etc: successive acid dissociation constants either on HRP-I or HRP-II as indicated; $k_{2\text{obs}}$ and $k_{3\text{obs}}$: pseudo first-order rate constants for the reactions of HRP-I and HRP-II with ferrocyanide; $k_{2\text{app}}$, $k_{3\text{app}}$: apparent second order rate constants of the reactions of HRP-I and HRP-II with ferrocyanide; k_1 , k_2 , etc: second order rate constants; v : initial reaction velocity; $[]$, $[]_0$: molar concentration and initial molar concentration without regard to state of protonation; V_t , V_∞ , A_t , A_∞ : voltage and absorbance at time t and time infinity: ΔV , ΔA : $|V_t - V_\infty|$ and $|A_t - A_\infty|$; $t_{1/2}$, reaction half time; μ , ionic strength.

years ago (Keilin and Mann, 1937). Theorell (1942) identified another compound, HRP-I, which was formed prior to HRP-II when HRP was treated with H_2O_2 .

The generally accepted reaction sequences and stoichiometries for the reaction of HRP and hydrogen peroxide with a substrate such as ferrocyanide are:



(George, 1952, 1953a; Chance, 1952c). Thus HRP-I contains two oxidizing equivalents more than HRP, and HRP-II contains one more equivalent than HRP. No particular states of ionization of the reactants are implied. The rate constants are labelled apparent rate constants, as $k_{2\text{app}}$ and $k_{3\text{app}}$, at least, show a marked dependence on pH. Ferrocyanide was chosen as a substrate because it undergoes a simple one-electron oxidation to ferricyanide without the production of free radical intermediates. A recent study on the HRP catalyzed oxidation of luminol by H_2O_2 at pH 8.0 has shown that the free radicals produced from the substrate are oxidized at kinetically comparable rates by HRP-I (Cormier and Prichard, 1968). Even though ferrocyanide is probably not a substrate of physiological significance for HRP, the analysis of the pH dependence of the $k_{2\text{app}}$ and $k_{3\text{app}}$ data can reveal information about ionizations at the active site of HRP-I and HRP-II.

Previous reports have indicated both that the action of HRP and H_2O_2 on substrates is pH dependent (Getchell and Walton, 1931; Balls and Hale, 1934; Wilder, 1962) and pH independent (Chance, 1952d). A previous kinetic study of the binding of fluoride and cyanide ligands to HRP indicated the presence of ionizable groups at the active site (Dunford and Alberty, 1967; Ellis and Dunford, 1968). A complete listing of the $\text{pK}'\text{s}$ of ionizable groups found on HRP are listed in Table (1.03).

This study shows that the kinetics of both the reactions of HRP-I and HRP-II with ferrocyanide show considerable pH dependence ($k_{2\text{app}}$ changes by a factor of 70 and $k_{3\text{app}}$ by a factor of over 50,000 over the pH ranges the reactions were studied) from which information has been deduced about kinetically significant ionizations at the active site of the two enzyme intermediates.

3.02 Experimental

Materials

Purified, lyophilized HRP, obtained from Boehringer-Mannheim was further purified by elution from a Sephadex C-50 (CM) column. The procedure is described in Appendix 3. The R.Z. of the HRP samples used, measured by taking the ratio of absorbance at 403 $\text{m}\mu$ and 280 $\text{m}\mu$, varied from 2.6 to 2.9. An R.Z. of about 3.0 is generally taken to indicate a highly purified sample of HRP. The concentration of HRP was determined spectrophotometrically

at 403 m μ using a molar absorptivity of $9.1 \times 10^4 \text{ M}^{-1} \text{ cm}^{-1}$ (Keilin and Hartree, 1951).

Doubly distilled water was used in the preparation of all solutions. The ionic strength of all reaction mixtures was kept constant at 0.11 with 0.01 contributed by the buffer and the remainder by KNO_3 and ferrocyanide. The solutions of ferrocyanide were prepared less than one hour before use from Baker reagent grade $\text{K}_4\text{Fe}(\text{CN})_6 \cdot 3\text{H}_2\text{O}$ under diffuse lighting and were protected from light during storage and use. This precaution was taken to prevent either thermal or photodissociation. The molar absorptivity of ferricyanide was measured to be $1060 \text{ M}^{-1} \text{ cm}^{-1}$ at 420 m μ in agreement with the published value of $1050 \text{ M}^{-1} \text{ cm}^{-1}$ (Birk, 1969). The molar absorptivity of ferrocyanide at 420 m μ is much less ($\sim 5 \text{ M}^{-1} \text{ cm}^{-1}$) than that of ferricyanide and can be neglected (Birk, 1969).

The concentrations of the H_2O_2 solutions were analyzed spectrophotometrically by an adaptation of methods used by Ovenston and Rees (1950) and Ramette and Sandford (1965). Five ml of freshly prepared 0.2 M KI solution, 0.1 ml of 0.5% ammonium molybdate and up to 4 ml of stock H_2O_2 solution were placed in a 10 ml volumetric flask and made up to the mark. The molybdate catalyzes the oxidation of 2I^- to I_2 by H_2O_2 which then reacts to form an equilibrium mixture of I_3^- . A blank solution was also made up in the same way as the sample solution but omitting the H_2O_2 . The blank solution is necessary

because of small amounts of oxidizing agents present in the water that interfere with the determination. The absorbance measurements were made against the blank at 353 mμ using an apparent molar absorptivity of $25,900 \text{ M}^{-1} \text{ cm}^{-1}$ for the I_3^- present in solution. Concentrations of stock H_2O_2 solutions of about $5 \times 10^{-5} \text{ M}$ can be measured quite accurately with this procedure.

Stopped-Flow Kinetic Experiments

Kinetic measurements were made on a pneumatically driven stopped-flow apparatus which is described in detail in Chapter 2. The driving syringes and reaction chambers were kept constant at 25.0° . The lamp source and power supply as well as the spectrophotometric detection system have been described elsewhere (Ellis and Dunford, 1968). The reactions were followed spectrophotometrically at 425 mμ. The total absorbance change was kept small ($\Delta A < 0.02$) so that the relative voltage changes observed on the oscilloscope, ΔV , were proportional to ΔA .

The buffer solution was not mixed with HRP prior to the commencement of the reaction in the stopped-flow apparatus to ensure that the HRP did not decompose at either high or low pH. The rate of the reaction under study was always much faster than the rate of decomposition of HRP at these pH extremes (Maehly, 1953).

Steady State Kinetic Measurements

Steady state kinetic measurements were conducted spectrophotometrically on a Cary 14 Recording Spectrophotometer equipped with a slide wire for the absorbance range 0 to 0.1. The cell compartments were kept at a constant temperature of 25.0°. The reaction was followed by measuring the increase in absorbance at 420 m μ due to the production of ferricyanide. Ferrocyanide, HRP, H₂O₂, and sufficient water equal to a constant total volume of 0.08 ml were added with Hamilton microliter syringes to a cuvette containing 2.00 ml of a buffer - KNO₃ solution. The final addition, which initiated the reaction, was made by stirring the solution with a glass rod on which microliter amounts of H₂O₂ solution had been deposited. The initial velocity, v , was computed at an extrapolated zero time by measuring the slope of the absorbance - time trace. Blank reaction rate runs were conducted without HRP present and in no case was a significant reaction rate measured for the uncatalyzed H₂O₂-ferrocyanide reaction.

3.03 Results

Neither ferrocyanide nor ferricyanide in solution with HRP were observed to change the absorption spectrum of HRP at least over a period of one hour. This experiment indicates that no spectroscopically detectable complex is formed between either of these compounds and HRP. It also indicates that dissociation of cyanide is not occurring

from either ferrocyanide or ferricyanide. The buffer solutions were chosen so that their effective pH ranges overlapped. From the continuous nature of the rate data as a function of pH it was concluded that there were no anomalous effects caused by buffers.

The ionization constants K_A and K_B of HFe(CN)_6^{3-} and $\text{H}_2\text{Fe(CN)}_6^{2-}$ were obtained by interpolation of data from an ionic strength study (Jordan and Ewing, 1962). The value of K_A and K_B at an ionic strength of 0.11 and 25.0° is 7.24×10^{-4} M and 6.0×10^{-2} M respectively. The other ionization constants for $\text{H}_4\text{Fe(CN)}_6$ are larger than 0.1 M.

Kinetics of the HRP-II - Ferrocyanide Reaction

It was found experimentally that HRP-II could be prepared by adding 1.1 molar equivalents of H_2O_2 and 0.5 molar equivalents of p-cresol to a 10^{-6} M solution of HRP. About 70% HRP-II and 30% HRP were formed initially as measured from their molar absorptivities (George, 1953c). The function of the p-cresol is to reduce preferentially the more reactive HRP-I to HRP-II. The HRP-II was converted directly to HRP over a period of minutes as shown by the return of the original HRP spectrum in Figure (3.01). An isosbestic point at 411 m μ was maintained, indicating the presence of only two absorbing species, HRP and HRP-II (Chance, 1963a). The original HRP spectrum was obtained when the reaction was allowed to go

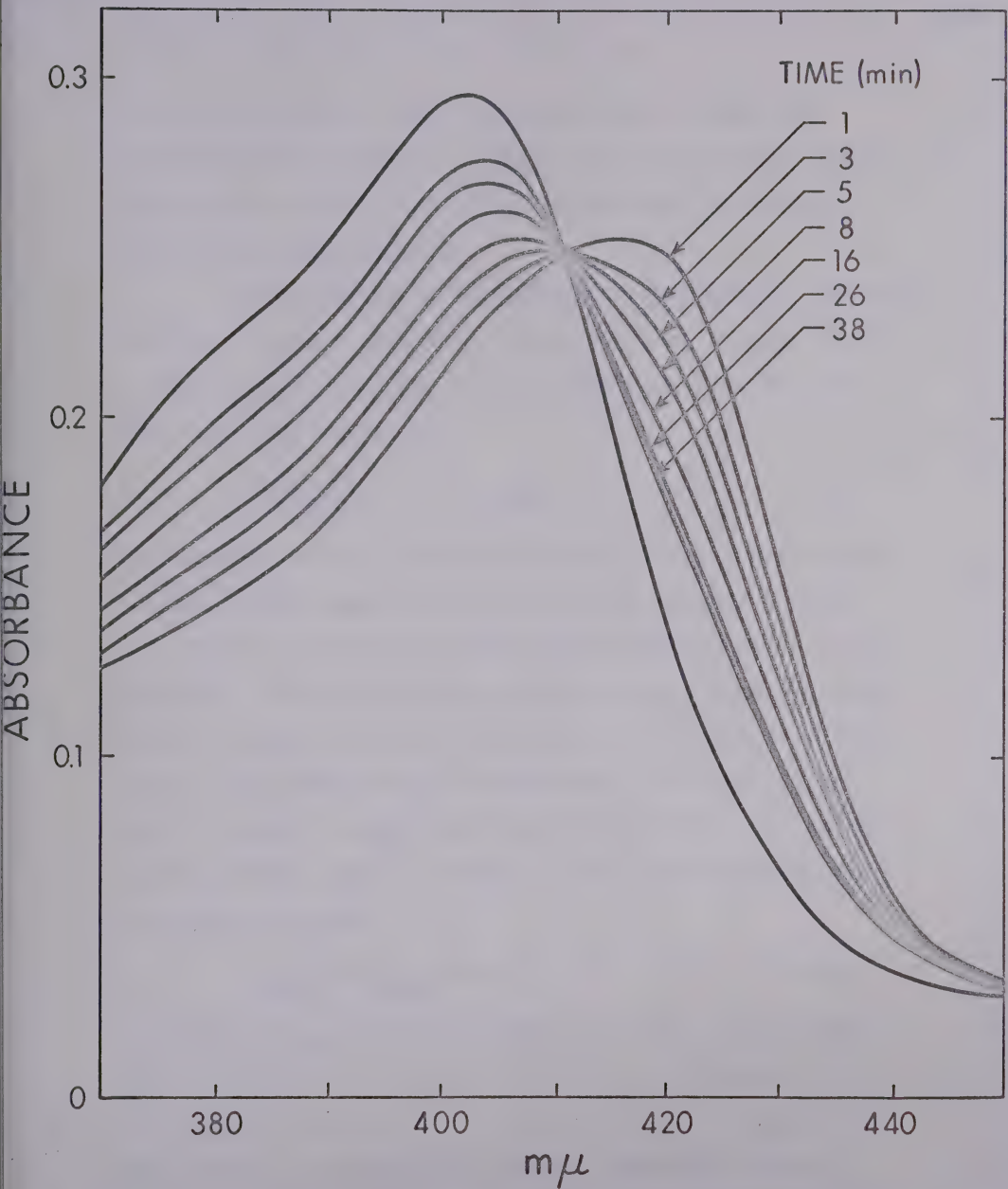


Figure 3.01: Plot of absorbance vs. wavelength at the times indicated showing the conversion of HRP-II to HRP. The isosbestic point at 411 mμ indicated the presence of only two absorbing species, HRP and HRP-II.

to completion over a long period of time or upon the addition of ferrocyanide. Sufficient quantities of HRP-II were present up to 0.5 hr after preparation to study the oxidation of ferrocyanide.

The kinetics of the HRP-II - ferrocyanide reaction (3.03) at a given pH and in the presence of a large excess of ferrocyanide over HRP-II are consistent with the differential rate expression:

$$-\frac{d[\text{HRP-II}]}{dt} = k_{3\text{obs}}[\text{HRP-II}] \quad (3.04)$$

The disappearance of HRP-II at each pH and for each ferrocyanide concentration was a first order process and this was proved by obtaining linear semilogarithmic plots of ΔV vs. time. From these plots values of $k_{3\text{obs}}$ were obtained. Values of $k_{3\text{obs}}$ obtained at pH 5.90 are plotted as a function of the ferrocyanide concentration in Figure (3.02). From a weighted linear least squares analysis, giving the solid straight line, in Figure (3.02) the following relationship was proven:

$$k_{3\text{obs}} = k_{3\text{app}}[\text{Fe}(\text{CN})_6^{4-}] \quad (3.05)$$

The slope, $k_{3\text{app}}$, of the straight line with its standard error is $(5.1 \pm 0.1) \times 10^5 \text{ M}^{-1}\text{sec}^{-1}$. The intercept with its standard error is $(3.0 \pm 1.5) \times 10^{-2}\text{sec}^{-1}$ which is zero within the interval of the 95% confidence limits.

It then follows that the total differential rate expression is:

$$-\frac{d[\text{HRP-II}]}{dt} = k_{3\text{app}}[\text{Fe}(\text{CN})_6^{4-}][\text{HRP-II}] \quad (3.06)$$

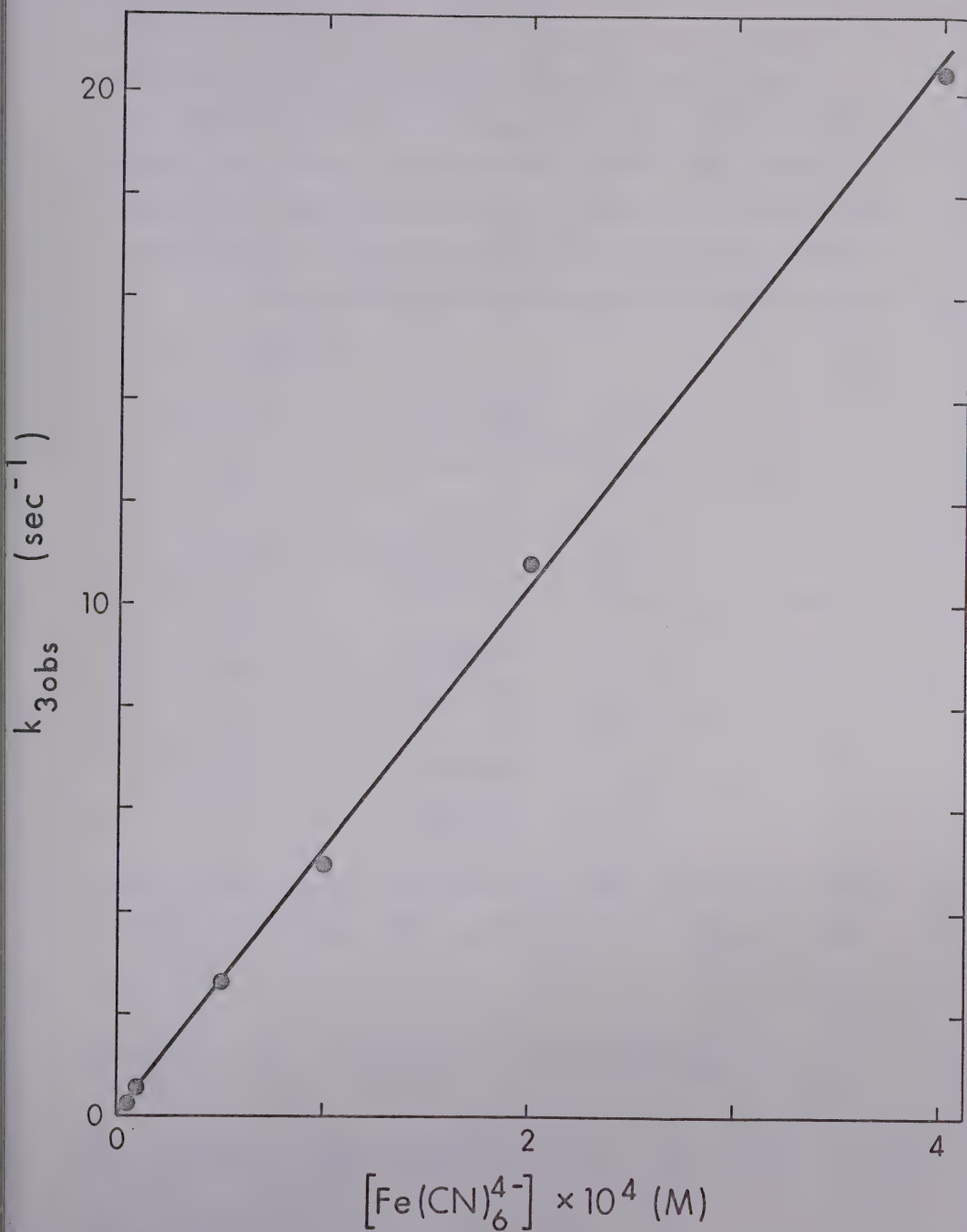
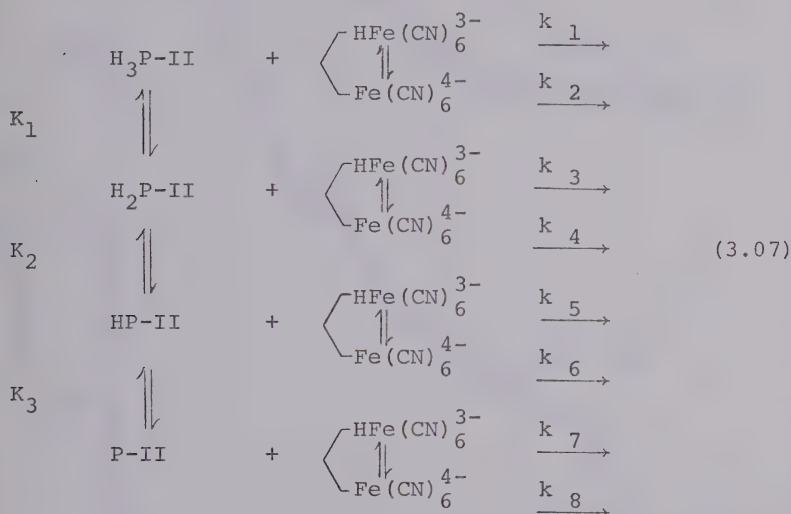


Figure 3.02: Plot of k_{3obs} vs. $[\text{Fe}(\text{CN})_6^{4-}]$ at pH 5.90 for the HRP-II-ferrocyanide reaction.

The total concentration of HRP in the reaction mixture was about 1.5×10^{-6} M and the $[\text{Fe}(\text{CN})_6^{4-}]$ was at least in a 10 fold excess at the lowest pH values and in a much larger excess at pH values greater than 4. The apparent second order rate constants, $k_{3\text{app}}$, are plotted semilogarithmically vs. pH in Figure (3.03) and listed in Table (3.01).

The simplest reaction that accounts satisfactorily for the $k_{3\text{app}}$ data is:



The vertical arrows denote fast non-rate determining proton transfer reactions. From reaction (3.07) it follows that:

$$\begin{aligned}
 k_{3\text{app}} = & \left\{ \frac{k_1 [\text{H}^+]}{K_A} + \left(k_2 + \frac{k_3 K_1}{K_A} \right) + \left(k_4 + \frac{k_5 K_2}{K_A} \right) \frac{K_1}{[\text{H}^+]} + \right. \\
 & \left. \left(k_6 + \frac{k_7 K_3}{K_A} \right) \frac{K_1 K_2}{[\text{H}^+]^2} + \frac{k_8 K_1 K_2 K_3}{[\text{H}^+]^3} \right\} / \left\{ \left(1 + \frac{K_1}{[\text{H}^+]} + \frac{K_1 K_2}{[\text{H}^+]^2} + \frac{K_1 K_2 K_3}{[\text{H}^+]^3} \right) \right. \\
 & \left. \left(1 + \frac{[\text{H}^+]}{K_A} \right) \right\} \quad (3.08)
 \end{aligned}$$

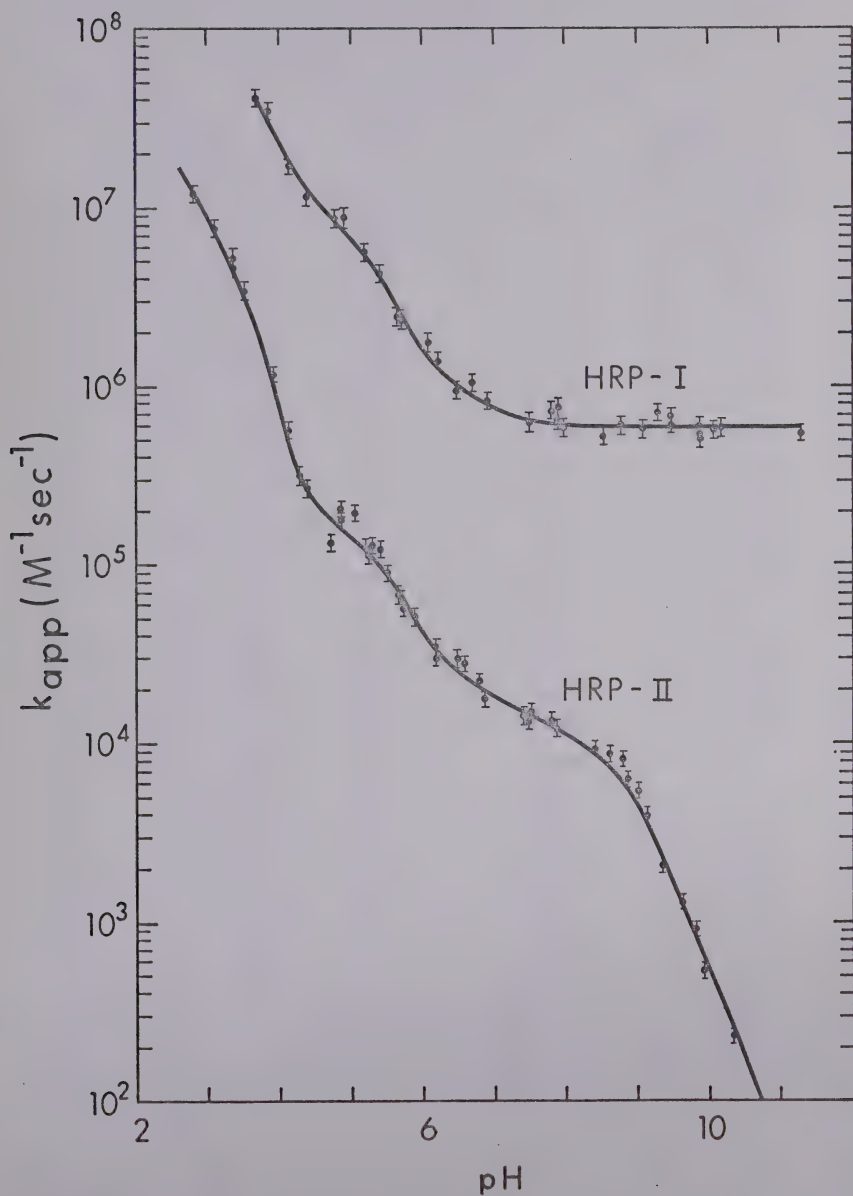


Figure 3.03: Semilogarithmic plot of k_{2app} and k_{3app} vs. pH for the reactions of HRP-I and HRP-II with ferrocyanide. The error limits are based on an estimated standard deviation of $\pm 10\%$.

Table 3.01
Apparent Rate Constants for the HRP-II-Ferrocyanide

Reaction at 25.0° and $\mu = 0.11$

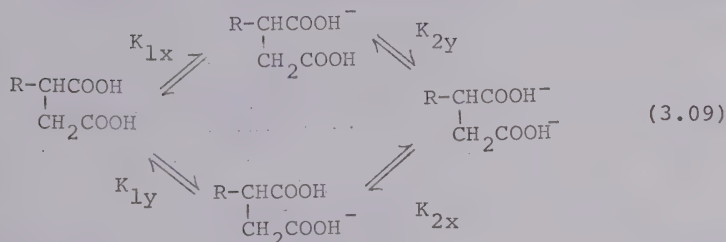
pH	k_{3app} ($M^{-1}sec^{-1}$)	Buffer ^a	pH	k_{3app} ($M^{-1}sec^{-1}$)	Buffer ^a
2.80	1.3×10^7	GH	6.18	3.0×10^4	M
3.12	7.6×10^6	GH	6.18	3.6×10^4	M
3.38	4.7×10^6	GH	6.47	3.0×10^4	M
3.39	5.0×10^6	GH	6.57	2.9×10^4	P
3.48	3.3×10^6	GH	5.78	2.3×10^4	M
3.87	1.1×10^6	A	5.83	1.8×10^4	P
4.11	5.6×10^5	A	7.39	1.5×10^4	P
4.28	3.1×10^5	A	7.43	1.4×10^4	T
4.41	2.8×10^5	A	7.38	3.6×10^4	P
4.71	1.4×10^5	A	7.79	1.4×10^4	T
4.83	2.1×10^5	A	7.86	1.3×10^4	T
4.83	1.9×10^5	M	8.41	9.5×10^3	T
5.02	2.0×10^5	M	8.58	8.9×10^3	T
5.22	1.1×10^5	A	8.81	8.4×10^3	GN
5.22	1.1×10^5	A	8.83	6.4×10^3	T
5.25	1.3×10^5	A	8.98	5.5×10^3	T
5.41	1.3×10^5	A	9.11	4.0×10^3	GN
5.46	9.0×10^4	M	9.35	2.1×10^3	C
5.65	6.8×10^4	M	9.61	1.4×10^3	GN
5.67	6.6×10^4	M	9.79	9.3×10^2	C
5.71	5.8×10^4	M	9.92	5.4×10^2	GN
5.90	5.2×10^4	P	10.32	2.4×10^2	GN

^aBuffer Key: A, acetic acid-NaOH; GH, glycine-HNO₃; M, maleic acid-NaOH; T, tris-HNO₃; C, NaHCO₃-NaOH; GN, glycine-NaOH; P, KH₂PO₄-NaOH.

A number of other reaction schemes in addition to that of reaction (3.07) were postulated in an attempt to fit the k_{3app} data. Reaction schemes that had HRP-II species with none, one or two ionizations did not explain the k_{3app} data satisfactorily. It was possible to explain the k_{3app} data with the use of only one ionization constant, K_A , for the protonated ferrocyanide species even though the ionization constant for the doubly protonated species, K_B , is known. The two acid dissociation constants for the ferrocyanide protonated species are separated by almost two pK units. In addition as experiments were conducted only as low as pH 2.80, 1.6 pK units away from pK_B , the relative concentration of the $H_2Fe(CN)_6^{2-}$ species was very low and as such its effect on the total rate of the reaction cannot be determined.

In a reaction involving two or more ionizations such as reaction (3.07) molecular rather than group ionizations are necessarily implied (Dixon and Webb, 1964). Group ionization constants, of which the molecular ionization constants consist, cannot be determined from the analysis of rate data alone. If the pK values of the group ionization constants are widely separated, the ionization

constants measured indicate the true value of the group ionization constant. The example of the unsymmetrical dibasic acid given by Dixon and Webb (1964) illustrates clearly the distinction between group and molecular ionization constants:



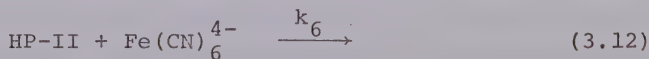
The relationship between the molecular ionization constants, K_1' and K_2' and the group ionization constants K_{1x} , K_{2x} , K_{1y} , and K_{2y} are given by the following expressions:

$$K_1' = K_{1x} + K_{1y} \quad (3.10)$$

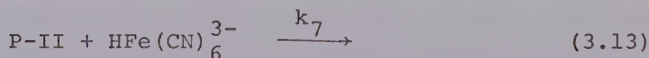
and

$$K_2' = \frac{K_{2x}K_{2y}}{K_{2x} + K_{2y}} \quad (3.11)$$

Two pathways of reaction (3.07) such as:



and



are kinetically indistinguishable and are combined together in one term of the expression relating $k_{3\text{app}}$ to the specific rate constants, ionization constants, and hydrogen ion concentrations. The only unambiguous rate constants obtainable

from equation (3.08) are k_1 and k_8 . The differential rate law for reaction (3.12) is:

$$-\frac{d[\text{HP-II}]}{dt} = k_6 [\text{HP-II}] [\text{Fe}(\text{CN})_6^{4-}] \quad (3.14)$$

and for reaction (3.13) it is:

$$-\frac{d[\text{P-II}]}{dt} = k_7 [\text{P-II}] [\text{HFe}(\text{CN})_6^{3-}] \quad (3.15)$$

but

$$[\text{P-II}] = \frac{K_3 [\text{HP-II}]}{[\text{H}^+]} \quad (3.16)$$

and

$$[\text{HFe}(\text{CN})_6^{3-}] = \frac{[\text{Fe}(\text{CN})_6^{4-}] [\text{H}^+]}{K_A} \quad (3.17)$$

Equations (3.16) and (3.17) substituted in equation (3.15) give:

$$-\frac{d[\text{P-I}]}{dt} = \frac{k_7 K_3}{K_A} [\text{HP-II}] [\text{Fe}(\text{CN})_6^{4-}] \quad (3.18)$$

which from inspection with equation (3.14) is of an identical form and hence the two reactions (3.12 and 3.13) are indistinguishable.

The $k_{3\text{app}}$ data in Figure (3.03) at pH values higher than 8.5 falls approximately on a line of slope -1 which indicates that the contribution of k_8 to the overall rate is insignificant (Dixon and Webb, 1964). After a preliminary graphical analysis of the semilogarithmic plot of $k_{3\text{app}}$ vs. pH to obtain approximate values for the ionization and rate constants, non-linear least squares computer analysis (IBM Share Library, 1964) was carried out on the $k_{3\text{app}}$ -pH data to obtain the best fit parameters for

equation (3.08). It is necessary to use a non-linear least squares analysis as equation (3.08) contains more than two parameters². In a preliminary computer non-linear least squares analysis (IBM Share Library, 1964) for values of the parameters in equation (3.08) it was found that the parameter $(k_2 + k_3 K_1/K_A)$ did not contribute significantly to computed values of k_{3app} . Consequently in the final analysis of the k_{3app} data $(k_2 + k_3 K_1/K_A)$ and k_8 were set equal to zero. The values of the remaining parameters obtained from a final analysis, listed in Table (3.02), were used to calculate the lower solid line in Figure (3.03). However upper limits for the value of $(k_2 + k_3 K_1/K_A)$ and k_8 can be calculated to be $1 \times 10^6 \text{ M}^{-1} \text{ sec}^{-1}$ and $25 \text{ M}^{-1} \text{ sec}^{-1}$ respectively by assuming that their terms can contribute up to a maximum of 10% of the value of k_{3app} . Any larger

² Given a model

$$\hat{Y}_i = f(X_{i1}, X_{i2}, \dots, X_{im}; b_1, b_2, \dots, b_k)$$

which predicts the value, \hat{Y} , of a dependent variable, Y , where the model f contains m independent variables X_{i1} and k parameters b_j and given n observations

$$(Y_i, X_{i1}, X_{i2}, \dots, X_{im}) \quad i = 1, 2, \dots, n,$$

the program will compute the least-squares estimates b_j . That is the program will adjust the b_j to minimize

$$\Phi = \sum_{i=1}^h (Y_i - \hat{Y}_i)^2$$

(IBM Share Library, 1964).

Table 3.02

Rate and Ionization Constants^a Obtained by
Non-linear Least Squares Analysis for the
Reaction of HRP-II with Ferrocyanide

k_1	$(2.3 \pm 0.4) \times 10^7 \text{ M}^{-1}\text{sec}^{-1}$
$\left(k_2 + \frac{k_3 K_1}{K_A}\right)$	0 ($< 10^6 \text{ M}^{-1}\text{sec}^{-1}$)
$\left(k_4 + \frac{k_5 K_2}{K_A}\right)$	$(2.2 \pm 0.3) \times 10^5 \text{ M}^{-1}\text{sec}^{-1}$
$\left(k_6 + \frac{k_7 K_3}{K_A}\right)$	$(1.6 \pm 0.1) \times 10^4 \text{ M}^{-1}\text{sec}^{-1}$
k_8	0 ($< 25 \text{ M}^{-1}\text{sec}^{-1}$)
<hr/>	
K_1	$(3.6 \pm 1.2) \times 10^{-4} \text{ M}$
K_2	$(6.1 \pm 1.5) \times 10^{-6} \text{ M}$
K_3	$(2.7 \pm 0.3) \times 10^{-9} \text{ M}$

^a Errors given are the standard errors of the parameter estimates obtained from non-linear least squares analysis.

contribution to k_{3app} presumably would have resulted in their detection in the non-linear least squares analysis. On kinetic grounds an upper limit of $1 \times 10^6 \text{ M}^{-1}\text{sec}^{-1}$ for $(k_2 + k_3K_1/K_A)$ is still significantly larger than the value of either of two other parameters, $(k_4 + k_5K_2/K_A)$ and $(k_6 + k_7K_3/K_A)$, that contribute to the value for k_{3app} . The large size of the k_1 parameter has swamped out the effect of the $(k_2 + k_3K_1/K_A)$ parameter in determining the value of k_{3app} .

It is not possible to exclude any of the rate constants from the parameters for exceeding the diffusion controlled bimolecular rate limit of $10^9 \text{ M}^{-1} \text{ sec}^{-1}$ (Amdur and Hammes, 1966b).

Kinetics of the HRP-I - Ferrocyanide Reaction

The rate constant for the reaction of HRP and H_2O_2 to form HRP-I (reaction 3.01) is about $1 \times 10^7 \text{ M}^{-1} \text{ sec}^{-1}$ (Chance, 1953b; Chance et al., 1967) at least in the neutral pH region. Advantage was taken of this known rate constant and the value for k_{3app} determined above to study the kinetics of reaction (3.02). By using a large excess of H_2O_2 ($1 \times 10^{-4} \text{ M}$) over HRP ($5 \times 10^{-7} \text{ M}$) and with only a small excess of ferrocyanide ($1.5 \times 10^{-6} \text{ M}$), reaction (3.01) occurs much faster than reaction (3.02). It can be calculated that under these conditions reaction (3.01) has a half life of about 0.5 msec whereas reaction (3.02) was observed to have a half life of tens of

milliseconds depending on the pH. In fact reaction (3.01) was, under the above conditions, too fast to be detected on the stopped flow apparatus which has a dead time of 5 msec. Thus reaction (3.01) can be considered complete before observation of reaction (3.02) is begun. Reaction (3.03), the reaction between HRP-II and ferrocyanide, also occurs simultaneously with the formation of HRP-II from reaction (3.02). Moreover, the ratio of k_{2app} to k_{3app} is always 40 or more depending on the pH. Thus reaction (3.02) is also separated in time from reaction (3.03) and can be studied without interference from reaction (3.03).

The reaction of HRP-I with ferrocyanide becomes faster at lower pH and could not be studied below pH 3.67 on the present stopped-flow apparatus. At pH values greater than 6, the reaction is sufficiently slow that it could be studied in the presence of a large excess of ferrocyanide. Under these conditions the kinetics of reaction (3.02) are consistent with the differential rate expression:

$$-\frac{d[\text{HRP-I}]}{dt} = k_{2obs} [\text{HRP-I}] \quad (3.19)$$

Non-linear least squares analysis of the ΔV -time data in the integrated form of equation (3.19) proved the validity of the rate law. Values of k_{2obs} at a constant pH of 7.86 are plotted in Figure (3.04) and show that:

$$k_{2obs} = k_{2app} [\text{Fe}(\text{CN})_6^{4-}] \quad (3.20)$$

Thus the complete differential rate law for reaction (3.02)

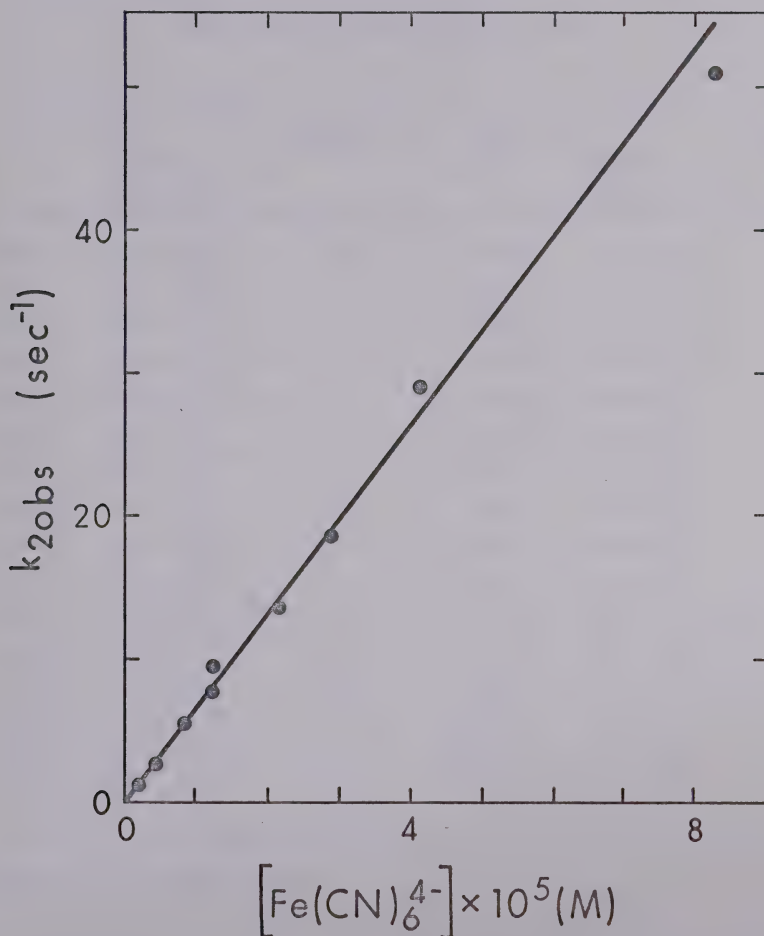


Figure 3.04: Plot of $k_{2\text{obs}}$ vs. $[\text{Fe}(\text{CN})_6^{4-}]$ at pH 7.86 for the HRP-I-ferrocyanide reaction. The straight line is the weighted least squares best fit line. The slope, $k_{2\text{app}}$, with its standard error is $(6.6 \pm 0.2) \times 10^5 \text{ M}^{-1} \text{ sec}^{-1}$. The intercept, $(-0.20 \pm 0.08) \text{ sec}^{-1}$, is zero within the interval of the 99% confidence limits.

Table 3.03

Apparent Rate Constants for the HRP-I-FerrocyanideReaction at 25.0° and $\mu = 0.11$

pH	k_{2app} ($M^{-1}sec^{-1}$)	Buffer ^a	pH	k_{2app} ($M^{-1}sec^{-1}$)	Buffer ^a
3.67	4.1×10^7	A	7.81	7.3×10^5	P
3.85	3.6×10^7	A	8.87	6.6×10^5	P
4.15	1.9×10^7	M	7.87	8.3×10^5	P
4.40	1.2×10^7	A	7.99	5.8×10^5	T
4.80	8.8×10^6	A	8.54	5.1×10^5	T
4.91	8.9×10^6	M	8.80	6.1×10^5	GN
5.21	5.6×10^6	A	9.09	5.9×10^5	GN
5.40	4.2×10^6	M	9.31	7.1×10^5	C
5.65	2.5×10^6	M	9.49	6.8×10^5	GN
5.70	2.5×10^6	M	9.52	6.1×10^5	C
6.10	1.8×10^6	P	9.88	5.3×10^5	C
6.22	1.5×10^6	M	9.90	5.9×10^5	GN
6.45	9.6×10^5	M	9.92	5.8×10^5	C
6.66	1.0×10^6	P	10.19	5.8×10^5	C
6.93	8.5×10^5	M	10.20	6.0×10^5	GN
7.47	6.3×10^5	T	11.32	5.5×10^5	C

^a Key as in Table (3.01)

is:

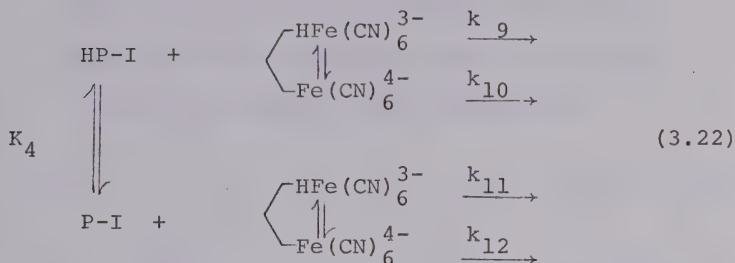
$$-\frac{d[\text{HRP-I}]}{dt} = k_{2\text{app}}[\text{Fe}(\text{CN})_6^{4-}][\text{HRP-I}] \quad (3.21)$$

In practice an integrated form of equation (3.21) (Frost and Pearson, 1961) was used in the determination of $k_{2\text{app}}$. A non-linear least squares fit to the ΔV -time curves were obtained using three parameters: the rate constant, $k_{2\text{app}}$, ΔV at zero time, and a small term for the placement of the base line at infinite time. A complete derivation of the equations used and the use of the non-linear least squares computer program for this problem is given in Appendix 1. To ensure a valid analysis 10 to 15 points were taken from each trace. At each pH, three or four oscilloscope traces were used to determine an average $k_{2\text{app}}$.

In experiments conducted at a constant pH but at two different wavelengths (411 and 426 m μ) values of $k_{2\text{app}}$ were found to be in agreement within experimental error, which indicates that only a single reaction is being observed. In other experiments also conducted at constant pH, in which $[\text{H}_2\text{O}_2]$ varied from 1×10^{-5} to 1×10^{-4} M, values of $k_{2\text{app}}$ agreed within experimental error. The validity of the procedure is verified and it can also be concluded that H_2O_2 does not react at any measurable rate with HRP-II to reform HRP-I. Under conditions where the $[\text{H}_2\text{O}_2]$ is larger (10^{-3} M) than that used in this study (10^{-4} M), H_2O_2 reacts slowly with HRP-II to form a third compound, HRP-III (Keilin and Hartree,

1951). The k_{2app} results are plotted vs. pH in Figure (3.03) and are listed in Table (3.03).

The simplest reaction consistent with the k_{2app} data has a single ionization on HRP-I:



from which

$$k_{2app} = \frac{\frac{k_9 [\text{H}^+]}{K_A} + \left(k_{10} + \frac{k_{11} K_4}{K_A} \right) + \frac{k_{12} K_4}{[\text{H}^+]}}{\left(1 + \frac{K_4}{[\text{H}^+]} \right) \left(1 + \frac{[\text{H}^+]}{K_A} \right)} \quad (3.23)$$

From non-linear least squares analysis of the k_{2app} data in equation (3.23) the values of the parameters listed in Table (3.04) were obtained. The upper solid line in the semilogarithmic plot of k_{2app} vs. pH in Figure (3.03) was computed with these values in equation (3.23)

Steady State Kinetics of the HRP Catalyzed H_2O_2 - Ferrocyanide Reaction

The stoichiometry of the H_2O_2 -ferrocyanide reaction was checked at each pH value as both the concentration of the H_2O_2 added and the ferricyanide produced in the reaction mixture were known. Within experimental error, two moles of ferricyanide were always produced per

Table 3.04

Rate and Ionization Constants^a Obtained by
Non-linear Least Squares Analysis for the
Reaction of HRP-I with Ferrocyanide

k_9	$(1.5 \pm 0.2) \times 10^8 \text{ M}^{-1}\text{sec}^{-1}$
$\left(k_{10} + \frac{k_{11}K_4}{K_A}\right)$	$(7.5 \pm 1.6) \times 10^6 \text{ M}^{-1}\text{sec}^{-1}$
k_{12}	$(6.0 \pm 0.2) \times 10^5 \text{ M}^{-1}\text{sec}^{-1}$
<hr/>	
K_4	$(4.9 \pm 1.6) \times 10^{-6} \text{ M}$
<hr/>	

^a Errors given are the standard error of the parameter estimates obtained from non-linear least squares analysis.

mole of H_2O_2 added. This check showed that no detectable amount of exogenous or endogenous donor reacted, or less than stoichiometric amounts of ferricyanide would have been produced.

The initial velocity expression under steady state conditions is derived in Appendix 2. Also included in Appendix 2 is a calculation of the attainment of steady state conditions which show that the steady state is 99% attained 21 msec after the start of the reaction.

$$v = \frac{2k_{1app}k_{2app}k_{3app}[\text{HRP}]_0[\text{Fe}(\text{CN})_6^{4-}]_0[\text{H}_2\text{O}_2]_0}{(k_{1app}k_{2app} + k_{1app}k_{3app})[\text{H}_2\text{O}_2]_0 + k_{2app}k_{3app}[\text{Fe}(\text{CN})_6^{4-}]_0} \quad (3.24)$$

where v is $d[\text{Fe}(\text{CN})_6^{3-}]/dt$. The proportionality of v and $[\text{HRP}]_0$ was checked at pH 4.79. The values of $[\text{Fe}(\text{CN})_6^{4-}]_0$ and $[\text{H}_2\text{O}_2]_0$ were kept constant at 1.00×10^{-4} M and 3.55×10^{-5} M and v was measured as a function of $[\text{HRP}]_0$. The results are plotted in Figure (3.05) and listed in Table (3.05). The slope and intercept of the weighted linear least squares best fit line, with their 95% confidence limits are $(42 \pm 4) \text{ sec}^{-1}$ and $(3 \pm 2) \times 10^{-8} \text{ M}^{-1}\text{sec}^{-1}$. The intercept is zero within the 99% confidence interval, which indicates that no additional constant term is required in equation (3.24).

From the results above it was found that k_{2app} is at least 40 times larger than k_{3app} . With the assumption that $k_{2app} \gg k_{3app}$ and rearrangement of equation (3.24):

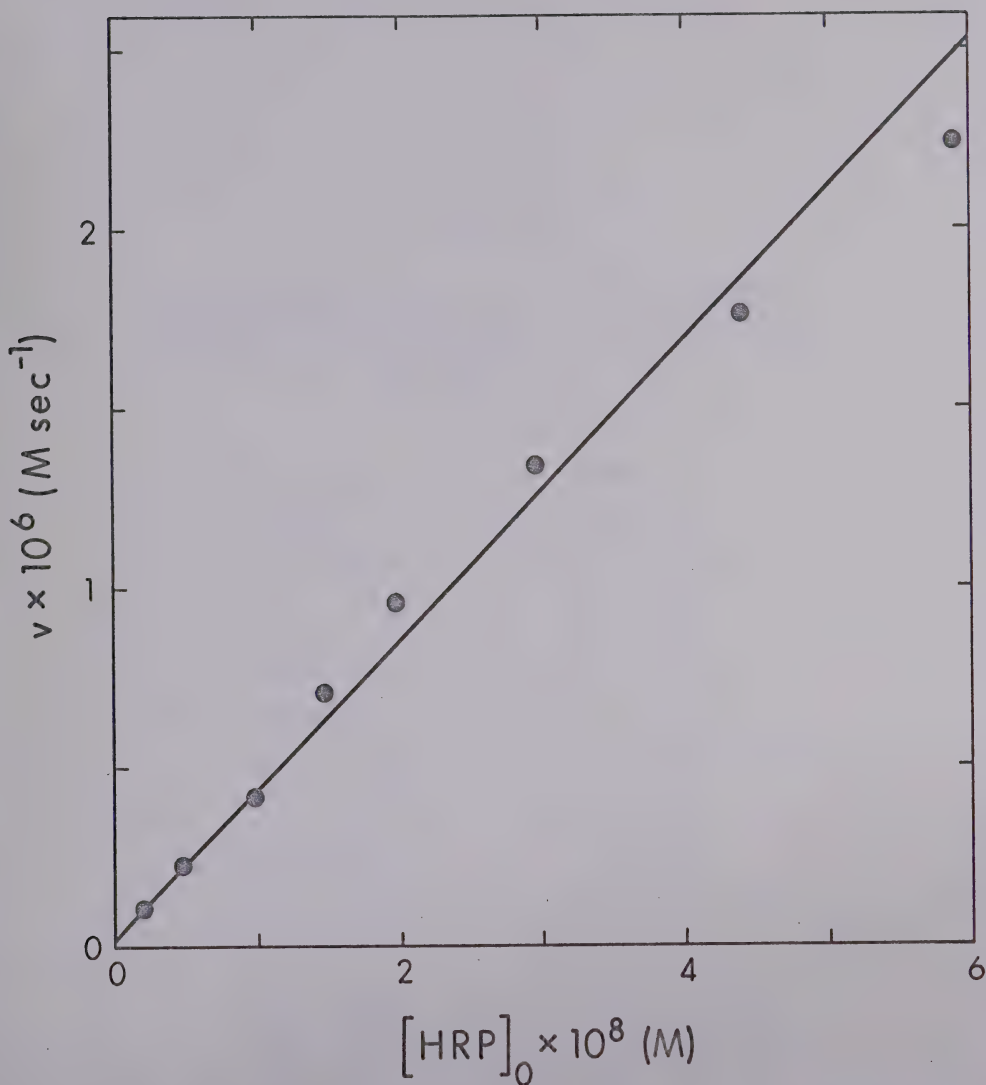


Figure 3.05: Plot of initial steady state velocity, v , vs. $[HRP]_0$ at pH 4.79 and constant initial concentrations of ferrocyanide and H_2O_2 of $1.00 \times 10^{-4} \text{ M}$ and $3.55 \times 10^{-5} \text{ M}$ respectively.

Table 3.05

Initial Velocity Data for the HRP Catalyzed
Oxidation of Ferrocyanide at 25.0°, $\mu = 0.11$ ^a
and pH = 4.79

v (M sec ⁻¹)	[HRP] ₀ (M)
2.5×10^{-6}	5.9×10^{-8}
1.9×10^{-6}	4.4×10^{-8}
1.3×10^{-6}	2.9×10^{-8}
8.5×10^{-7}	2.0×10^{-8}
6.4×10^{-7}	1.5×10^{-8}
4.4×10^{-7}	9.8×10^{-9}
2.4×10^{-7}	4.9×10^{-9}
1.1×10^{-7}	2.0×10^{-9}

^a The $[\text{H}_2\text{O}_2]_0$, and $[\text{Fe}(\text{CN})_6^{4-}]_0$ were held constant for each determination at 3.6×10^{-5} and 1.0×10^{-4} M respectively.

$$\frac{[\text{HRP}]_0}{v} = \frac{1}{2k_{1\text{app}}[\text{H}_2\text{O}_2]_0} + \frac{1}{2k_{3\text{app}}[\text{Fe}(\text{CN})_6^{4-}]_0} \quad (3.25)$$

From equation (3.25) it is predicted that a plot of $[\text{HRP}]_0/v$ vs. $1/[\text{Fe}(\text{CN})_6^{4-}]_0$ at a constant $[\text{H}_2\text{O}_2]_0$ should be linear with the slope equal to $1/2k_{3\text{app}}$ and an intercept equal to $1/2k_{1\text{app}}[\text{H}_2\text{O}_2]_0$. Data obtained at three values of pH are plotted in Figure (3.06) and listed in Table (3.06). Weighted linear least squares analysis gave the rate constants and error limits listed in Table (3.07).

It can also be shown from equation (3.25) that a plot of $[\text{HRP}]_0/v$ vs. $1/[\text{H}_2\text{O}_2]_0$ at constant pH and $[\text{Fe}(\text{CN})_6^{4-}]_0$ should be linear with a slope of $1/2k_{1\text{app}}$ and an intercept of $1/2k_{3\text{app}}[\text{Fe}(\text{CN})_6^{4-}]_0$. Data obtained at a single pH of 4.82 are plotted in Figure (3.07) and listed in Table (3.06). The solid lines in Figure (3.06) were calculated from a weighted linear least square analysis.

Values of $k_{1\text{app}}$ and $k_{3\text{app}}$ obtained from a weighted linear least squares analysis of the data are also listed in Table (3.07).

Values of $k_{3\text{app}}$ obtained from the steady state kinetics and from stopped flow kinetics agree within the error limits shown in Table (3.07). The error in the determination of $k_{1\text{app}}$ by the steady state method is necessarily large because of the small value of the intercepts in Figure (3.06) and the uncertainty in drawing an accurate slope through the data points in Figure (3.07).

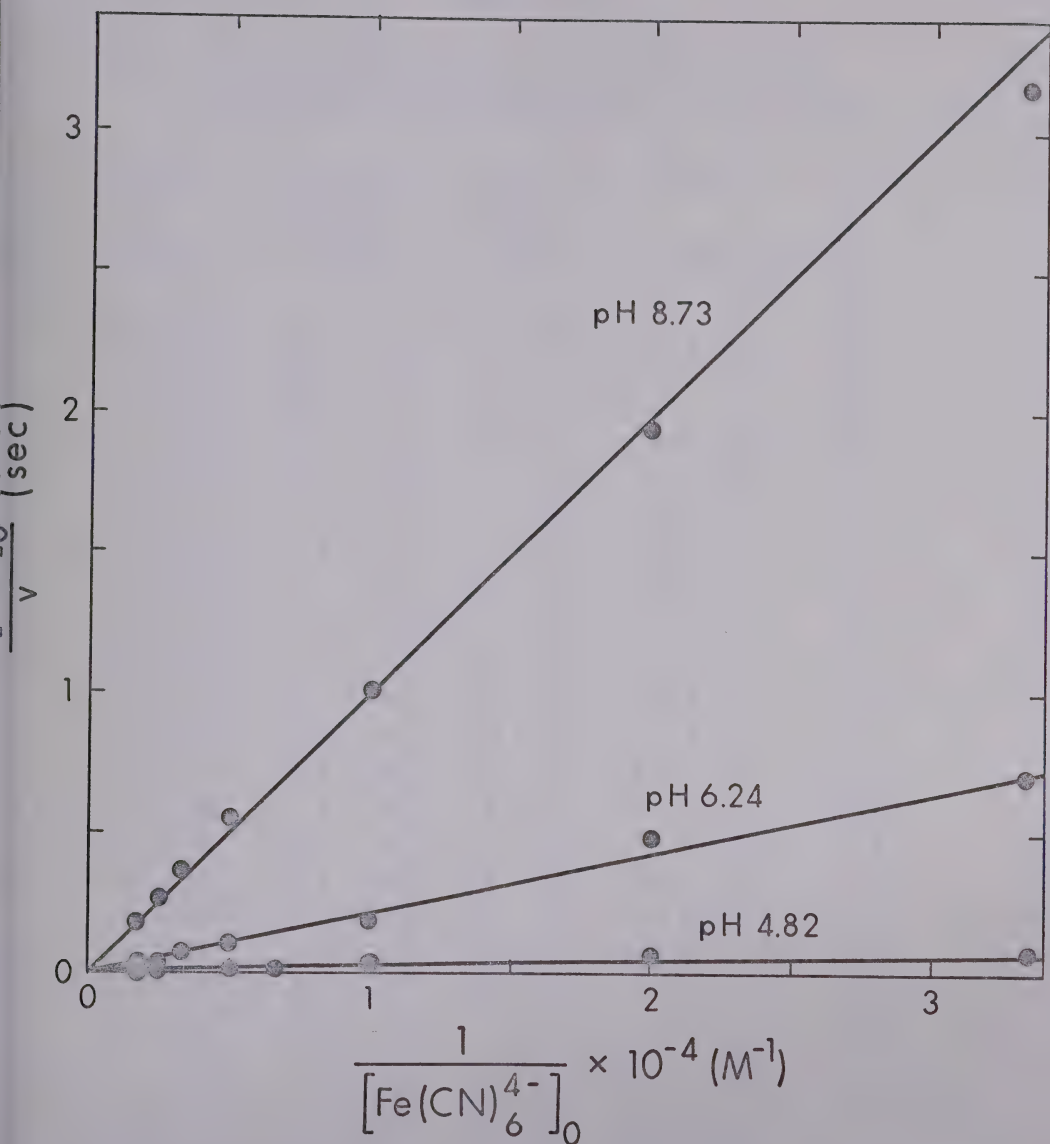


Figure 3.06: Plot of $[HRP]_0/v$ vs. $1/[Fe(CN)_6^{4-}]_0$ at the pH values shown. For each plot, pH, $[H_2O_2]_0$ and $[HRP]_0$ are constant and their respective values are: 4.82, 3.55×10^{-5} M, and 1.96×10^{-8} M; 6.24, 3.79×10^{-5} M and 9.00×10^{-8} M; 8.73, 4.03×10^{-5} M and 4.50×10^{-7} M.

Table 3.06

Initial Velocity Data for the HRP Catalyzed
Oxidation of Ferrocyanide at 25.0° and $\mu = 0.11$

$\frac{[\text{HRP}]_0}{v}$ (sec)	$\frac{1}{[\text{Fe}(\text{CN})_6^{4-}]_0}$ (M^{-1})	$\frac{1}{[\text{H}_2\text{O}_2]_0}$ (M^{-1})	$[\text{HRP}]_0$ (M)	pH
6.9×10^{-3}	2.0×10^3	2.8×10^4	2.0×10^{-8}	4.82
8.1×10^{-3}	2.5×10^3	2.8×10^4	2.0×10^{-8}	4.82
1.2×10^{-2}	5.0×10^3	2.8×10^4	2.0×10^{-8}	4.82
1.6×10^{-2}	6.7×10^3	2.8×10^4	2.0×10^{-8}	4.82
2.0×10^{-2}	1.0×10^4	2.8×10^4	2.0×10^{-8}	4.82
4.5×10^{-2}	2.0×10^4	2.8×10^4	2.0×10^{-8}	4.82
8.0×10^{-2}	3.3×10^4	2.8×10^4	2.0×10^{-8}	4.82
1.8×10^{-1}	1.7×10^3	2.5×10^4	4.5×10^{-7}	8.73
2.7×10^{-1}	2.5×10^3	2.5×10^4	4.5×10^{-7}	8.73
3.6×10^{-1}	3.3×10^3	2.5×10^4	4.5×10^{-7}	8.73
5.5×10^{-1}	5.0×10^3	2.5×10^4	4.5×10^{-7}	8.73
1.0×10^0	1.0×10^4	2.5×10^4	4.5×10^{-7}	8.73
2.0×10^0	2.0×10^4	2.5×10^4	4.5×10^{-7}	8.73
3.2×10^0	3.3×10^4	2.5×10^4	4.5×10^{-7}	8.73
3.9×10^{-2}	1.7×10^3	2.6×10^4	9.0×10^{-8}	6.24
4.5×10^{-2}	2.5×10^3	2.6×10^4	9.0×10^{-8}	6.24
7.9×10^{-2}	3.3×10^4	2.6×10^4	9.0×10^{-8}	6.24
1.1×10^{-1}	5.0×10^4	2.6×10^4	9.0×10^{-8}	6.24
2.0×10^{-1}	1.0×10^4	2.6×10^4	9.0×10^{-8}	6.24
4.8×10^{-1}	2.0×10^4	2.6×10^4	9.0×10^{-8}	6.24
7.0×10^{-1}	3.3×10^4	2.6×10^4	9.0×10^{-8}	6.24
2.5×10^{-2}	1.0×10^4	6.8×10^3	2.6×10^{-8}	4.82
2.6×10^{-2}	1.0×10^4	7.9×10^3	2.6×10^{-8}	4.82
2.6×10^{-2}	1.0×10^4	1.2×10^4	2.6×10^{-8}	4.82
2.7×10^{-2}	1.0×10^4	1.6×10^4	2.6×10^{-8}	4.82
2.3×10^{-2}	1.0×10^4	2.4×10^4	2.6×10^{-8}	4.82
2.9×10^{-2}	1.0×10^4	4.7×10^4	2.6×10^{-8}	4.82

Table 3.07

Rate Constants for the HRP Catalyzed Oxidation of
Ferrocyranide by H_2O_2 at 25.0° and $\mu = 0.11$

$k_{3\text{app}}^{\text{a}}$ ($\text{M}^{-1}\text{sec}^{-1}$) (stopped flow)	$k_{3\text{app}}^{\text{b}}$ ($\text{M}^{-1}\text{sec}^{-1}$) (steady state)	$k_{\text{lapp}}^{\text{b}}$ ($\text{M}^{-1}\text{sec}^{-1}$) (steady state)	pH	Buffer ^c
$(1.7 \pm 0.5) \times 10^5$	$(2.5 \pm 0.3) \times 10^{5\text{d}}$	$(5.2 \pm 2.2) \times 10^{6\text{d}}$	4.82	M
$(1.7 \pm 0.5) \times 10^5$	$(2.0 \pm 0.2) \times 10^{5\text{e}}$	$(8.0 \pm 15.5) \times 10^{6\text{e}}$	4.82	M
$(3.2 \pm 0.9) \times 10^4$	$(2.3 \pm 0.3) \times 10^{4\text{d}}$	-- ^f	6.24	M
$(6.6 \pm 1.9) \times 10^3$	$(5.1 \pm 0.2) \times 10^{3\text{d}}$	$(6.3 \pm 5.3) \times 10^{5\text{d}}$	8.73	GN

- ^a Rate constants calculated from parameters in Table (3.02) in eq. (3.08). Error limits calculated from 95% confidence limits of the computer fit.
- ^b Error limits are 95% confidence limits from weighted linear least squares analysis of data in Figure (3.06 and (3.07).
- ^c Buffer key as in Table (3.01).
- ^d From weighted linear least squares analysis of data in Figure (3.06) obtained at constant $[\text{H}_2\text{O}_2]_0$.
- ^e From weighted linear least squares analysis of data in Figure (3.07) obtained at constant $[\text{Fe}(\text{CN})_6^{4-}]_0$.
- ^f Negative intercept found.

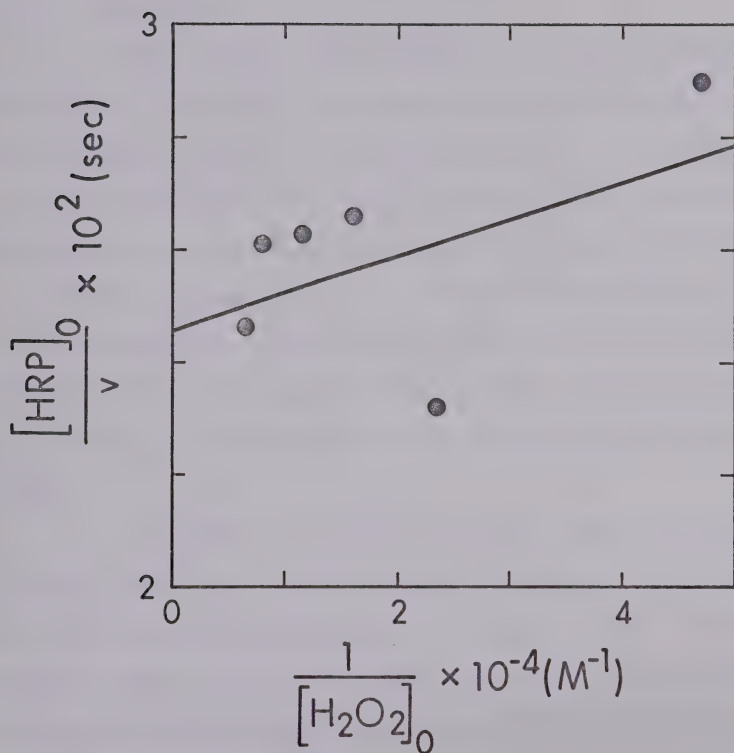


Figure 3.07: Plot of $[\text{HRP}]_0/v$ vs. $1/[\text{H}_2\text{O}_2]_0$ at a pH of 4.82 and at constant initial concentrations of ferrocyanide and HRP of $1.00 \times 10^{-4} \text{M}$ and $2.55 \times 10^{-8} \text{M}$ respectively. The solid line was calculated from a weighted linear least squares analysis. The large errors are caused because the term $1/2 k_{\text{lapp}} [\text{H}_2\text{O}_2]_0$ is small.

This arises because the term $1/2k_{3app}[\text{Fe}(\text{CN})_6^{4-}]_0$ in equation (3.25) is, under typical experimental conditions, approximately 100 times larger than the $1/2k_{1app}[\text{H}_2\text{O}_2]_0$ term effectively swamping out the smaller term.

3.04 Discussion

The steady state kinetic study has shown that equations (3.01-3.03) represent the minimum reaction sequences for the HRP catalyzed oxidation of ferrocyanide by H_2O_2 at a fixed pH. The inclusion of fast non-rate determining steps would also lead to an equation of the same form as equation (3.25). Since the values of k_{3app} obtained from the steady state method agree with those obtained from the stopped-flow studies, no detectable loss of activity of HRP occurs in the steady state reaction cycle.

A number of kinetic studies, including the present ones, have indicated the presence of ionizations on HRP associated with the active site and are listed in Table (3.08). It is generally agreed that the pK values on HRP measured to be in the range 10.8 to 11.3 are associated with the formation of a hydroxide complex (Ellis and Dunford, 1969). The temperature jump study of fluoride binding to HRP over the pH range 4.1 to 7.9 (Dunford and Alberty, 1967; Ellis and Dunford, 1968) showed the presence of two ionizations at the active site with pK values of 4.3 and 6.1. In substantial agreement was a subsequent

Table 3.08

The pK Values for Ionizations in the Active Site
of HRP deduced from Kinetic Studies at 25.0° and $\mu = 0.11$

The values listed for each of the first and second ionizations are believed to represent pK values of the same group, with changes in the constants reflecting local environmental changes.

Species	pK Value			Ref.
	First Ionization	Second Ionization	Third Ionization (6th Co-ordination position)	
HRP-II	3.4	5.2	8.6	This work
HRP-I	-	5.3	-	This work
HRP	4.2 ^{c,d}	6.2 ^c	10.8	a
HRP-F	5.2	- ^e		a,b
HRP-CN	6.7	10.7		a

^a (Ellis and Dunford, 1968).

^b (Dunford and Alberty, 1967).

^c Mean of two independent values which agree within experimental error.

^d pK values of 4 and 5 were deduced from small spectral changes (Theorell and Paul, 1944).

^e The study could not be conducted above pH 7.9.

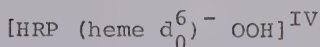
study of cyanide binding to HRP over the pH range 4.2 to 11.3 which showed the presence of three ionizations at the active site with pK values of 4.1, 6.4, and 10.8 (Ellis and Dunford, 1968). Both the cyanide and fluoride ligands would be expected to carry a negative charge to the active site. In both studies it was found that the pK values of the molecular ionizations were increased when the complexed HRP was compared to free HRP, as might be expected from simple electrostatic considerations (Alberty and Massey, 1954).

If the mean pK values of the molecular ionization constants on free HRP of 4.2 and 6.2 are related consecutively to those on HRP-II, then decreases of about 0.8 and 1.0 pK units appear to occur when HRP is converted to HRP-II. This would indicate that HRP-II has a more positively charged active site than HRP (Alberty and Massey, 1954).

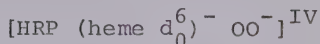
The molecular ionization of pK 5.3 on HRP-I appears to correlate with the pK of 5.2 on HRP-II, which implies that the effective charge on the active site of HRP-I is unchanged from that of HRP-II. No ionization on HRP-I was observed that corresponded to the ionizations with pK values of 3.4 on HRP-II or pK 4.2 on HRP, which may indicate that it has disappeared. Alternatively, if the corresponding pK on HRP-I were shifted to a smaller value it might not have been detectable as kinetic experiments could be conducted only as low as pH 3.67 on HRP-I in this study. Also an ionization on HRP-I corresponding to

the one of pK 8.6 on HRP-II does not appear to be present.

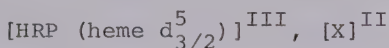
A number of structures have been proposed for HRP-I and HRP-II. For HRP-II these include the Fe(IV) and the Fe(IV)O structures proposed by George (1953c). Brill and Williams (1961) agreed that the ferryl structure describes HRP-II but proposed for HRP-I the existence of two components (1) a simple complex with hydroperoxide in the sixth co-ordination position and (2) an oxidized porphyrin ring compound. Brill and Sandberg (1968) later put forward proposals for the structure of HRP-I including (1) iron in a quadrivalent state plus a free radical or (2) iron in the ferric state plus a biradical on the porphyrin or protein. Moss et al. (1969) stated that the results of their Mossbauer study on HRP-I and HRP-II were compatible with a Fe(IV) type structure for HRP-II but they also concluded that there was no difference in the configuration of the iron between HRP-I and HRP-II, indicating that the second oxidizing equivalent on HRP-I is not stored on the iron. Peisach et al. (1968) and Blumberg et al. (1968) put forth a series of comprehensive proposals for the structures of HRP-I and HRP-II consistent with low temperature optical spectra, electron paramagnetic resonance spectra and previously reported magnetic susceptibility data. Structures are written for HRP-II in which two oxygen atoms reside in the sixth ligand position of the iron atom:



and in the ionized form



For the structure of HRP-I it was suggested that the z axial ligands are not present or that they provide only a weak component to the ligand field consistent with:



The two oxidizing equivalents are stored not on a ligand but either on the protein or the porphyrin represented as group X.

The results are consistent with a number of these structural proposals. The shift in the pK values observed in going from HRP to HRP-II (Table 3.06) are consistent with the Fe(IV) type structure for HRP-II proposed by George (1953c) which would have an active site more positively charged than free HRP. The results of Moss et al. (1969) indicating the configuration about the iron of HRP-I and HRP-II to be the same is consistent with the pK of 5.3 on HRP-I and 5.2 on HRP-II remaining nearly constant. Any structure proposed for HRP-I and HRP-II that has an active site more positively charged than HRP is consistent with the shift in pK values found from this study. However, the proposals of Peisach et al. (1968) are the most consistent with these results because of deductions that follow from a consideration of their structures. The first is the presence of an ionization on the ligand of the sixth

co-ordination position of HRP-II which may very well correspond to the ionization of pK 8.6 found from this study. The second is that HRP-I has lost its axial ligands from the iron and hence the lack of evidence in this kinetic study for ionizations on HRP-I that could correspond to the pK of 8.6 on HRP-II or to the ones of pK 3.4 on HRP-II and 4.2 on HRP. This may be consistent with the loss of axial ligands from HRP-I proposed by Peisach et al. (1968).

An alternate explanation for the lack of kinetically distinguishable ionizations on HRP-I might be that the reaction site of each of HRP-I and HRP-II with ferrocyanide may be different. Consistent with this conclusion is the suggestion by Moss et al. (1969) that one of the oxidizing equivalents on HRP-I is not stored on the iron. If the oxidizing equivalents are not transferred through the iron in each case then the kinetics of the oxidation of ferrocyanide by HRP-I may be reflecting a different set of ionizations than the HRP-II - ferrocyanide reaction. The fact that all of the ionizations appearing on free HRP can be correlated with ionizations on HRP-II could also indicate that the reaction site of the cyanide and fluoride ligands with HRP is the same as the reaction site of ferrocyanide with HRP-II, namely at the iron where it has been proposed the oxidizing equivalent of HRP-II is stored (Moss et al., 1969; George, 1953a).

The reaction of HRP and H_2O_2 to form HRP-I is pH independent at least over the neutral pH region (Chance, 1953b; Chance et al., 1967) which may indicate that the neutral H_2O_2 species takes part in the rate controlling step. Hence H_2O_2 would not be expected to be as sensitive to ionizations at the active site as would the highly charged ferrocyanide species in reaction with HRP-I and HRP-II.

The pK of 3.4 on HRP-II and 4.2 on HRP fall in the normal range for a carboxyl ionization. Carboxyl groups on horseradish peroxidase include glutamic and aspartic acid residues and two propionic acid groups of protoporphyrin IX (Shannon et al., 1966). The pK values of 5.2 on HRP-II, 5.3 on HRP-I, and 6.2 on HRP fall most closely in the range of an imidazolium group of a histidine residue, of which horseradish peroxidase has an average of one gm residue per 100 gm of protein (Shannon et al., 1966). Similar correlations have been made for lactoperoxidase (Dolman et al., 1968).

Brill (1966) in a recent review has compiled rate constants obtained mainly by Chance and co-workers for the reaction of a number of organic substrates with HRP-I and HRP-II most of which were obtained primarily at only a single pH value. These results are listed in Table (3.09) along with the apparent rate constants for the oxidation of ferrocyanide at the same pH by HRP-I and HRP-II. The rate constants given in Table (3.09) are all apparent rate

Table 3.09

Apparent Rate Constants for the Reaction of HRP-I
and HRP-II with Substrates^a

Substrate	k_{2app} ($M^{-1}sec^{-1}$)	k_{3app} ($M^{-1}sec^{-1}$)	pH
Ferrocyanide ^b	8×10^5	2×10^4	7
Ferrocyanide ^b	9×10^6	2×10^5	4.7
Guaiacol	9×10^6	3×10^5	7
Ascorbic Acid	--	2×10^4	4.7
Aniline	--	7×10^4	7
p-aminobenzoic acid	9×10^6	2×10^3	--
luminol ^c	2×10^6	7×10^4	8

^a Except as marked the data was obtained primarily by Chance and co-workers at 25-30° and was compiled by Brill (1966).

^b Interpolated from rate constants plotted in Figure (3.03).

^c From Cormier and Prichard (1968).

constants. A comparison of the apparent rate constants is not necessarily informative as in the case of the substrates other than ferrocyanide specific rate constants were not determined. Only from an analysis of the pH-rate profile for a substrate can the specific rate constants be obtained.

CHAPTER 4

The Temperature Jump Kinetics of the Binding of
Imidazole to Ferriprotoporphyrin IX

The material covered in this chapter represents a more detailed description of results previously published (Hasinoff et al., 1969; Angerman et al., 1969).

4.01 Introduction

Ferriprotoporphyrin IX is the prosthetic group of a number of heme proteins including methemoglobin, metmyoglobin, horseradish peroxidase, and catalase. The simpler name, hemin, is henceforth used for ferriprotoporphyrin IX. Four co-ordination positions about the ferric ion of hemin are surrounded by the approximately planar dianionic porphyrin ring. The fifth and sixth co-ordination positions trans to each other above and below the plane of the porphyrin ring are available in solution for further co-ordination by the solvent. X-ray crystallographic studies (Hoard et al., 1967) have shown that for the five co-ordinate high-spin chloroiron(III) derivative of tetraphenyl porphine that the iron atom is displaced approximately 0.38 \AA out-of-plane of the four nitrogen atoms. A more recent x-ray crystallographic study (Countryman et al., 1969) of the bis(imidazole)- $\alpha, \beta, \gamma, \delta$ -tetraphenylporphinatoiron(III) chloride has shown that the iron atom can be considered

six co-ordinate as the displacement out-of-plane is very slight, 0.009 Å. By comparison the distances from the iron to the imidazole nitrogens were found to be 1.96 and 1.99 Å. The iron-porphine nitrogen distance was 1.99 Å.

In aqueous alkaline solution hemin is known to dimerize (Clark and Perkins, 1940; Cowgill and Clark, 1952; Davies, 1940; Inada and Shibata, 1962; Jordan and Bednarski, 1964; Maehly and Akeson, 1958). It has also been established that the monomer-dimer equilibrium is shifted in favour of the monomer in solutions containing a high concentration of ethanol (Davies, 1940; Jordan and Bednarski, 1964; Maehly and Akeson, 1958; Vestling, 1940; Davis and Martin, 1966). Maehly and Akeson (1958) found that 50 volume % ethanol caused the dimer to dissociate completely to the monomer. These observations were confirmed by the polarographic study of Davis and Martin (1966) which showed that hemin undergoes a reversible one electron reduction in aqueous ethanol. Thus, by working in aqueous ethanol solutions, complications due to dimer formation may be avoided. The kinetics of imidazole binding to hemin were studied in solutions that were 44.5 weight % in ethanol.

Imidazole is a part of the amino acid histidine and because of its properties it has been implicated in a number of enzyme reactions. The imidazole of histidine occupies the fifth co-ordination position of the iron of both myoglobin and hemoglobin. Ligand binding to heme proteins has been used as a probe to obtain information about the active site of proteins (Diven et al.; 1965;

Goldsack et al., 1966; Dunford and Alberty, 1967; Ellis and Dunford, 1968). It was felt that the binding of imidazole to hemin would provide a useful model for the binding of ligands to the heme proteins.

4.02 Experimental

Apparatus and Method

The kinetic measurements were conducted on a temperature-jump apparatus constructed in this laboratory and based on the concepts put forth by Eigen (1963). The electronic detection circuit, monochromator, light source and power supply were identical to those described elsewhere (Ellis and Dunford, 1968). The temperature jump was obtained by triggering the discharge of a high voltage capacitor (Plastic Capacitors Inc., LK 500-104 ZND, 0.1 μ F, 50 kV). The trigger module (TM-11) was obtained from E G & G Inc. The voltage for charging the capacitor was supplied by a Spellman high voltage power supply model 2040. The temperature-jump cell was constructed of Plexiglas and its geometry was such that 1 ml of solution was heated. Two quartz cylindrically shaped lenses provided for the transmission of light through the solution in the cell. The cell was constructed in such a way that it was possible to perform experiments on a minimum of 5 ml of solution. The cell fitted snugly into a brass thermostatic jacket enclosed in a light-tight cannister. The temperature-jump cell was thermostatically controlled at 19.0° and a voltage of 20.5 kV was discharged through the solution which was sufficient

to give a 6.0° rise in temperature.

A monochromator setting of 413 m μ was employed which corresponded to the maximum of the difference spectrum of the two absorbing species in solution. Changes in absorbance caused by the temperature perturbation were observed by monitoring the output voltage of a photo-multiplier circuit on an oscilloscope with a differential high gain d.c. amplifier. The relaxation curve was photographed from the oscilloscope screen. The single observed relaxation time, τ , was determined by the use of a photographic enlarger to match the negative of the oscilloscope trace with one of a series of exponential curves specially constructed for the purpose. A typical trace is shown in Figure (4.01). Further details concerning the construction of the temperature-jump apparatus are given by Ellis (1968).

Materials

Imidazole and hemin of White Label grade were obtained from Eastman Organic Chemicals and were used without further purification. The solvent, 44.5 weight % ethanol, was prepared from distilled, filtered, deionized water and reagent grade 95% ethanol. The stock hemin was prepared by dissolving hemin in 0.1M NaOH and diluting until the stock was 1.00×10^{-3} M in hemin and 1.0×10^{-2} M in NaOH. This stock solution was stored under refrigeration and from it freshly diluted solutions, 4.00×10^{-5} M in hemin, were prepared for each day's experiments. Kinetic and equilibrium measurements were conducted on

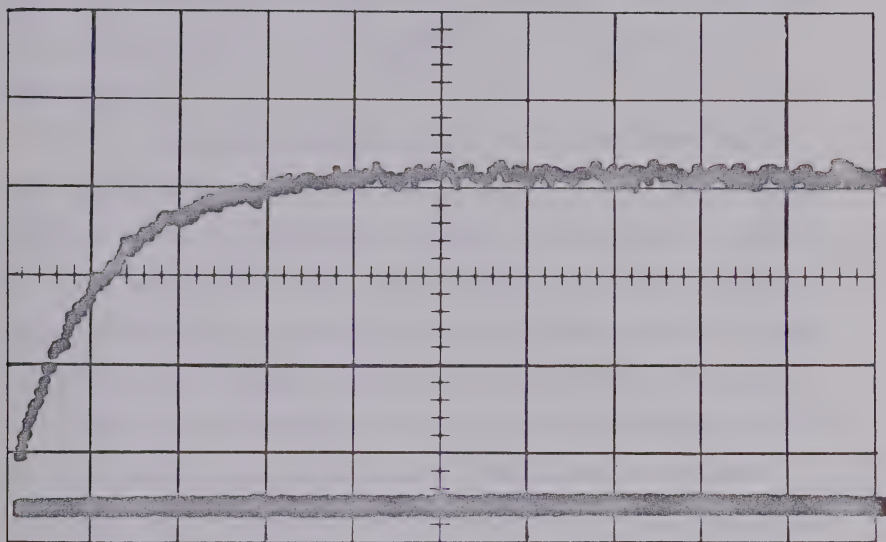


Figure 4.01: Oscilloscope trace of voltage vs. time. Concentration of hemin was $4.0 \times 10^{-6} \text{M}$ and of imidazole $1.2 \times 10^{-3} \text{M}$. The pH was 7.5 and ionic strength 0.11 with 0.01 contributed by maleate buffer. The horizontal scale is 1 msec/cm and the vertical scale 100 mV/cm. Monochromator setting was 413 m μ .

4.00×10^{-6} M hemin solutions within minutes of their preparation. For all experiments the imidazole concentration was at least 50 times larger than the hemin concentration. Thus the total concentration of imidazole in solution was very nearly equal to the equilibrium concentration of imidazole.

An operational pH scale was established using the method described by Bates et al. (1963). Their nomenclature is used in which the symbol pH^* is used for pH in a mixed aqueous solvent. An accurate measure of pH^* can be obtained with an aqueous glass pH electrode in a mixed aqueous solvent system provided the electrode is stored in a solution of composition, pH^* , and ionic strength similar to that used in the experiments. The glass electrode (Beckman long thin probe combination 38183) was stored and standardized with a triethanol ammonium chloride-triethanol-amine buffer of pH^* 7.05 (Bates et al., 1963). This electrode was used in combination with a Beckman Expanded Scale pH meter. All solutions contained a buffer contributing 0.01 to a total ionic strength of 0.11 with the remainder contributed by the inert electrolyte, KNO_3 . In the pH^* range 4.5 to 6.0 acetate buffer was used, 6.2 to 7.5 maleate buffer, 6.3 to 8.3 phosphate buffer, and 8.8 to 10.3 borate buffer.

N.M.R. Line Broadening Experiments

The n.m.r. spectra were run on 5 samples of hemin dissolved in 48.8 mole % aqueous ethanol in the

concentration range 1.25×10^{-3} to 5.00×10^{-3} M. The line broadenings were found to vary linearly with the concentration of hemin. Shifts were measured from the internal reference, sodium 3-(trimethylsilyl)-1-propanesulfonate (Eastman Organic Chemicals) which was dissolved at the minimum concentration for the detection of the methyl resonance signal. The line broadening data were obtained at pH* 11, but it was found that the line widths were independent of hydroxide ion concentration over the range 10^{-6} to 0.1M.

The n.m.r. spectra for the temperature study (Angerman et al., 1969) were run on a Varian A-56/60 spectrometer equipped with a variable temperature probe and temperature controller. All full linewidths at half height and chemical shifts were reproducible to ± 2 Hz. A Du Pont 310 Curve Resolver was used to separate the contribution of the water and the ethanol to the hydroxy proton resonance.

4.03 Results

Monomer-dimer Equilibrium

A spectrophotometric study was undertaken to determine the monomer-dimer equilibrium constant. For the equilibrium



where M represents monomer and D represents dimer, the equilibrium constant is given as:

$$K_1 = \frac{[D]}{[M]^2} \quad (4.02)$$

The extinction coefficient of the dimeric species and the monomeric species were determined in a 1.0×10^{-5} M solution of hemin at a wavelength of 400 mμ and at 5 and 64.8 mole % ethanol. It was assumed that the dimer is completely formed at 5 mole % ethanol and that the monomer is the only species in 64.8 mole % ethanol. The equilibrium constant, K_1 , for the dimerization, was calculated from absorbance measurements on solutions 5.0×10^{-3} M in hemin and 48.8 mole % ethanol, the solvent for the n.m.r. study. The values for K_1 at 25.0° and 34.8° are 25 and 34 M^{-1} for the solvent composition used in the n.m.r. study. Therefore there is about 10% of the hemin present as dimer under the conditions of the n.m.r. study. Similarly, K_1 was measured to be 140 and 520 M^{-1} at 25.0 and 34.8° respectively under the conditions used in the temperature-jump study. The dimer concentration in the more dilute solutions used in the temperature-jump study is calculated to be about 0.1% of the total concentration of hemin and is insignificant. Furthermore at a constant pH* the hemin solutions were found to obey Beer's law for a single absorbing species in solution over an appreciable range of hemin concentrations, indicating that the hemin species did not change as a function of concentration.

The Acid Dissociation on Hemin

An acid dissociation constant on hemin was

measured by spectrophotometric titration. From a pH^* of 8 to a solution 3.6 M in NaOH no significant spectral changes were noted in the Soret band at 400 m μ of hemin solutions. Using the absorbance of an alkaline solution as a reference, it was possible by using the method of Coward and Kiser (1966) to show that the absorbance changes corresponded quite closely to that for a single proton dissociation with an acid association constant of pK_a 6.63. For the equilibrium,



where M and MOH are hemin and the presumed hydroxy hemin, the acid dissociation constant is defined as:

$$K_a = \frac{[\text{MOH}][\text{H}^+]}{[\text{M}]} \quad (4.04)$$

The titration results, plotted as the fraction of the protonated species present, α , vs. pH^* are shown in Figure (4.02). Below a pH^* value of 5.8, solutions of hemin were observed to precipitate upon standing. Thus it was impossible to obtain absorbance readings corresponding to complete conversion to the acid form of hemin. The scatter in the data points in Figure (4.02) below pH^* 5.8 are caused by the unstable hemin solution. No attempt was made to measure possible pK' s occurring in more acid solutions and kinetic experiments were not conducted below pH^* 6.00.

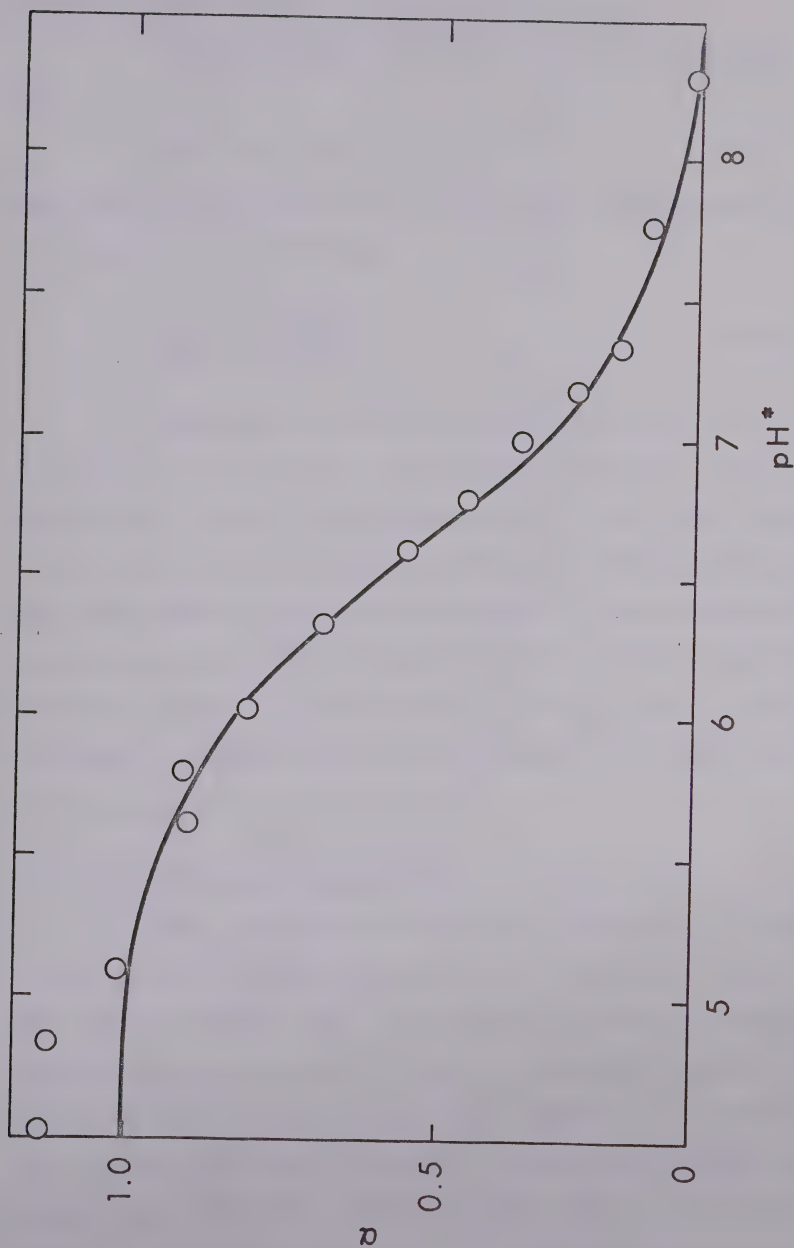


Figure 4.02: Plot of, α , the fraction of protonated hemin present, vs. pH^* . The solid line is a theoretical sigmoid curve for the dissociation of a single proton from an acid group with a pK of 6.63.

The Acid Dissociation of the Imidazolium Ion

The acid dissociation constant of imidazolium ion,



where ImH^+ and Im are the protonated and unprotonated forms of imidazole, is given by:

$$K_{\text{ImH}} = \frac{[\text{Im}][\text{H}^+]}{[\text{ImH}^+]} \quad (4.06)$$

The acid dissociation constant, K_{ImH} , was measured in 44.5 weight % ethanol at a constant ionic strength of 0.11 and at a temperature of 25.0°, by titrating a solution of 0.01 M imidazole with concentrated HNO_3 so that the volume changeover the course of the titration was negligibly small. The inflection point of the sigmoidal titration curve (a plot of pH^* vs. volume of HNO_3 added) indicated the acid dissociation constant of imidazolium ion, K_{ImH} , to be 1.8×10^{-7} M.

The Hemin-Imidazole Equilibrium

When imidazole is added to a solution of hemin, large spectral changes occur as shown in Figure (4.03). The spectra exhibit four well-defined isosbestic points indicating the presence of only two absorbing species in solution which, as discussed below, appear to be hemin and the bisimidazole hemin complex. No spectral evidence could be obtained for the existence of the singly co-ordinated species, monoimidazole hemin. If the state of ionization

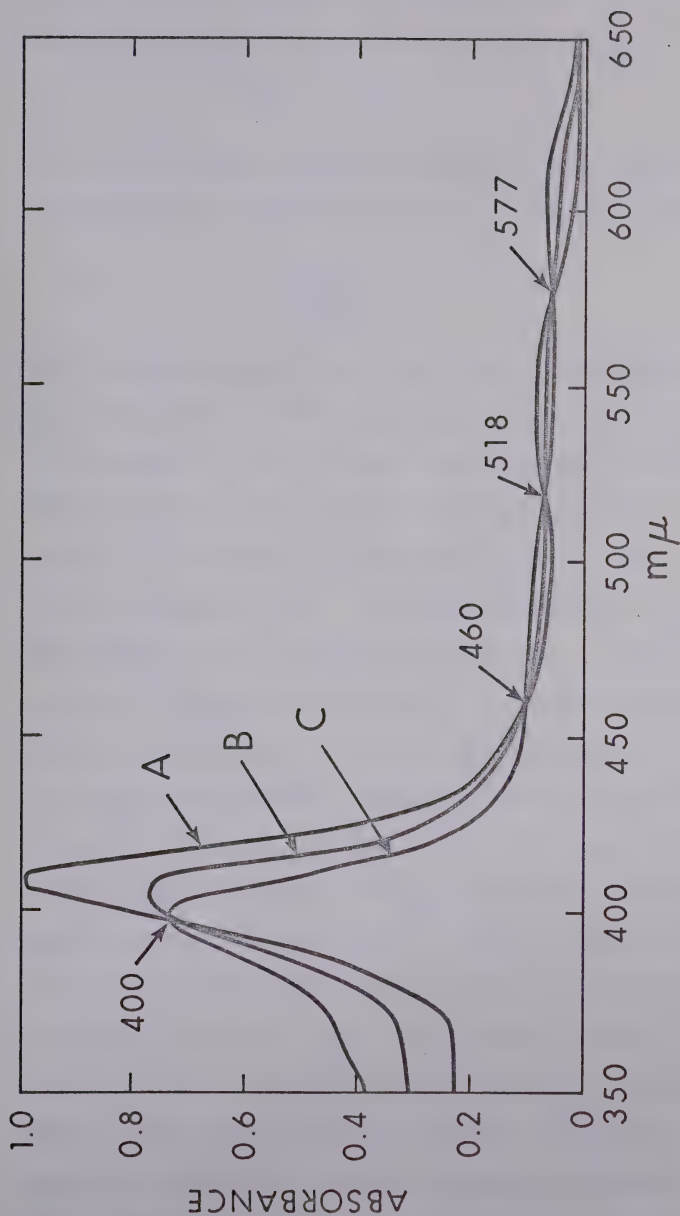


Figure 4.03: Plot of absorbance vs. wavelength in $m\mu$ for concentration of hemin was $8.0 \times 10^{-6} M$ and concentrations of imidazole for curves, C, B, and A were 0, 1×10^{-3} and $1 \times 10^{-2} M$. The pH^* was 7.6 and the ionic strength 0.11. Curve A is the spectrum of fully complexed bisimidazole hemin.

of the various species is neglected the association of hemin and imidazole may be represented as:



The corresponding apparent association constant, apparent because it is a function of pH^* , is given by the expression:

$$K_{app} = \frac{[MIm_2]}{[M] [Im]^2} \quad (4.08)$$

The bracketed quantities with bars indicate equilibrium concentrations. The proof that the equilibrium expression of equation (4.08) is valid was obtained by two methods. The slope of a plot of $\log [(A_R - A_S)/(A_S - A_\infty)]$ indicates the number of molecules of imidazole binding to a molecule of hemin (Scheler, 1960). The quantities A_R , A_S and A_∞ are the absorbances of hemin solutions in a 1 cm cuvette with no added imidazole (reference), a known amount of imidazole added (sample) and a large excess of imidazole added such that the bisimidazole complex is completely formed. The slope of a typical plot is shown in Figure (4.04) and has a value of 1.9 which, within experimental error, confirms equations (4.07) and (4.08). Also if equation (4.08) is the valid equilibrium expression a plot of $\Delta A/[Im]^2$ vs. ΔA should be linear with the absolute value of the slope equal to the association constant, K_{app} , (Coward and Kiser, 1966). The quantity ΔA is $(A_S - A_R)$. This type of linear plot is useful when a large excess of ligand is required for complete formation of the complex. Linear plots were

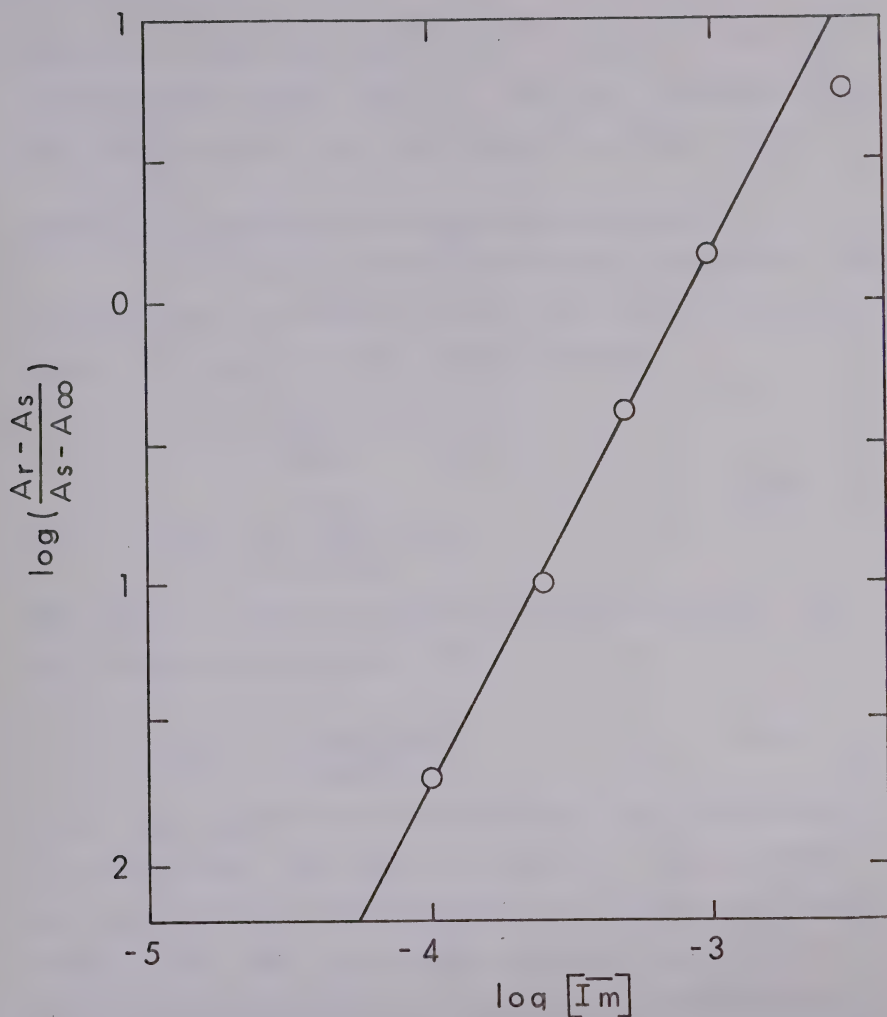


Figure 4.04: Plot of $\log [(A_r - A_s)/(A_s - A_\infty)]$ vs. $\log [\text{Im}]$.

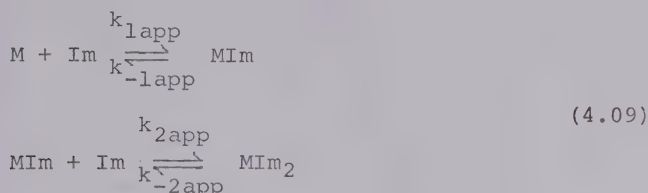
The concentration of hemin was 4.0×10^{-6} M. The pH^* was 7.5

The slope of 1.9 indicates that 2 moles of imidazole co-ordinate per molecule of hemin.

obtained over the entire pH* range. A typical example is shown in Figure (4.05). The K_{app} data as a function of pH* are listed in Table (4.01) and plotted in Figure (4.06).

Kinetics of the Hemin-Imidazole Binding Reaction

The overall reaction represented in equation (4.07) may be written as occurring in two steps, again neglecting states of ionization of the species involved:



The relation between the association constant, K_{app} , and the apparent rate constants is:

$$K_{app} = \frac{k_{1app}k_{2app}}{k_{-1app}k_{-2app}} \quad (4.10)$$

In all the temperature-jump experiments only one relaxation, τ , was observed. The observed values of τ were dependent upon the equilibrium concentrations of imidazole and ranged from 0.1 to 2 msec. The single relaxation time and the lack of any spectroscopically observable intermediate provides evidence that the steady state approximation for the intermediate is valid:

$$\frac{d[MIm]}{dt} = 0 \quad (4.11)$$

Without the steady state approximation two relaxation times would be expected (Alberty et al., 1963). The reciprocal

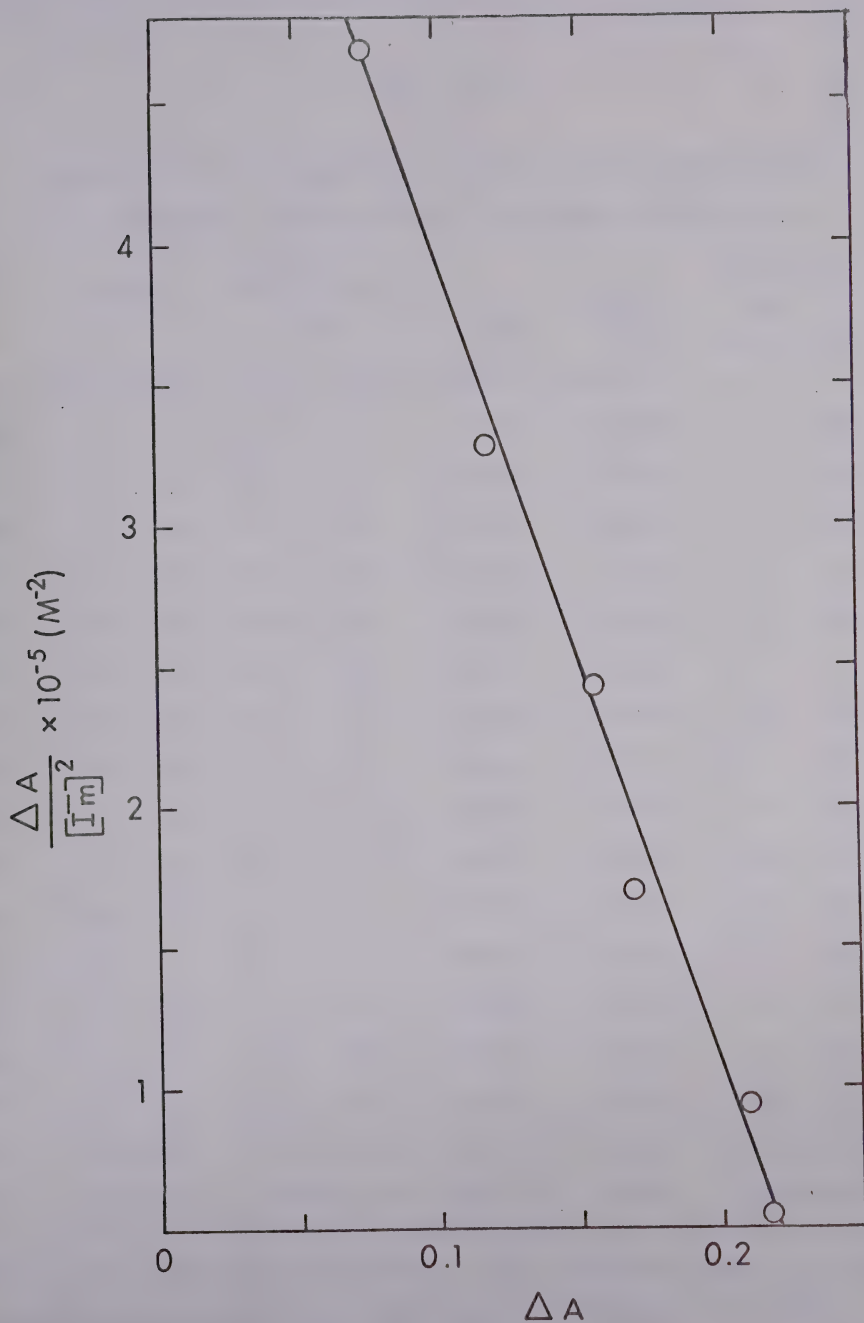


Figure 4.05: Plot of $\Delta A/[\text{Im}]^2$ vs. ΔA . Concentration of hemin was $4.0 \times 10^{-6} \text{ M}$. The pH^* was 6.7. K_{app} from the slope of the line is $2.8 \times 10^6 \text{ M}^{-2}$.

Table 4.01

Apparent Rate and Equilibrium Constants for the Binding
Of Imidazole to Hemin at 25° and Ionic Strength 0.11

pH*	k_{1app} $\times 10^{-6}$ ($M^{-1}sec^{-1}$)	Spectro- photometric K_{app} $\times 10^{-6}$ (M^{-2})	k_{-2app} (sec^{-1})	$\frac{k_{2app}}{k_{-1app}}$ (M^{-1})	Kinetic K_{app} $\times 10^{-6}$ (M^{-2})
6.00	0.75 \pm .15	0.76 \pm .08	470 \pm 260	220 \pm 340	1.6 \pm 0.6
6.20	0.92 \pm .09	1.2 \pm .1	580 \pm 40	330 \pm 80	1.1 \pm 0.9
6.40	1.12 \pm .11	1.6 \pm .2	710 \pm 50	640 \pm 120	0.7 \pm 0.6
6.62	1.40 \pm .14	2.4 \pm .2	650 \pm 20	510 \pm 50	1.4 \pm 0.4
6.70	1.44 \pm .14	2.8 \pm .3	650 \pm 70	620 \pm 180	1.0 \pm 0.4
6.70	1.44 \pm .14	2.6 \pm .3	760 \pm 70	880 \pm 220	0.7 \pm 1.1
6.80	1.46 \pm .15	2.8 \pm .3	480 \pm 100	90 \pm 260	0.15 \pm 0.13
6.90	1.34 \pm .13	3.2 \pm .3	720 \pm 50	1370 \pm 170	6.5 \pm 7.5
7.12	1.40 \pm .14	3.5 \pm .3	640 \pm 90	720 \pm 290	1.0 \pm 0.6
7.30	1.15 \pm .11	2.0 \pm .2	580 \pm 70	440 \pm 160	0.36 \pm 0.04
7.53	0.88 \pm .09	1.5 \pm .1	550 \pm 10	510 \pm 30	2.0 \pm 0.6
7.76	0.74 \pm .07	1.2 \pm .1	550 \pm 40	520 \pm 90	1.3 \pm 1.0
7.79	0.64 \pm .06	1.0 \pm .1	440 \pm 80	400 \pm 210	1.1 \pm 3.6
8.32	0.26 \pm .03	0.35 \pm .03	410 \pm 20	650 \pm 60	0.9 \pm 0.2
8.82	0.12 \pm .01	0.11 \pm .01	340 \pm 30	270 \pm 40	0.23 \pm 0.27
9.72	0.042 \pm .004	0.0095 \pm .001	290 \pm 30	26 \pm 10	0.024 \pm 0.043
10.30	0.028 \pm .003	0.0069 \pm .001	359 \pm 100	70 \pm 30	0.0012 \pm 0.011

Error limits given are the standard error except on the k_{1app} and the spectrophotometric K_{app} data which are estimated at $\pm 10\%$.

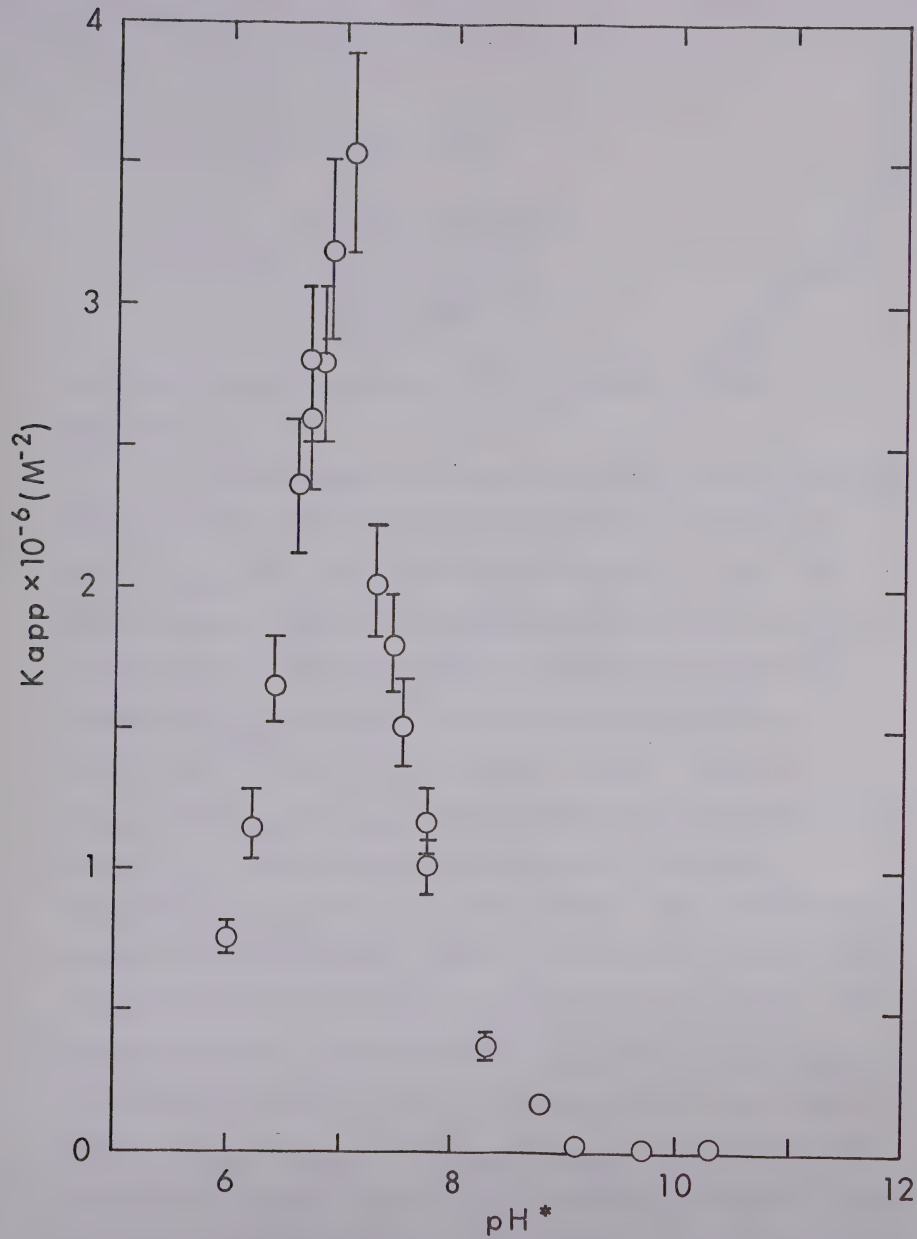


Figure 4.06: Plot of K_{app} vs. pH^* . Error limits given are estimates.

relaxation time is given by:

$$\frac{1}{\tau} = \frac{k_{-2app} + \frac{k_{2app}k_{1app}}{k_{-1app}} [\overline{Im}]^2}{1 + \frac{k_{2app}}{k_{-1app}} [\overline{Im}]} \quad (4.12)$$

The derivation of equation (4.12) is given in full in Appendix 4.

Under conditions where the equilibrium imidazole concentration is large, equation (4.12) is reduced to $1/\tau = k_{1app}[\overline{Im}]$. Therefore from plots of $1/\tau$ vs. $[\overline{Im}]$ the limiting slope at large $[\overline{Im}]$ yields values of k_{1app} . A typical limiting slope plot is shown in Figure (4.07). Values of k_{1app} obtained in this way are plotted in Figure (4.08) and listed in Table (4.01). Values of k_{-2app} and k_{2app}/k_{-1app} were computed from equation (4.12) using K_{app} from the spectrophotometric titration, τ , and $[\overline{Im}]$ as input data for a non-linear least squares program (IBM Share Library, 1964). A complete listing of the program as well as its use is given by Ellis (1968). The values found for the parameters k_{-2app} and k_{2app}/k_{-1app} are listed in Table (4.01). In addition the three parameters, K_{app} , k_{-2app} , and k_{2app}/k_{-1app} , were regarded as unknown parameters and best fit values were obtained using the same computer program. The values of K_{app} obtained in this way are listed in Table (4.01) also. Additional proof of the validity of the steady state assumption and equation (4.12) is the observed behavior of the reciprocal relaxation

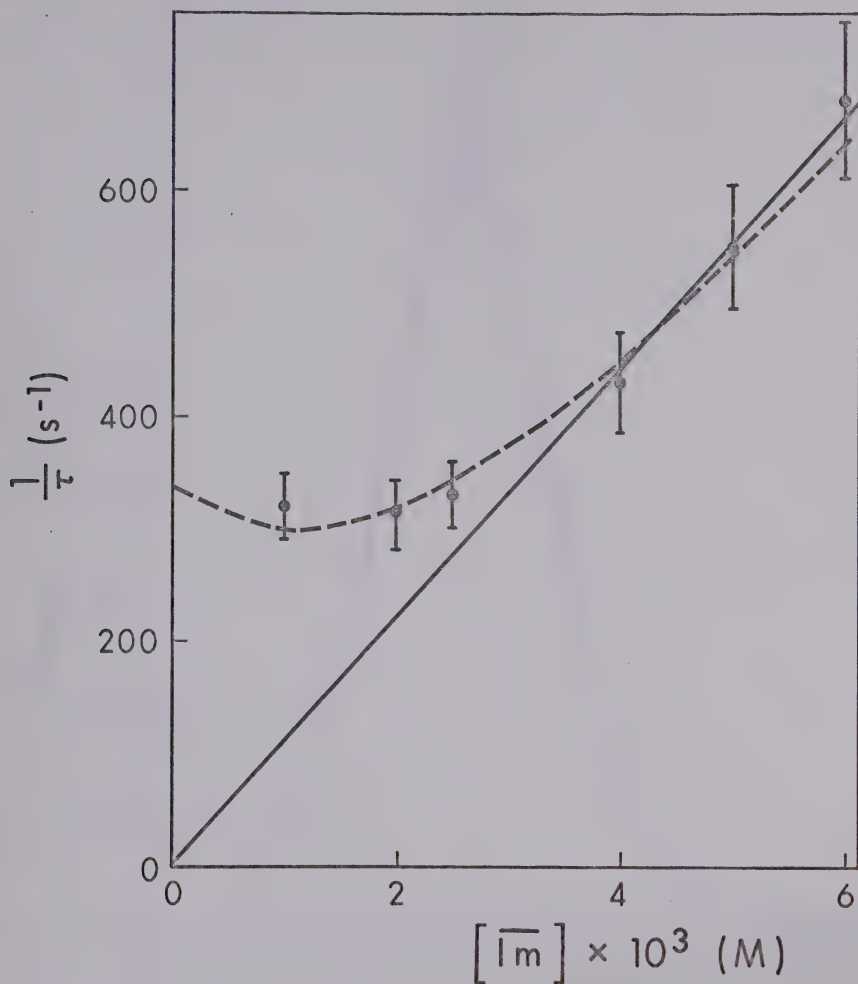


Figure 4.07: Plot of $1/\tau$ vs. $[\overline{Im}]$ for imidazole binding to hemin at $pH^* 8.82$. The solid line is an estimated limiting slope and the dashed line was computed from eq. (4.12) using K_{app} determined spectrophotometrically and best-fit values for k_{-2app} and k_{2app}/k_{-1app} .

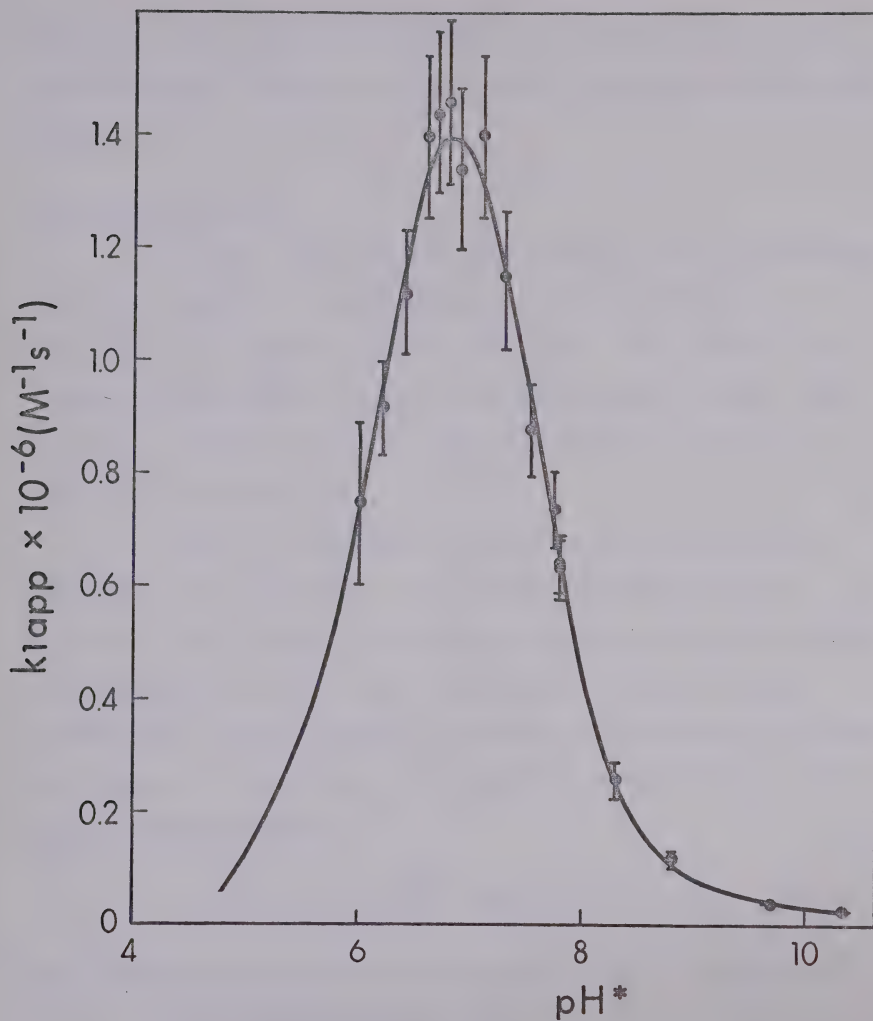


Figure 4.08: Plot of k_{lapp} vs. pH^* . The solid line is that predicted using the best four-parameter fit to equation (4.20). The circles are experimental points and error limits are estimated.

time, $1/\tau$, as a function of $[\overline{\text{Im}}]$ as in Figure (4.07) and the successful fitting of the $1/\tau$ and $[\overline{\text{Im}}]$ data to equation (4.12)

The N.M.R. Results

It was observed that the solvent n.m.r. resonances had their natural linewidths when a 100 fold excess of imidazole was added to a hemin solution. This result confirms that imidazole binds to the paramagnetic center and displaces solvent molecules from the inner co-ordination sphere of the metal ion.

From an analysis of the transverse relaxation time, T_{2p} , of the methyl ($-\text{CH}_3$) and methylene ($-\text{CH}_2-$) protons of the ethanol as a function of the water to ethanol concentration ratio it was concluded by Angerman et al. (1969) that the replacement of water or hydroxide by ethanol or ethoxide in the first co-ordination sphere of the iron may be represented by:



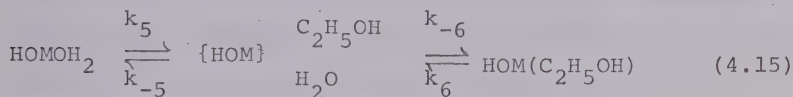
The equilibrium constant for equation (4.13) is given as:

$$K_4 = \frac{[\text{H}_2\text{O}][\text{HOM}(\text{C}_2\text{H}_5\text{OH})]}{[\text{C}_2\text{H}_5\text{OH}][\text{HOMOH}_2]} \quad (4.14)$$

and was found to have a value of 8.7 at 35° (Angerman et al., 1969). If it is assumed that this value of K_4 is independent of temperature then it can be estimated that under the conditions of the n.m.r. temperature study

the hemin is 90% in the ethanol form. Similarly under the conditions of the temperature-jump study the hemin is 70% in its ethanol form.

The analysis of the temperature dependence of the line broadening data indicated that the average rate constant for ethanol exchange is $1.8 \times 10^6 \text{ sec}^{-1}$ and for water exchange $6 \times 10^5 \text{ sec}^{-1}$ both at 25° (Angerman et al., 1969). It was also concluded that if a limiting S_N1 mechanism is assumed for the solvent exchange then the mechanism can be represented by:



It also follows that:

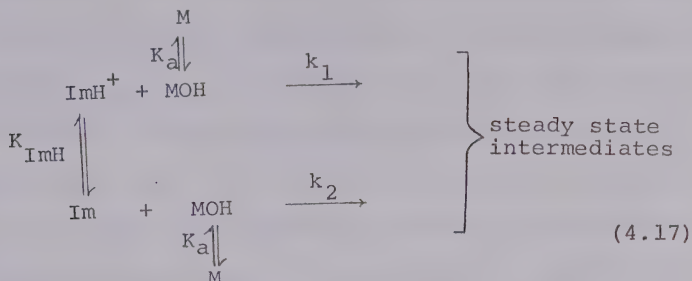
$$K_4 = \frac{k_5 k_{-6}}{k_{-5} k_6} = 8.7 \quad (4.16)$$

The values of k_5 and k_6 are at 25° , $6 \times 10^6 \text{ sec}^{-1}$ and $1.8 \times 10^6 \text{ sec}^{-1}$ therefore k_{-6}/k_{-5} is approximately 25. The high ratio of k_{-6}/k_{-5} is not consistent with the known nucleophilic order of water and ethanol may be due to preferential solvation of the hemin by ethanol in the outer co-ordination spheres.

4.04 Discussion

There are two kinetically indistinguishable reactions which explain successfully the pH^* dependence of

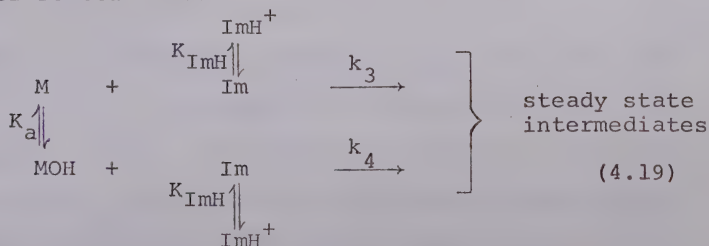
the k_{lapp} rate data. In one imidazole and imidazolium ion are postulated to react only to the basic form of hemin:



The vertical arrows indicate fast non-rate determining proton transfer reactions in buffered solutions. The horizontal arrows indicate the slower rate determining association reactions. According to equation (4.17) the apparent forward rate constant is given by:

$$K_{\text{lapp}} = \frac{\frac{k_1 [\text{H}^+]}{\text{K}_{\text{ImH}}} + k_2}{\left(1 + \frac{[\text{H}^+]}{\text{K}_{\text{ImH}}}\right) \left(1 + \frac{[\text{H}^+]}{\text{K}_a}\right)} \quad (4.18)$$

The other reaction is:



for which k_{lapp} is:

$$k_{\text{lapp}} = \frac{\frac{k_3 [\text{H}^+]}{\text{K}_a} + k_4}{\left(1 + \frac{[\text{H}^+]}{\text{K}_{\text{ImH}}}\right) \left(1 + \frac{[\text{H}^+]}{\text{K}_a}\right)} \quad (4.20)$$

It is easily seen from a comparison of equations (4.18) and (4.20) that the equations are of an identical form; the parameter k_1/K_{ImH} in equation (4.18) corresponding to the parameter k_3/K_a in equation (4.20) and the parameter k_2 in equation (4.18) corresponding to the parameter k_4 in equation (4.20). The unknown parameters in equations (4.18) and (4.20) were determined using the non-linear least squares program that was modified to minimize the sums of the squares of the relative rather than absolute residuals. Several different approaches were taken in the determination of the unknown parameters. In the first, all four parameters of equation (4.18); k_1 , k_2 , K_{ImH} , and K_a were regarded as unknown and best fit values were obtained by non-linear least squares analysis. It is readily seen from equations (4.18) and (4.20) that the two equilibrium constants, K_{ImH} , and K_a are distinguishable due to the symmetry of these two equations. The results of the four-parameter analysis are listed in Table (4.02). In the next approach, all parameters excepting K_{ImH} , for which the value 1.8×10^{-7} M obtained by titration was used, were regarded as unknown. No ambiguity exists for the determination of K_a as existed with the four-parameter fit. The results obtained are listed in Table (4.02). The discrepancy in the value of K_a measured spectrophotometrically and from the analysis of the kinetic data may be due to the ethanol and water forms of hemin having different acid dissociation constants. The equilibrium could conceivably

Table (4.02)

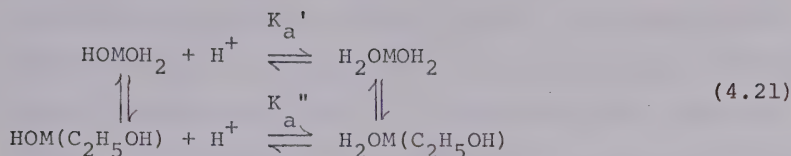
Rate and Equilibrium Constants Determined from
Non-linear Least Squares Analysis of pH* Dependence
of the k_{lapp} Data^{a,b}

Rate and Equilibrium Constants	Four Parameter Computer Fit	Three Parameter Computer Fit
k_1	$(2.4 \pm 0.2) \times 10^6 \text{ M}^{-1} \text{ sec}^{-1}$	$(8.8 \pm 0.5) \times 10^6 \text{ M}^{-1} \text{ sec}^{-1}$
k_2	$(2.7 \pm 0.2) \times 10^4 \text{ M}^{-1} \text{ sec}^{-1}$	$(2.9 \pm 0.2) \times 10^4 \text{ M}^{-1} \text{ sec}^{-1}$
k_3	$(2.4 \pm 0.2) \times 10^6 \text{ M}^{-1} \text{ sec}^{-1}$	$(4.4 \pm 0.2) \times 10^6 \text{ M}^{-1} \text{ sec}^{-1}$
k_4	$(2.7 \pm 0.2) \times 10^4 \text{ M}^{-1} \text{ sec}^{-1}$	$(2.9 \pm 0.2) \times 10^4 \text{ M}^{-1} \text{ sec}^{-1}$
K_a	$(4.8 \pm 0.8) \times 10^{-7} \text{ M}$	$(9.1 \pm 0.8) \times 10^{-8} \text{ M}$
K_{ImH}	$(4.1 \pm 0.5) \times 10^{-8} \text{ M}$	-

^a Errors on the parameters are the standard errors obtained for the parameter estimated by the non-linear least squares computer program.

^b Values of K_a and K_{ImH} in the four-parameter analysis are interchangeable giving an equivalent fit to the k_{lapp} data as explained in the text.

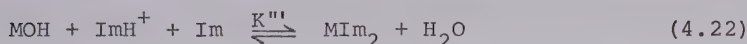
be of the type:



The value of the measured K_a would be a combination of K_a' and K_a'' . It is known from the n.m.r. data that water and ethanol undergo different rates of exchange from that of the hydroxy hemin species (Angerman et al., 1969).

In addition, any reaction that is a combination of reaction (4.17) and (4.19) will provide an equally valid fit to the k_{lapp} data.

From an examination of the equilibrium data at least two sets of equilibria provide a rough explanation of the K_{app} data:



for which,

$$K_{\text{app}} = K''' (1 + [\text{H}^+]/K_a)^{-1} (1 + [\text{H}^+]/K_{\text{ImH}})^{-1} (1 + K_{\text{ImH}}/[\text{H}^+])^{-1} \quad (4.23)$$

and



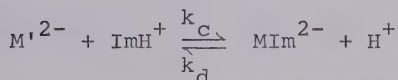
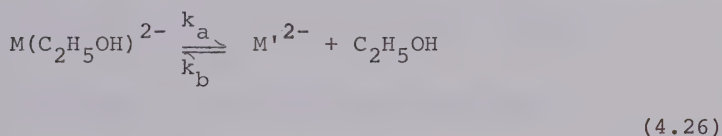
for which

$$K_{\text{app}} = K^{\text{iv}} (1 + [\text{H}^+]/K_{\text{ImH}})^{-2} (1 + K_a/[\text{H}^+])^{-1} \quad (4.25)$$

From a simple electrostatic consideration the presence of an OH^- ligand trans to the ethanol and water

on the two hemin species would be expected to have a labilizing influence on these ligands. For example the water exchange on $\text{Fe}(\text{OH}_2)_5\text{OH}^{2+}$ is faster than on $\text{Fe}(\text{OH}_2)_6^{3+}$ (Eigen and Wilkins, 1965). On this basis the reaction scheme (4.19) appears less plausible if the solvent exchange rate has an important influence on the rate of substitution.

If a S_N1 limiting mechanism or dissociation mechanism is considered (Seewald and Sutin, 1963) then the first reaction in (4.17) becomes:



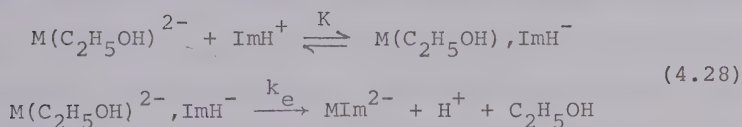
where M'^{2-} is a pentaco-ordinate intermediate and $\text{M}(\text{C}_2\text{H}_5\text{OH})^{2-}$ is hydroxyethanol hemin with only the most labile and prevalent ligand shown. The total charges on reactions (4.26) are shown as superscripts. Since no inhibition of the rate is observed at a large concentration of ligand (Sutin, 1966),

$$k_1 = \frac{k_a k_c}{k_b [\text{EtOH}]} \quad (4.27)$$

The value of k_a is $2 \times 10^6 \text{ sec}^{-1}$ from the n.m.r. results and an average $k_1 = 6 \times 10^6 / 0.7 = 9 \times 10^6 \text{ M}^{-1} \text{ sec}^{-1}$. The correction of 0.7 is applied to k_1 since the n.m.r. results indicated that the hemin is 70% in its ethanol form. The concentration of ethanol is 8.2 M so that k_c/k_b is predicted

to be approximately 40. This means that imidazolium ion is predicted to be 40 times better as a nucleophile than ethanol. Also as $k_1 \gg k_2$ the imidazolium ion is predicted to be a better nucleophile than imidazole. Both of these predictions are highly questionable. Similarly, if the same argument is applied to reaction (4.19) imidazole is again predicted to be approximately 20 times as good a nucleophile as ethanol - again a questionable prediction.

However if an ion pair mechanism is considered. the faster reaction in reaction (4.17) becomes



where K is the ion pair formation constant. The ligand substitution rate constant is, if the ion pair equilibrium is established rapidly:

$$k_1 = \frac{k_e K}{1 + K[Im]} \quad (4.29)$$

As there was no inhibition of the reaction at high imidazole concentrations equation (4.29) simplifies to:

$$k_1 = k_e K \quad (4.30)$$

Also if it is assumed that the rate of solvent exchange is not affected by the ion pair formation, (Sutin, 1966) then the exchange rate for ethanol is $k_e = 2 \times 10^6 \text{ sec}^{-1}$, and since $k_1 = 9 \times 10^6 \text{ M}^{-1} \text{ sec}^{-1}$ as before then

$K = 4 \text{ M}^{-1}$. The value of 4 M^{-1} is reasonable for an ion pair formed by a double and single oppositely charged species, as are the ImH^+ and hemin species. By comparison, the ion pair constant between the $\text{Co}(\text{NH}_3)_5\text{Cl}^{2+}$ and CH_3CO_2^- species has been measured directly to be 5 M^{-1} (Archer et al., 1965).

If solvent removal is faster in the ion pair, then the value found of K represents an upper limit. On a similar basis the "ion pair" constant for Im in reaction (4.17) is about 0.02 M^{-1} . A decrease in K is expected when a cation is replaced by a neutral ligand in the ion pair. Similarly, if an ion pair constant is calculated for reaction (4.19) values of K equal to 2 and 0.02 M^{-1} are obtained. The K of 2 M^{-1} is larger than that expected for an ion pairing between a neutral and charged species. Thus reaction (4.17) appears the most reasonable on the basis of the "ion pair" calculation.

Fleischer et al. (1968) have studied ligand binding to cobalt(III) hematoporphyrin IX presumably in monomeric form in aqueous solutions. Hematoporphyrin IX has two $\text{CH}_3\text{CH}(\text{OH})-$ substituents in place of the vinyl substituents in ferriprotoporphyrin IX. It can be shown that if a reaction scheme similar to reaction (4.09) is assumed for their cyanide-iron(III) hematoporphyrin IX reaction then their observed pseudo first order rate constant, k_{obs} , corresponds to $(\tau)^{-1}$. Similar behavior of

$(\tau)^{-1}$ and k_{obs} are observed at high ligand concentrations for both systems; a plot of k_{obs} or $1/\tau$ is linear with an intercept of zero. However Fleischer et al. (1968) were unable to observe any leveling off in k_{obs} as they operated at a much larger excess of ligand than in the temperature-jump experiments. They were able to obtain evidence for a limiting S_N1 ligand substitution mechanism for the cobalt but not the iron porphyrin.

The binding of imidazole to ferrimyoglobin, a heme protein containing the prosthetic group ferriproto-porphyrin IX, has been studied by Diven et al. (1965) and Goldsack et al. (1966). The apparent association rate constants were much smaller ($< 350 \text{ M}^{-1}\text{sec}^{-1}$) than those measured in this study presumably because of the hindered nature of the environment of the prosthetic group in ferri-myoglobin.

Bibliography

- Alberty, R.A., Yagil, G., Diven, W.F. and Takahashi, M. (1963), Acta Chem. Scand. 17, S34.
- Amdur, I. and Hammes, G.G. (1966a), Chemical Kinetics, New York, McGraw-Hill, p. 136.
- Amdur, I. and Hammes, G.G. (1966b), Chemical Kinetics, New York, McGraw-Hill, p. 62.
- Angerman, N.S., Hasinoff, B.B., Dunford, H.B. and Jordan, R.B. (1969), Can. J. Chem. 47, 3218.
- Archer, D.W., East, D.A., and Monk, C.B. (1965), J. Chem. Soc., 720.
- Balls, A.K., and Hale, W.S. (1934), J. Biol. Chem. 107, 767.
- Bates, R.G., Paabo, M. and Robinson, R.A. (1963), J. Phys. Chem. 67, 1833.
- Birk, J.P. (1969), J. Amer. Chem. Soc. 91, 3189.
- Blauer, G. and Ehrenberg, A. (1963), Acta Chem. Scand. 17, 8.
- Blumberg, W.E., Peisach, J., Wittenberg, B.A. and Wittenberg, J.B. (1968), J. Biol. Chem. 243, 1854.
- Brill, A.S. and Williams, R.J.P. (1961), Biochem. J. 78, 246.
- Brill, A.S. and Sandberg, H.E. (1968), Biophys. J. 8, 669.

Caldin, E.F. (1964a), Fast Reactions in Solution, New York, Wiley, p. 8.

Caldin, E.F. (1964b), Fast Reactions in Solution, New York Wiley, p. 39.

Caldin, E.F. (1964c), Fast Reactions in Solution, New York, Wiley, p. 29.

Chance, B. (1949a), Arch. Biochem. Biophys. 21, 416.

Chance, B. (1949b), Arch. Biochem. Biophys. 22, 224.

Chance, B. (1952a), Arch. Biochem. Biophys. 41, 404.

Chance, B. (1952b), Arch. Biochem. Biophys. 37, 235.

Chance, B. (1952c), Arch. Biochem. Biophys. 41, 416.

Chance, B. (1952d), Arch. Biochem. Biophys. 40, 153.

Chance, B. (1963a), in Techniques in Organic Chemistry, Vol. VIII, Part II, p. 1343.

Chance, B. (1963b), in Techniques in Organic Chemistry, Vol. VIII, Part II, p. 728.

Chance, B. (1964a), Rapid Mixing and Sampling Techniques in Biochemistry, New York, Academic Press, p. 39.

Chance, B. (1964b), Rapid Mixing and Sampling Techniques in Biochemistry, New York, Academic Press, p. 125.

- Chance, B., De Vault, D., Legallais, U., Mela, L. and Yonetani, T. (1967), *Fast Reactions and Primary Processes in Chemical Kinetics*, Stockholm, Interscience Publishers, p. 437.
- Cormier, M.J. and Prichard, P.M. (1968), J. Biol. Chem. 243, 4706.
- Clark, W.M. and Perkins, M.E. (1940), J. Biol. Chem. 135, 643.
- Coryell, C.D., Stitt, F. and Pauling, L. (1937), J. Amer. Chem. Soc. 59, 633.
- Countryman, R., Collins, D.M. and Hoard, J.C. (1969), J. Amer. Chem. Soc. 91, 5166.
- Coward, N.A. and Kiser, R.W. (1966), J. Phys. Chem. 70, 213.
- Cowgill, R.W. and Clark, W.M. (1952), J. Biol. Chem. 198, 33.
- Czerlinski, G.H. (1966a), *Chemical Relaxation*, New York, Marcel Dekker Inc., p. 292.
- Czerlinski, G.H. (1966b), *Chemical Relaxation*, New York, Marcel Dekker Inc., p. 275.
- Davies, T.H. (1952), J. Biol. Chem. 198, 33.
- Davis, D.G. and Martin, R.F. (1966), J. Amer. Chem. Soc. 88, 1365.
- Dempsey, B., Lowe, M.B. and Phillips, J.N. (1961), in *Haematin Enzymes*, Falk, J.E., Lemberg, R. and Mortin, K.K.,

Eds., London, Pergamon, p. 29.

Diven, W.F., Goldsack, D.E. and Alberty, R.A. (1965), J. Biol. Chem. 240, 2437.

Dixon, M. and Webb, E.C. (1964), *Enzymes*, 2nd Ed, London Longmans, Green, p. 116.

Dolman, D. (1969), Personal communication.

Dolman, D., Dunford, H.B., Chowdhury, D.M. and Morrison, M. (1968), Biochemistry 7, 3991.

Dunford, H.B. and Alberty, R.A. (1967), Biochemistry 6, 447.

Eigen, M. and Hammes, G.G. (1963), Advan. Enzymol. 25, 1.

Eigen, M. and de Maeyer, L. (1963) in *Techniques in Organic Chemistry*, Vol. VIII, Part II, p. 895.

Eigen, M. Wilkins, R.G. (1965), in *Mechanisms of Inorganic Reactions*, ACS Monograph Series, p. 64.

Ellis, W.D. (1968), Ph.D. Thesis, University of Alberta, Edmonton.

Ellis, W.D. and Dunford, H.B. (1968), Biochemistry 7, 2054.

Ellis, W.D. and Dunford, H.B. (1969), Arch. Biochem. Biophys. 133, 313.

Evett, M.K. (1968), Dissertation, University of California, Berkeley.

Falk, J.E. (1964), *Porphyrins and Metalloporphyrins*, New York, Elsevier Publishing Co.

Fleischer, E.B., Jacobs, S. and Mestichelli, L. (1968), J. Amer. Chem. Soc. 90, 2527.

Frost, A.A. and Pearson, R.G. (1961), *Kinetics and Mechanism*, 2nd ed., New York, John Wiley and Sons Inc., p. 16.

Gallagher, W.A. and Elliott, W.G. (1965), Biochem. J. 97, 187.

Gallagher, W.A. and Elliott, W.B. (1967), Biochem. J. 105, 461.

Gallagher, W.A. and Elliott, W.B. (1968), Biochem. J. 108, 131.

George, P. (1952), Nature 169, 612.

George, P. (1953a), Biochem. J. 54, 267.

George, P. (1953b), J. Biol. Chem. 201, 413.

George, P. (1953c), Biochem. J. 55, 220.

Getchell, R.W. and Walton, J.H. (1931), J. Biol. Chem. 91, 419.

Gibson, Q.H. (1954), Discussions Faraday Society 17, 137.

Goldsack, D.E., Eberlein, W.S. and Alberty, R.A. (1966), J. Biol. Chem. 241, 2653.

Hammes, G.G. (1968a) in *Advances in Protein Chemistry*, Vol. 23, Academic, p. 1.

Hammes, G.G. (1968b) in *Advances in Protein Chemistry*, Vol. 23, Academic, p. 12.

- Harbury, H.A. (1957), J. Biol. Chem. 225, 1009.
- Harbury, H.A. and Loach, P.A. (1960), J. Biol. Chem. 235, 3646.
- Hartridge, H. and Roughton, F.J.W. (1923), Proc. Roy. Soc. Ser. A 104, 376.
- Hasinoff, B.B., Dunford, H.B. and Horne, D.G. (1969), Can. J. Chem. 47, 3225.
- Hoard, J.L., Cohen, G.H. and Glick, M.D. (1967), J. Amer. Chem. Soc. 89, 1992.
- IBM SHARE Library (1964), Program SDA 3094.
- Inada, Y. and Shibata, K. (1962), Biochem. Biophys. Res. Comm. 9, 323.
- Jordan, J. and Ewing, G.J. (1962), Inorg. Chem. 1, 587.
- Jordan, J. and Bednarski, T.M. (1964), J. Amer. Chem. Soc. 86, 5690.
- Kasinky, H.E. and Hackett, D.P. (1968), Phytochemistry 7, 1147.
- Keilin, D. and Mann, T. (1937), Proc. Roy. Soc. B 122, 199.
- Keilin, J. (1949), Biochem. J. 45, 448.
- Keilin, D. and Hartree, E.F. (1951), Biochem. J. 49, 88.
- Koenig, D.F. (1965), Acta Cryst. 18, 663.

- Kuhn, R., Hand, D. and Florkin, M. (1931), Z. Physiol. Chem. 201, 255.
- Maehly, A.C. (1953), Arch. Biochem. Biophys. 44, 430.
- Maehly, A.C. (1958), Acta Chem. Scand. 12, 1254.
- Moss, T.H., Ehrenberg, A. and Bearden, A.J. (1969), Biochemistry 8, 4159.
- Nobbs, C.L., Watson, H.C. and Kendrew, J.C. (1966), Nature 209, 339.
- Ovenston, T.C. and Rees, W.T. (1950), Analyst (London) 75, 204.
- Paul, K.G. (1958), Acta Chem. Scand. 12, 1312.
- Paul, K.G. (1963), in The Enzymes, Vol. 8, Part B, 2nd ed., Boyer, P.D., Hardy, H. and Myrback, K. Eds., New York, p. 227.
- Pauling, L. and Coryell, C.D. (1936), Proc. Natl. Acad. Sci. U.S. 22, 159.
- Peisach, J., Blumberg, W.E., Wittenberg, B.A. and Wittenberg, J.B. (1968), J. Biol. Chem. 243, 1871.
- Phillips, J.N. (1960), Rev. Pure Appl. Chem. 10, 35.
- Planche (1810), Bull. Phar. 2, 578.
- Ramette, R.W. and Sandford, R.W. (1963), J. Amer. Chem. Soc. 87, 5001.

Rawlinson, W.A. and Scutt, P.B. (1952), Aus. J. Sci. Res. 5, 173.

Roughton, F.J.W. (1963), in *Techniques in Organic Chemistry*, Vol. VIII, Part II, 2nd ed., New York, Interscience, p. 704.

Saunders, B.C., Holmes-Siedle, A.G. and Stark, B.P. (1964), *Peroxidase*, London, Butterworths.

Seewald, D. and Sutin, N. (1963), Inorg. Chem. 2, 643.

Scheler, W. (1960), Biochem. Z. 332, 542.

Shack, J. and Clark, W.M. (1947), J. Biol. Chem. 171, 143.

Shannon, L.M, Kay, E. and Lew, J.Y. (1966), J. Biol. Chem. 241, 2166.

Smith, J.H.C. (1957), *Proceedings of the 2nd International Congress of Photobiology*, Minerva Medica, Turin, p. 333.

Strittmatter, P. (1964) in *Rapid Mixing and Sampling Techniques in Biochemistry*, Chance, B., Eisenhardt, R.H., Gibson, Q.H. and Lonberg-Holm, K.K. Eds., New York, Academic Press, p. 71.

Sutin, N. (1966), Ann. Rev. Phys. Chem. 17, 119.

Theorell, H. (1941), Enzymologia 10, 250.

Theorell, H. (1942), Arkiv. Kemi. Mineral. Geol 16A, No. 2.

Theorell, H. and Paul, K.G. (1944), Arkiv. Kemi. Mineral.

Geol. 18A, No. 2.

Tohjo, M. and Shibata, K. (1963), Arch. Biochem. Biophys.
103, 401.

Vestling, C.S. (1940), J. Biol. Chem. 135, 623.

Wilder, C.J. (1962), J. Food Sci. 27, 567.

Appendix 1

The Analysis of Second Order Kinetic Data Obtained
on a Stopped-Flow Apparatus

In the study of a second order reaction such as:



for which the rate law is:

$$\frac{dx}{dt} = k[A][B] \quad (A1.02)$$

where x is the concentration of B that has reacted at time t , it is experimentally advantageous to study the reaction if possible by pseudo first order kinetics. Under conditions where one of the reactants is in much greater excess than the other and remains effectively constant throughout the course of the reaction, it is not necessary to know the concentration of the other reactant but only, some physically measurable quantity that is directly proportional to it. When the reaction rate becomes fast, however, (reaction half time less than 10 msec) it becomes necessary to lower the concentration, of the reactant that is in excess, to slow the reaction. The treatment of the data is different since pseudo first order conditions no longer exist.

A method was developed with a consideration for the experimental limitations imposed by the stopped-flow apparatus that used the integrated second order rate

expression (Frost and Pearson, 1961):

$$\frac{1}{(a-b)} \ln \frac{b(a-x)}{a(b-x)} = kt \quad (\text{Al.03})$$

where a and b are the initial concentrations of A and B.

For the following derivation the following assumptions are made:

1. $a > b$
2. A is assumed not to absorb appreciably compared to B
3. Voltage changes as specified are proportional to absorbance changes which is true if absorbance changes are less than 0.02 absorbance units.

Figure (Al.01) is a hypothetical stopped-flow oscilloscope trace where the voltage output of a photomultiplier circuit is measured as a function of time. The axes represented by the solid straight lines do not represent the true zero time or the true base line at infinite time.

Starting from the left of the oscilloscope trace, the nearly vertical solid line marks the start of the flow. The long horizontal portion of the trace is the "driving time"; the time period over which the flow exists and has been experimentally measured to be about 55 msec. The break in the horizontal portion of the trace, where the vertical axis is placed, marks the point at which the flow is stopped. However it does not represent the true start of the reaction as the reactants are mixed not in the

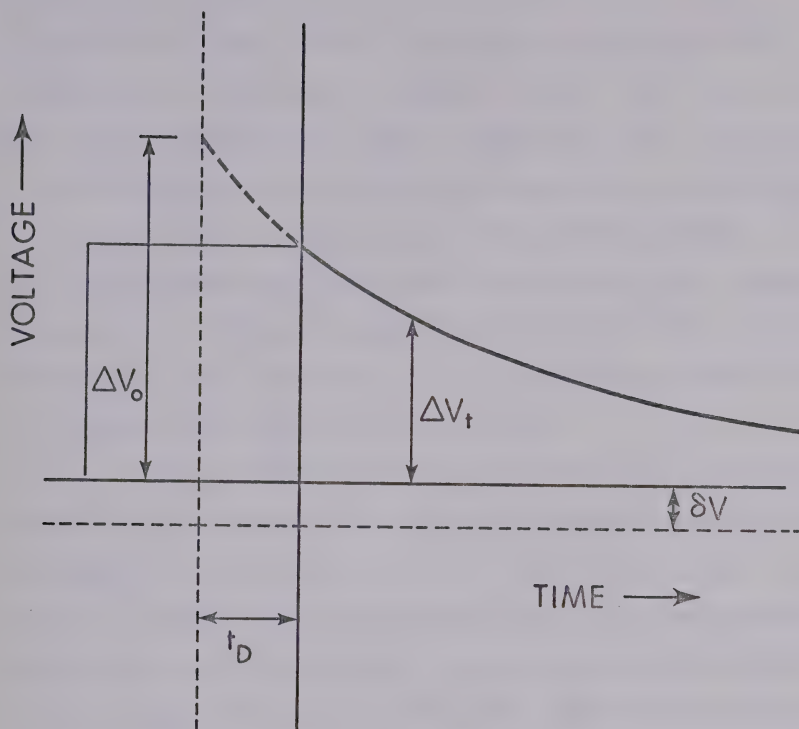


Figure A1.01: A hypothetical stopped-flow oscilloscope trace of voltage vs. time. The solid axes represent the arbitrarily places axes and the dashed axes indicate the true axes at the true zero time and the true base line.

observation chamber but in the mixing chamber. The time that it takes for the reactants to flow from the mixing to the observation chamber is the "dead time", t_D , and was measured to be 5 msec. These and other parameters that characterize the stopped-flow apparatus are discussed in greater detail in Chapter 2. The voltage change, ΔV_t , at the arbitrary zero time does not represent the voltage change due to 100% B present. The voltage change corresponding to 100% B present, ΔV_o , is therefore hidden due to the finite dead time of the apparatus.

The parameter δV represents the error present in choosing the true baseline which is theoretically attained at infinite time or not at all if the product formed decomposes. The horizontal solid line is the arbitrary base line from which the quantity ΔV_t is measured and differs from the true base line by the amount δV , which can be positive or negative. To each of the quantities ΔV_t and ΔV_o is thus added the correction δV . It follows then that the fraction that the voltage change has been decreased is the fraction of x that has formed, hence:

$$x = b \left(1 - \left(\frac{\Delta V_t + \delta V}{\Delta V_o + \delta V} \right) \right) \quad (A1.04)$$

Solving for x in equation (A1.04):

$$x = \frac{ab(e^{(a-b)kt} - 1)}{(ae^{(a-b)kt} - b)} \quad (A1.05)$$

Combining equations (Al.04) and (Al.05) and solving for ΔV_t :

$$\Delta V_t = \frac{\Delta V_o - a(e^{(a-b)kt} - 1)(\Delta V_o + \delta V)}{(ae^{(a-b)kt} - b)} \quad (\text{Al.06})$$

The equation is solved for ΔV_t as this is the quantity that is experimentally measured as a function of time. Equation (Al.06) is in a form that is amenable to non-linear least squares analysis to obtain the three unknown parameters, k , ΔV_o , and δV . A non-linear least squares computer program has been described by the IBM SHARE Library program SDA 3094 (1964) and modified by Ellis (1968) that is suitable to find the unknown parameters.

With equation (Al.06) as the model equation in the program and ΔV_t and t as input data, initial guesses are estimated for each of the unknown parameters k , ΔV_o , and δV . With these initial guesses observed and calculated values of ΔV_t are compared and corrections calculated until the least squares criterion is satisfied. This involves minimizing the sums of the squares of the residuals, that is the observed minus the calculated values of ΔV_t .

FORTRAN Listing of Sub-programs and Comments

The FORTRAN listing of the two subroutines FCODE and SUBZ are given on the next page.

The various FORTRAN parameters and variables are defined accordingly:


```

ISN 0002      SUBROUTINE SUBR2(Y,X,B,PPNT,NPNT,N)
ISN 0003      IMPLICIT REAL*8(A-H,O-Z)
ISN 0004      DIMENSION Y(500),X(500,10),B(50),PRNT(5)
ISN 0005      DO 1 I=1,N
ISN 0006      1 X(I,1)=X(I,1)*B(6)*B(7)+0.005
ISN 0007      NPNT=4
ISN 0008      RETURN
ISN 0009      END

```

***** END OF COMPILE *****

```

ISN 0002      SUBROUTINE FCODE(Y,X,B,PPNT,F,I)
ISN 0003      IMPLICIT REAL*8(A-H,O-Z)
ISN 0004      DIMENSION Y(500),X(500,10),B(50),PRNT(5)
ISN 0005      A1=DEXP((B(3)-B(4))*B(1)*X(I,1))
ISN 0006      A2=B(3)*(A1-1.0)
ISN 0007      A3=P(3)*A1-B(4)
ISN 0008      F=B(5)-A2*(B(5)+B(2))/A3
ISN 0009      PRNT(1)=(X(I,1)-0.005)/(B(6)*B(7))
ISN 0010      PRNT(2)=B(4)*A2/A3
ISN 0011      PRNT(3)=X(I,1)
ISN 0012      PRNT(4)=DLOG((B(4)*(B(3)-B(4)*A2/A3))/(B(3)*(B(4)-B(4)*A2/A3)))/(B
ISN 0013      1(3)-B(4))
ISN 0014      RETURN
ISN 0015      END

```

***** END OF COMPILE *****

Unknown parameters

B(1): k

B(2): δV

B(5): ΔV_o

Constant parameters and conversion factors

B(3): a

B(4): b

B(6): the number of graticule divisions per inch of graph paper on which the enlarged oscilloscope trace is read out on.

B(7): the number of seconds per graticule division or the sweep speed of the oscilloscope time base.

Variables

Y(I): the dependent variable is the number of inches measured on the vertical scale of the graph paper and is directly proportional to ΔV_t .

X(I,1): the independent variable is the number of inches measured on the horizontal scale of the graph paper and is proportional to time t.

The purpose of subroutine SUBZ is to convert the experimental measurements of distance on the graph paper to true time. This is accomplished with a DO loop which in turn multiplies each of the input data points, X(I,1), by the two conversion factors B(6) and B(7) and to this adds the dead time 0.005 sec to obtain the true time measured from the true start of the reaction.

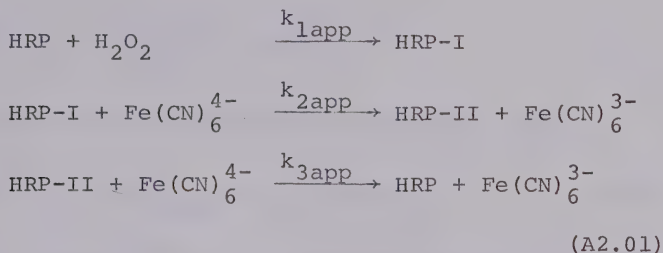
Subroutine FCODE contains the FORTRAN version of equation (A1.06), the model equation. Also included in this subroutine is the option for printing out auxiliary data: the original input data, the true time, and the different concentrations.

In the limit for $a \gg b$, the second order integrated rate expression gives the pseudo first order expression and the subroutines as written, are also applicable to a pseudo first order kinetic analyses.

Appendix 2

Derivation of the Initial Velocity Expression for the
Steady State HRP Catalyzed Oxidation of Ferrocyanide
by Hydrogen Peroxide

The reaction sequences of the HRP catalyzed oxidation of ferrocyanide by hydrogen peroxide are:



where no particular state of ionization is implied for any of the reactants. From inspection of equations (A2.01) the following conservation relations apply throughout the course of the reaction:

$$[\text{HRP}] + [\text{HRP-I}] + [\text{HRP-II}] = [\text{HRP}]_0 \tag{A2.02}$$

$$[\text{Fe}(\text{CN})_6^{4-}] + [\text{Fe}(\text{CN})_6^{3-}] = [\text{Fe}(\text{CN})_6^{4-}]_0 \tag{A2.03}$$

where the concentrations with the subscript zeros are initial concentrations.

For reactions (A2.01) the following differential rate expressions apply:

$$\frac{d[\text{HRP-I}]}{dt} = k_{1\text{app}}[\text{HRP}][\text{H}_2\text{O}_2] - k_{2\text{app}}[\text{HRP-I}][\text{Fe}(\text{CN})_6^{4-}]
 \tag{A2.04}$$

$$\frac{d[\text{HRP-II}]}{dt} = k_{2\text{app}}[\text{HRP-I}][\text{Fe}(\text{CN})_6^{4-}] - k_{3\text{app}}[\text{HRP-II}][\text{Fe}(\text{CN})_6^{4-}] \quad (\text{A2.05})$$

$$\frac{d[\text{HRP}]}{dt} = k_{3\text{app}}[\text{HRP-II}][\text{Fe}(\text{CN})_6^{4-}] - k_{1\text{app}}[\text{HRP}][\text{H}_2\text{O}_2] \quad (\text{A2.06})$$

The steady state assumption applied to each form of HRP is:

$$\frac{d[\text{HRP-I}]}{dt} = \frac{d[\text{HRP-II}]}{dt} = \frac{d[\text{HRP}]}{dt} = 0 \quad (\text{A2.07})$$

and when applied to equations (A2.04-A2.06) gives:

$$k_{1\text{app}}[\text{HRP}][\text{H}_2\text{O}_2] = k_{2\text{app}}[\text{HRP-I}][\text{Fe}(\text{CN})_6^{4-}] \quad (\text{A2.08})$$

$$k_{2\text{app}}[\text{HRP-I}][\text{Fe}(\text{CN})_6^{4-}] = k_{3\text{app}}[\text{HRP-II}][\text{Fe}(\text{CN})_6^{4-}] \quad (\text{A2.09})$$

$$k_{3\text{app}}[\text{HRP-II}][\text{Fe}(\text{CN})_6^{4-}] = k_{1\text{app}}[\text{HRP}][\text{H}_2\text{O}_2] \quad (\text{A2.10})$$

Substitution of equations (A2.09-A2.10) in equation (A2.02) gives:

$$\begin{aligned} [\text{HRP-II}] + \frac{k_{3\text{app}}[\text{HRP-II}]}{k_{2\text{app}}} + \frac{k_{3\text{app}}[\text{Fe}(\text{CN})_6^{4-}][\text{HRP-II}]}{k_{1\text{app}}[\text{H}_2\text{O}_2]} \\ = [\text{HRP}]_0 \end{aligned} \quad (\text{A2.11})$$

The differential rate expression for the production of ferricyanide is:

$$\frac{d[\text{Fe}(\text{CN})_6^{3-}]}{dt} = k_{2\text{app}}[\text{HRP-I}][\text{Fe}(\text{CN})_6^{4-}] + k_{3\text{app}}[\text{HRP-II}][\text{Fe}(\text{CN})_6^{4-}] \quad (\text{A2.12})$$

Substitution of equation (A2.09) in equation (A2.12) gives:

$$\frac{d[\text{Fe}(\text{CN})_6^{3-}]}{dt} = 2k_{3\text{app}}[\text{HRP-II}][\text{Fe}(\text{CN})_6^{4-}] \quad (\text{A2.13})$$

Solving equation (A2.11) for [HRP-II] and substituting the result in equation (A2.13) gives:

$$\frac{d[\text{Fe}(\text{CN})_6^{3-}]}{dt} = \frac{2k_{1\text{app}}k_{2\text{app}}k_{3\text{app}}[\text{HRP}][\text{Fe}(\text{CN})_6^{4-}][\text{H}_2\text{O}_2]}{(k_{1\text{app}}k_{2\text{app}} + k_{1\text{app}}k_{3\text{app}})[\text{H}_2\text{O}_2] + k_{2\text{app}}k_{3\text{app}}[\text{Fe}(\text{CN})_6^{4-}]} \quad (\text{A2.14})$$

Defining the initial velocity, v , as $\frac{d[\text{Fe}(\text{CN})_6^{3-}]_0}{dt}$ at zero time then:

$$v = \frac{2k_{1\text{app}}k_{2\text{app}}k_{3\text{app}}[\text{HRP}]_0[\text{Fe}(\text{CN})_6^{4-}]_0[\text{H}_2\text{O}_2]_0}{(k_{1\text{app}}k_{2\text{app}} + k_{1\text{app}}k_{3\text{app}})[\text{H}_2\text{O}_2]_0 + k_{2\text{app}}k_{3\text{app}}[\text{Fe}(\text{CN})_6^{4-}]_0} \quad (\text{A2.15})$$

Both $k_{2\text{app}}$ and $k_{3\text{app}}$ have been measured as shown in Chapter 3 and it was found that $k_{2\text{app}}$ was 40 or more times k larger than $k_{3\text{app}}$. With the approximation ($k_{2\text{app}} \gg k_{3\text{app}}$) equation (A2.15) simplifies to:

$$\frac{[\text{HRP}]_0}{v} = \frac{1}{2k_{3\text{app}}[\text{Fe}(\text{CN})_6^{4-}]_0} + \frac{1}{2k_{1\text{app}}[\text{H}_2\text{O}_2]_0} \quad (\text{A2.16})$$

Calculation of the Attainment of the Steady State Conditions

Three approximations have been made in the derivation of initial velocity steady state expression, equation (A2.15), and each of these will be dealt with in turn - generally and then with a specific case.

In the first approximation where $d[\text{HRP-II}]/dt$ is set equal to zero and equation (A2.09) is derived, it is implicitly assumed in equation (A2.11) that $(d[\text{HRP-II}])/(dt k_{2\text{app}}[\text{Fe}(\text{CN})_6^{4-}]_0) \ll [\text{HRP}]$. Equivalently if $k_{2\text{app}}[\text{Fe}(\text{CN})_6^{4-}]_0 = k_{2\text{obs}}$ a pseudo first order rate constant, then it is assumed:

$$\frac{d[\text{HRP-II}]}{dt k_{2\text{obs}}[\text{HRP}]_0} \ll 1 \quad (\text{A2.17})$$

Reactions (A2.01), described by the differential equations (A2.04-2.06), under pseudo first order conditions where each of the substrates, hydrogen peroxide and ferrocyanide, are in large excess of HRP and HRP compounds, are soluble for concentrations and concentration derivatives at any time. A more complete description of the procedure is given by Evett (1968)*. The relative concentrations are plotted in Figure (A2.01) vs. time for a typical case at a pH of 4.79. The following are the pseudo first order rate constants used in the calculation of the time course of the reaction progress curves of Figure (A2.01):

$$\begin{aligned} k_{1\text{obs}} &= k_{1\text{app}}[\text{H}_2\text{O}_2]_0 = (1.6 \times 10^7 \text{ M}^{-1}\text{sec}^{-1})(10^{-4}\text{M}) \\ &= 1.6 \times 10^3 \text{ sec}^{-1} \end{aligned} \quad (\text{A2.18})$$

$$\begin{aligned} k_{2\text{obs}} &= k_{2\text{app}}[\text{Fe}(\text{CN})_6^{4-}]_0 = (8.9 \times 10^6 \text{ M}^{-1}\text{sec}^{-1})(3.6 \times 10^{-5}\text{M}) \\ &= 3.2 \times 10^2 \text{ sec}^{-1} \end{aligned} \quad (\text{A2.19})$$

* I am indebted to Dr. M. Evett for his assistance in supplying a computer solution for the evaluation of the time course of the three component reaction system.

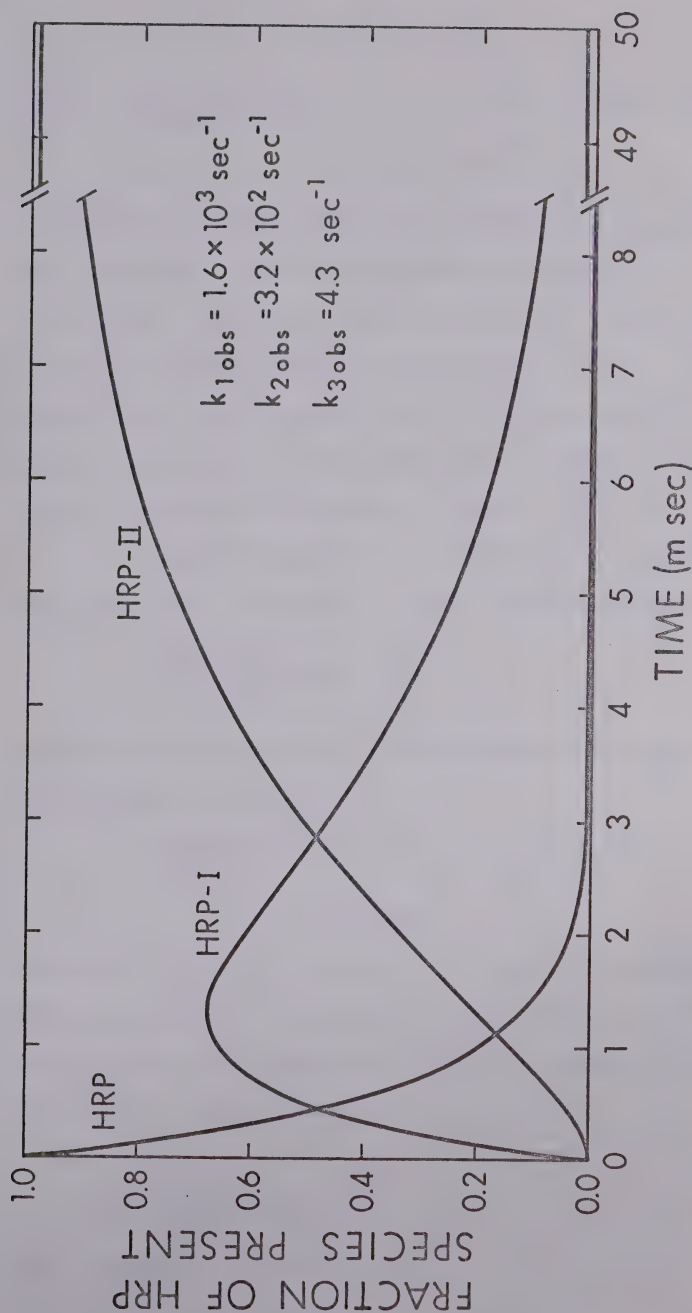


Figure A2.01: Computer calculated relative concentrations of various HRP species vs. time at pH 4.79. The values of $k_{1\text{obs}}$, $k_{2\text{obs}}$, and $k_{3\text{obs}}$ are 1.6×10^3 , 3.2×10^2 , and 4.3 sec^{-1} respectively. Note that HRP attains steady state conditions much before HRP-I and HRP-II.

$$\begin{aligned}
 k_{3\text{obs}} &= k_{3\text{app}} [\text{Fe(CN)}_6^{4-}]_0 = (1.2 \times 10^5 \text{ M}^{-1} \text{sec}^{-1}) (3.6 \times 10^{-5} \text{ M}) \\
 &= 4.3 \text{ sec}^{-1} \quad (\text{A2.20})
 \end{aligned}$$

The apparent second order rate constants $k_{2\text{app}}$ and $k_{3\text{app}}$ were obtained from data collected in Chapter 3. The value of $k_{1\text{app}}$ was obtained from Dolman (1969) which corresponds closely to values obtained by Chance (1963a). In Table (A2.01) are also listed normalized concentration derivatives at a number of representative reaction times for the reaction courses described in Figure (A2.01).

Assume then that equation (A2.17) is valid when only some small fraction, F , of 1 is attained or:

$$\frac{d[\text{HRP-II}]}{dt k_{2\text{obs}} [\text{HRP}]_0} = F \quad (\text{A2.21})$$

For 99% attainment of the steady state condition for this approximation or when $F = 0.01$:

$$\begin{aligned}
 \frac{d[\text{HRP-II}]}{dt [\text{HRP}]_0} &= 0.01 \times 3.2 \times 10^2 \text{ sec}^{-1} \\
 &= 3.2 \text{ sec}^{-1} \quad (\text{A2.22})
 \end{aligned}$$

From Table (A2.01) a value of 3.2 sec^{-1} for $d[\text{HRP-II}]/(dt [\text{HRP}]_0)$ is reached in approximately 15 msec. Similarly it can be shown that equation (A2.10) in equation (A2.11) involves the approximation:

$$\frac{d[\text{HRP}]}{dt k_{1\text{obs}} [\text{HRP}]_0} = F \quad (\text{A2.23})$$

and if again $F = 0.01$

Table A2.01

Normalized Concentration Derivatives Under
Pseudo First Order Conditions at pH 4.79
for Reactions (A2.01)

time (msec)	$\frac{d[\text{HRP}]}{dt} [\text{HRP}]_0^{-1}$ (sec ⁻¹)	$\frac{d[\text{HRP-I}]}{dt} [\text{HRP}]_0^{-1}$ (sec ⁻¹)	$\frac{d[\text{HRP-II}]}{dt} [\text{HRP}]_0^{-1}$ (sec ⁻¹)
1	-3.2×10^2	1.1×10^2	2.1×10^2
2	-6.5×10^1	-1.3×10^2	1.9×10^2
4	-2.3×10^0	-1.1×10^2	1.1×10^2
6	8.3×10^{-2}	-5.7×10^1	5.7×10^1
8	9.6×10^{-2}	-3.0×10^1	3.0×10^1
10	5.2×10^{-2}	-1.6×10^1	1.6×10^1
12	2.7×10^{-2}	-8.1×10^0	8.1×10^0
14	1.4×10^{-2}	-4.2×10^0	4.2×10^0
16	7.4×10^{-3}	-2.2×10^0	2.2×10^0
18	3.9×10^{-3}	-1.2×10^0	1.2×10^0
20	2.0×10^{-3}	-6.0×10^{-1}	6.0×10^{-1}
30	7.9×10^{-5}	-2.3×10^{-2}	2.3×10^{-2}
40	2.9×10^{-6}	-8.9×10^{-4}	8.9×10^{-4}

$$\begin{aligned}\frac{d[\text{HRP}]}{dt}[\text{HRP}]_0 &= 0.01 \times 1.6 \times 10^3 \text{ sec}^{-1} \\ &= 16 \text{ sec}^{-1}\end{aligned}\quad (\text{A2.24})$$

From Table (A2.01), HRP reaches 99% of steady state conditions when the reaction has preceeded for only 3 msec, an even shorter time than for HRP-II as previously shown.

The steady state approximation is used a third and final time and that is in equation (A2.13) which is derived from equation (A2.12) by assuming that:

$$\frac{d[\text{HRP-II}]}{dt} \ll \frac{d[\text{Fe}(\text{CN})_6^{3-}]}{dt} \quad (\text{A2.25})$$

Or if $d[\text{HRP-II}]/dt$ has obtained some fractional portion, F ,

of $\frac{d[\text{Fe}(\text{CN})_6^{3-}]}{dt}$ the result may be written as:

$$\frac{d[\text{HRP-II}]}{dt}[\text{HRP}]_0 = \frac{F \frac{d[\text{Fe}(\text{CN})_6^{3-}]}{dt}}{[\text{HRP}]_0} \quad (\text{A2.26})$$

or:

$$\frac{d[\text{HRP-II}]}{dt}[\text{HRP}]_0 = \frac{Fv}{[\text{HRP}]_0} \quad (\text{A2.27})$$

The value of $v/[\text{HRP}]_0$ is simply the slope of a plot of v vs. $[\text{HRP}]_0$ at a pH of 4.79 in Chapter 3 (Figure 3.05) and has been determined to be 42 sec^{-1} by a weighted linear least squares analysis. If $F = 0.01$ again or the steady state conditions for this approximation are 99% attained then:

$$\begin{aligned}\frac{d[\text{HRP-II}]}{dt}[\text{HRP}]_0 &= 0.01 \times 42 \text{ sec}^{-1} \\ &= 0.42 \text{ sec}^{-1}\end{aligned}\quad (\text{A2.28})$$

From Table (A2.01) this value of $\frac{d[\text{HRP-II}]}{dt[\text{HRP}]_0}$ is attained at approximately 21 msec after the start of the reaction. The last approximation takes the longest to become valid and thus determines the attainment of the steady state conditions- 99% attained 21 msec after the start of the reaction. The value of 21 msec is a much shorter time than that over which the initial velocities were calculated (a few seconds) and hence the steady state approximations are valid for the determination of v .

Appendix 3

Purification of HRP by Sephadex Column Chromatography

A procedure was developed for the purification of HRP in Sephadex column chromatography. Sephadex is a high molecular weight polysaccharide that is highly cross-linked. Molecules larger than the pores present in swollen Sephadex do not penetrate and pass through the column first. Smaller molecules penetrate into the pores and are eluted last. Molecules, in general, are eluted from a Sephadex column in order of decreasing molecular weight.

The Sephadex used in this purification of HRP was a cation exchange gel, Sephadex C-50 (CM), and contains a large number of carboxylic acid groups. At a pH value larger than the pK 's of the carboxylic acid groups the acid groups are negatively charged and absorb positively charged solutes. Thus, separation of solute components on Sephadex C-50 (CM) is due partly to charge effects and to the molecular weight of the solute.

Experimental Procedure

Sephadex C-50 (CM) (7.5 gm) was equilibrated for 48 hours in 0.1 ionic strength phosphate buffer of pH 6.2 with several changes of supernatant to ensure complete equilibration with buffer. The column (Sephadex Laboratory Column type K25/45; 2.5 x 45 cm) was equipped with a gradient

apparatus to give a continuously linearly increasing ionic strength gradient. With the gradient apparatus the ionic strength increases linearly from 0.1 to 0.2.

The HRP (purified, lyophilized from Boehringer-Mannheim) (0.5 gm) was dissolved in 5 ml of water and added to the top of the column and eluted with a pressure head of about 5 cm of water. About 60 ml of effluent were allowed to pass through the column before the first samples were collected. Generally the major peak was observed to pass through the column at an effluent volume of 90 ml. In addition to the major peak two small poorly separated peaks remained at the top of the column. These components did not pass through the column even after a large volume of 0.2 ionic strength phosphate buffer had been applied.

The effluent was monitored by taking successive 5 ml samples and measuring their absorbance after a 10:1 dilution at 403 $m\mu$ and 280 $m\mu$. The absorbance at 403 $m\mu$ is due mainly to the heme prosthetic group of HRP and the absorbance at 280 $m\mu$ is due mainly to the apoprotein. The ratio of the absorbance at 403 $m\mu$ to that at 280 $m\mu$ is called the R.Z. and is often taken as an index of HRP purity, the higher the R.Z. the greater the purity of the enzyme preparation.

Absorbances at 403 and 280 $m\mu$ as well as R.Z. are plotted vs. the effluent volume in Figure (A3.01). The elution profile is not flattened at the center indicating that the sample size was not excessive for the type

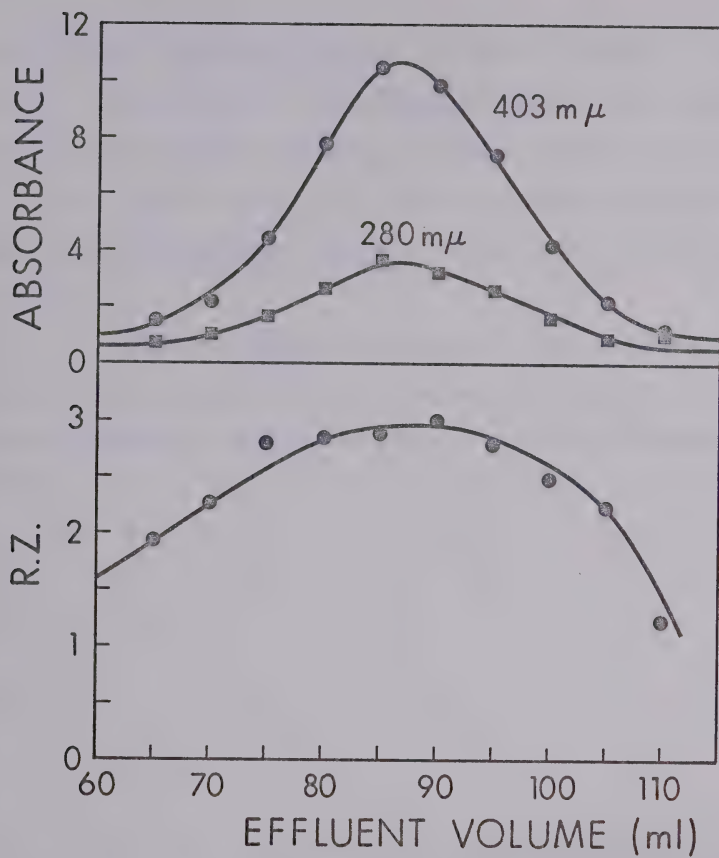


Figure A3.01: Absorbances at 403 and 280 m μ and R.Z. plotted vs. effluent volume.

of column used.

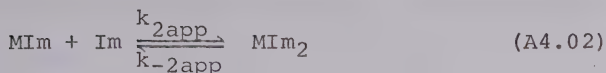
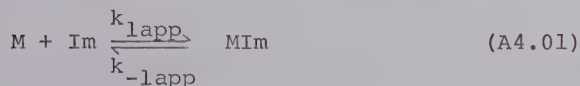
In general the effluent volume samples from 75 to 95 ml were combined together to give a sample of HRP of R.Z. 2.8 or higher. The combined samples were precipitated with an 80% saturated ammonium sulfate solution by spinning on a centrifuge at 4°C. The resulting ammonium sulfate precipitate containing the HRP was stored under refrigeration at about 5°.

Before use the precipitate was dissolved in water (5 ml), dialyzed exhaustively against cold distilled water and centrifuged and filtered with a Millipore filter.

Appendix 4

Derivation of the Steady State Relaxation Time for the
Binding of Imidazole to Hemin

For the reactions,



where M is the metalloporphyrin, ferriprotoporphyrin IX, Im is imidazole and MIm and MIm₂ are the monoimidazole and bisimidazole hemin complexes, all without regard to state of protonation of the reactants. The differential rate expression is:

$$\begin{aligned} \frac{d[\text{MIm}]}{dt} = & k_{1\text{app}}[\text{M}][\text{Im}] + k_{-2}[\text{MIm}_2] - k_{-1\text{app}}[\text{MIm}] \\ & - k_{2\text{app}}[\text{MIm}][\text{Im}] \end{aligned} \quad (\text{A4.03})$$

With the steady state approximation $d[\text{MIm}]/dt = 0$ in equation (A4.03) and solving for [MIm]:

$$[\text{MIm}] = \frac{k_{1\text{app}}[\text{M}][\text{Im}] + k_{-2\text{app}}[\text{MIm}_2]}{k_{-1\text{app}} + k_{2\text{app}}[\text{Im}]} \quad (\text{A4.04})$$

The differential rate expression in terms of [MIm₂] is:

$$\frac{d[\text{MIm}_2]}{dt} = k_{2\text{app}}[\text{MIm}][\text{Im}] - k_{-2\text{app}}[\text{MIm}_2] \quad (\text{A4.05})$$

From reactions (A4.01) and (A4.02) it is also easily shown that:

$$K_{app} = \frac{k_{1app} k_{2app}}{k_{-1app} k_{-2app}} = \frac{[\overline{MIm}_2]}{[\overline{M}] [\overline{Im}]^2} \quad (A4.06)$$

where the barred concentrations are equilibrium concentrations.

Assuming a perturbation from the equilibrium concentrations of the amount $\Delta[MIm_2]$, the conservation relations are then:

$$[M] = [\overline{M}] - \Delta[MIm_2] \quad (A4.07)$$

$$[Im] = [\overline{Im}] - 2\Delta[MIm_2] \quad (A4.08)$$

$$[MIm_2] = [\overline{MIm}_2] + \Delta[MIm_2] \quad (A4.09)$$

Substituting equation (A4.07-4.09) in equation (A4.05)

$$\begin{aligned} \frac{d([\overline{MIm}_2] + \Delta[MIm_2])}{dt} &= \{k_{2app} k_{1app} ([\overline{M}] - \Delta[MIm_2]) ([\overline{Im}] - \\ &\quad 2\Delta[MIm_2])^2 - k_{-2app} k_{-1app} ([\overline{MIm}_2] + \Delta[MIm_2]) \} \\ &\quad / \{k_{-1app} + k_{2app} ([\overline{Im}] - 2\Delta[MIm_2])\} \end{aligned} \quad (A4.10)$$

First making the approximation:

$$[\overline{Im}] = [\overline{Im}] - 2\Delta[MIm_2] \quad (A4.11)$$

and

$$(\Delta[MIm_2])^2 \ll \Delta[MIm_2] \quad (A4.12)$$

and then substituting equation (A4.06) in equation (A4.10), the result is:

$$\frac{d \Delta[MIm_2]}{dt} = \frac{k_{2app}k_{1app}[\overline{Im}]^2 + k_{-2app}k_{-1app}}{k_{-1app} + k_{2app}[\overline{Im}]} \quad (A4.13)$$

The reciprocal relaxation time is given by the identity

$$(d (\Delta [MIm_2])/dt)/\Delta[MIm_2] \equiv (\tau)^{-1} \quad (A4.14)$$

Thus with equations (A4.14) and (A4.06) equation (A4.13) reduces to:

$$\frac{1}{\tau} = \frac{k_{-2app}(1 + K_{app}[\overline{Im}]^2)}{1 + \frac{k_{2app}}{k_{-1app}}[\overline{Im}]} \quad (A4.15)$$

B29945